Title	Thermal, Metallurgical and Mechanical Behavior of Welded Structures based on CFD Process Simulations
Author(s)	Na, Suck-Joo
Citation	DIMECC 9th Annual Seminar, 14 - 15 November 2016, Helsinki, Finland
Date	2016
Rights	This presentation may be downloaded for personal use only.

Thermal, Metallurgical and Mechanical Behavior of Welded Structures based on CFD Process Simulations

Professor Suck-Joo NA, Dr.-Ing.
Department of Mechanical Engineering, KAIST, Korea
FiDiPro Professor, VTT, Finland

Thanks to:
KAIST: W.I.Cho, D.W.Cho, J.H.Cho, S.W.Han, H.P.Cheon, M.Sohail, D.V.Kiran, L.Zhang, L.Wu, S.D.Kim
POSCO: M.H.Cho, J.S.Lee, POSTECH: J.B.Lee, KITECH: C.H.Kim, D.C.Kim
BAM: A.Gumenyuk, M.Rethmeier, BIAS: F.Volloertsen, C.Thomy, VTT: V.Kujanpaa, M.Siren

Current State of Design of Welded Machine Structures

[Design example: Excavator Boom]

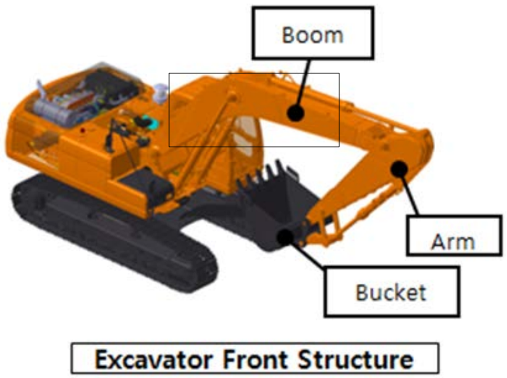

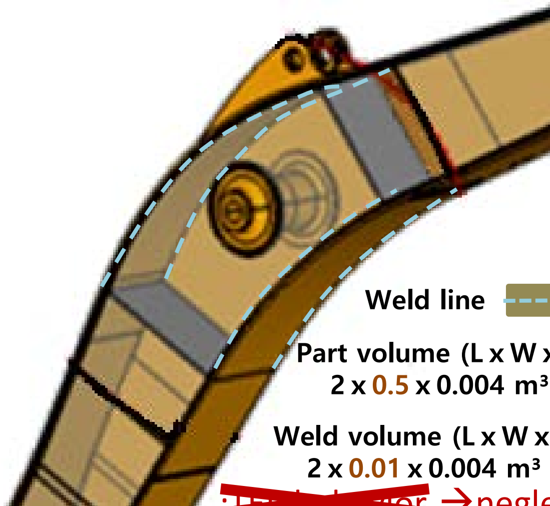

Weld line

Part volume (L x W x t) :Elastic behavior
2 x 0.5 x 0.004 m³

Weld volume (L x W x t) →
2 x 0.01 x 0.004 m³
~~:TEP behavior~~ → neglected

Very small cross section: ~1%
Large temperature change: 20°C ~ 2000°C
Large plastic strain: ~0.1

Multi-physics phenomena in welding

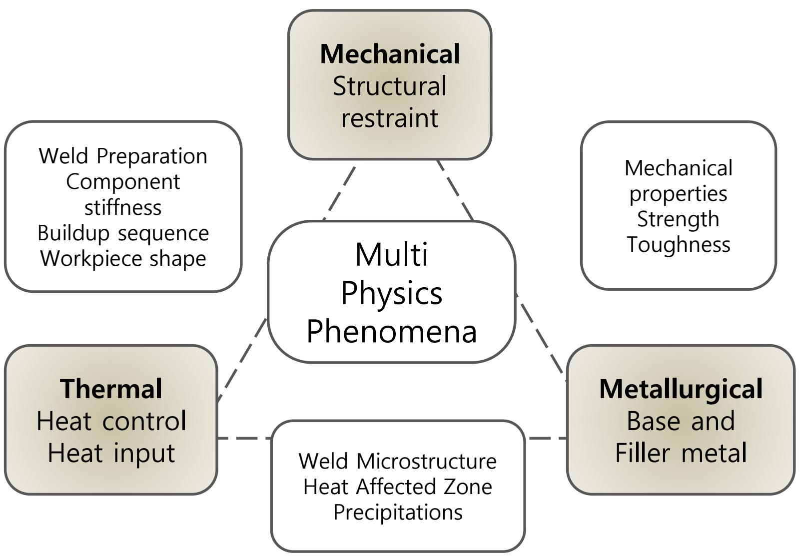

Fine element

Design of whole structure:
Large part: elastic +
Small weld: thermal-elasto-plastic (TEP)

Numerical Simulation

Fine element for whole domain: Excessive computation time
→ Elastic design of welded structures
+ Welding process by welder's skill

→ Mismatching by welding distortion

Welding Distortion and its Prevention

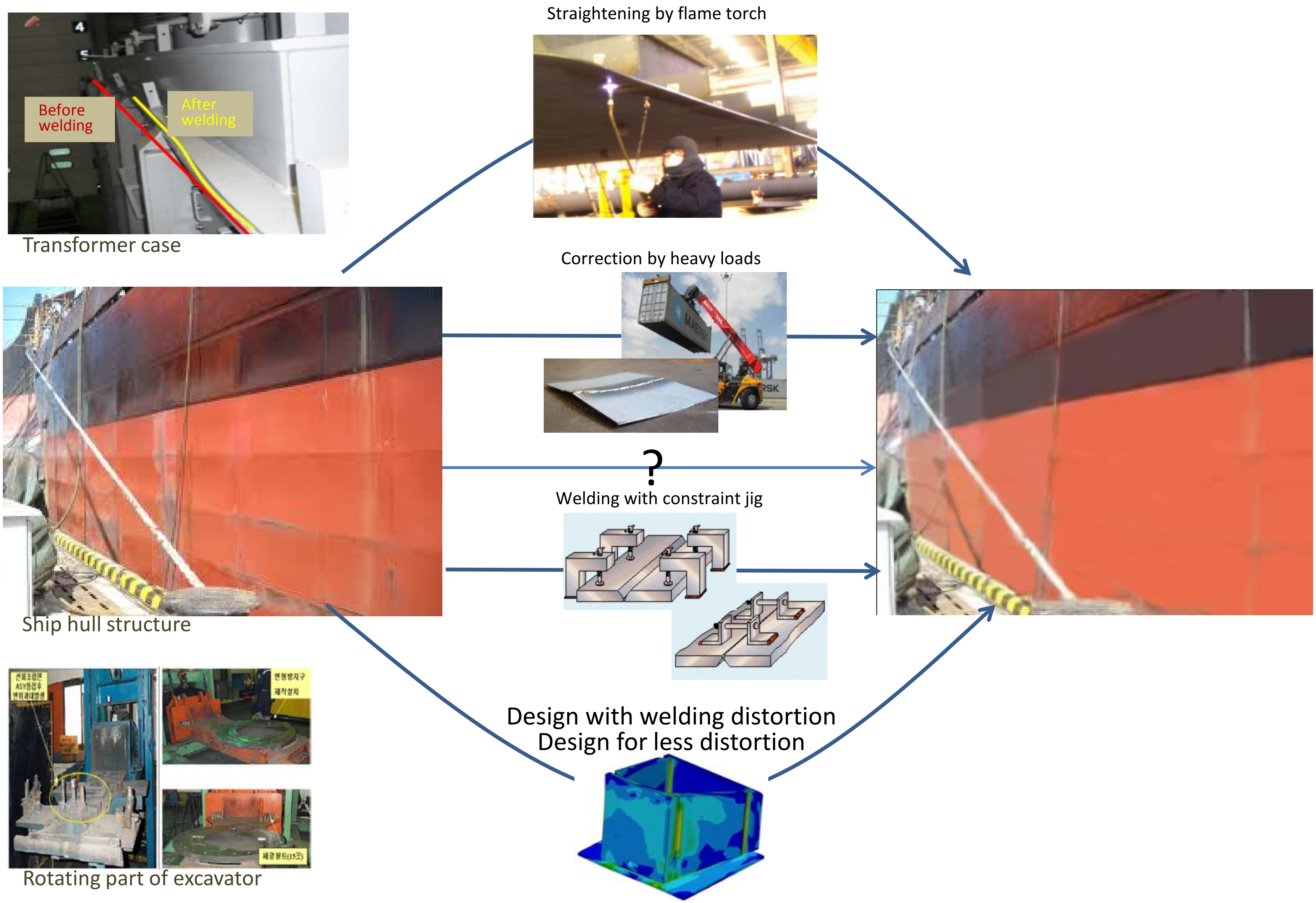

Prediction of Welding Distortion

[Design example: Excavator Boom]

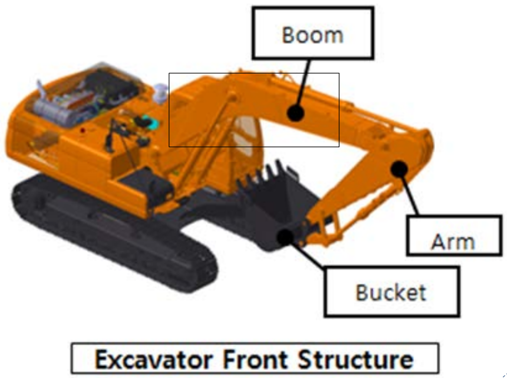

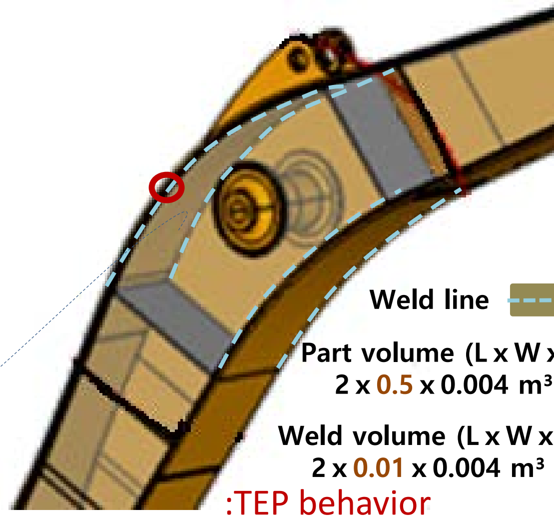

Weld line

Part volume (L x W x t) :~~Elastic behavior~~ → neglected
2 x 0.5 x 0.004 m³

Separation of weldment from structure

Weld volume (L x W x t)
2 x 0.01 x 0.004 m³ →
:TEP behavior

- Very small cross section: ~1%
- Large temperature change: 20ºC ~ 2000ºC
- Large plastic strain: ~0.1

Heat and fluid flow in weldment

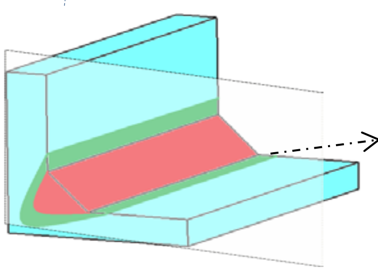

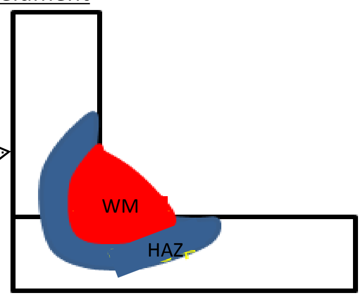

Heat flow by heat source
Fluid flow by EMF, etc.
Free surface by VOF

Very fine mesh

Temperature distribution
Element mixing

Data for metallurgical and mechanical analysis of weldments

Phase transformation → Microstructure

TEP (Thermal-Elasto-Plastic) behavior:
Weld metal and HAZ:

$$\varepsilon^{*} = \varepsilon - \varepsilon^{e} = \varepsilon^{p}$$

ε^{*} Inherent strain

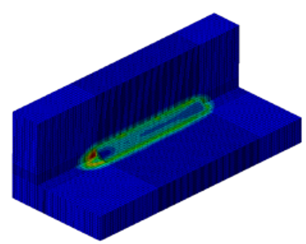

Plastic strain → Welding inherent strain
Residual stress

Welding distortion of machine structure

Inherent strain of weldment:
Boundary condition → Elastic FEM simulations

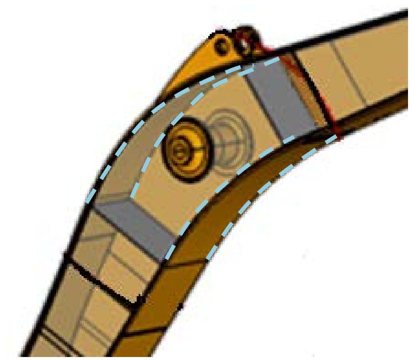

Strength of weldments

Simulations of heat and fluid flow → Analysis of inherent strain in weldment
→ Prediction of welding distortion for design of welded machine structures

Thermal-Metallurgical-Mechanical (T-M-M) Analysis of Weldment

Fully coupled Thermal-Metallurgical-Mechanical analysis

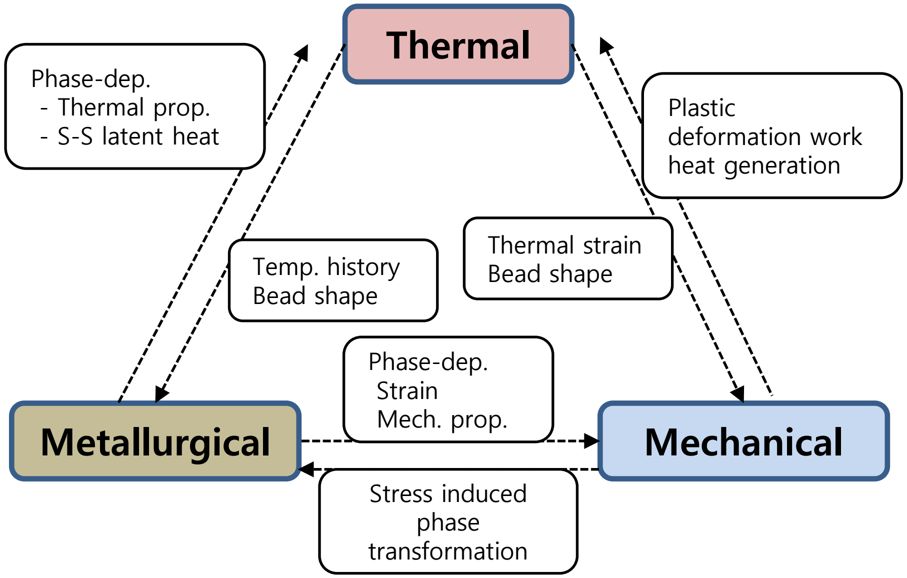

Thermal-Metallurgical-Mechanical analysis in this study

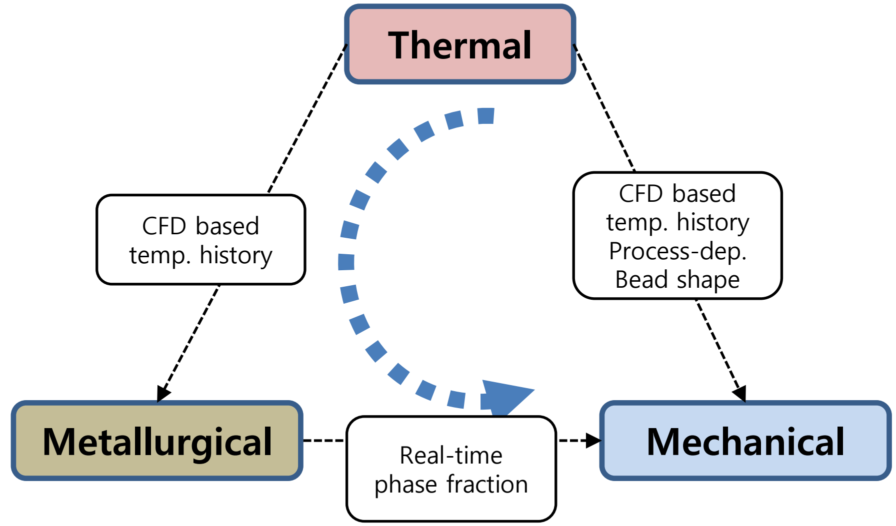

- **T-M-M Analysis of Bead-on-plate welding**
  - CFD analysis of welding process
  - Metallurgical analysis of weldment
  - Mechanical analysis of weldment

Governing Equations for Heat and Mass Flow in Welding

Pre-assumption: incompressible Newtonian fluid, laminar flow

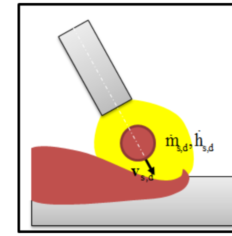

Mass Conservation (Continuity Equation)

$$\nabla \cdot \mathbf{v} = \frac{\dot{m}_s}{\rho}$$

$\mathbf{v}$: velocity vector, $\dot{m}_s$: mass source , ρ : density

Momentum Conservation Equation (Navier-Stokes Equation)

$$\frac{\partial \mathbf{v}}{\partial t} + \mathbf{v} \cdot \nabla \mathbf{v} = -\frac{1}{\rho}\nabla P + \nu \nabla^2 \mathbf{v} - K\mathbf{v} + \frac{\dot{m}_{s,d}}{\rho}(\mathbf{v}_{s,d} - \mathbf{v}) + \mathbf{G}$$

ν : dynamic viscosity, K : Drag coefficient, $\mathbf{v}_{s,d}$: droplet velocity,

$\mathbf{G}$: body acceleration

Energy Conservation Equation (Phase Change)

$$\frac{\partial h}{\partial t} + \mathbf{v} \cdot \nabla h = \frac{1}{\rho}\nabla \cdot (k \nabla T) + \dot{h}_s$$

h : enthalpy, k : thermal conductivity, $\dot{h}_s$: enthalpy source

VOF Equation (Free Surface Tracking)

$$\frac{\partial F}{\partial t} + \nabla \cdot (\mathbf{v}F) = \dot{F}_s$$

F: fluid fraction, $\dot{F}_s$: fluid fraction source associated with droplets

All the governing equations : implemented in the base software package

Key issue in welding simulations: how to model the welding process

Arc Welding Models for Bead-on-Plate Welding

- Arc Heat Source Model: Gaussian

$$\eta_A q_A(x,y) = \eta_A \frac{VI}{2\pi r_A^2}\exp\left(-\frac{x^2+y^2}{2r_A^2}\right)$$

η_A: Heat input efficiency(0.54),
V: Voltage, I: Arc current,
r_A: Heat distribution parameter(2.4mm)

- Arc Pressure Model

$$p_A \cong \frac{\mu_0 I^2}{4\pi^2 r_A{}^2}\exp\left(-\frac{r^2}{2r_A{}^2}\right)$$

μ_0: vacuum permeability

Z. Cao, Z. Yang and X. L. Chen: *Weld. J.*, 2004, **83**, 169s-176s

- Electromagnetic Force Model

$$J_z = \frac{I}{2\pi}\int_0^\infty \lambda J_0(\lambda r)\exp(-\lambda^2 r_A{}^2/12)\frac{\sinh[\lambda(c-z)]}{\sinh(\lambda c)}d\lambda$$

$$J_r = \frac{I}{2\pi}\int_0^\infty \lambda J_1(\lambda r)\exp(-\lambda^2 r_A{}^2/12)\frac{\cosh[\lambda(c-z)]}{\sinh(\lambda c)}d\lambda$$

$$B_\theta = \frac{\mu_m I}{2\pi}\int_0^\infty J_1(\lambda r)\exp(-\lambda^2 r_A{}^2/12)\frac{\sinh[\lambda(c-z)]}{\sinh(\lambda c)}d\lambda$$

S. Kou and D. K. Sun: Metall. Trans. A, 1985, **16A**, 203

- Surface Tension Model

$$\mu\frac{\partial v_t}{\partial n} = -\frac{\partial \gamma}{\partial T}\frac{\partial T}{\partial r}$$

μ: dynamic viscosity, v_t : tangential velocity, n: normal to the free surface, r: tangential direction

- Buoyancy Model

$$F_b = \rho g \beta (T - T_0)$$

ρ: density, g: gravity, β: thermal expansion rate, T: temperature, T_0: reference temperature

- Drag Force Model

$$\frac{\tau}{\rho_p u_0^2}\mathrm{Re}_0^{1/2}\left(\frac{H}{D}\right)^2 = g_2\left(\frac{r}{H}\right)$$

τ: shear stress, ρ_p: density, u_0: initial plasma velocity, Re_0: Reynolds number, H: nozzle height, D: nozzle diameter, r: radius from the center, g_2: universal function

D. J. Phares, G. T. Smedley and R. C. Flagan: *J. Fluid Mech.*, 2000, **418**, 351-375

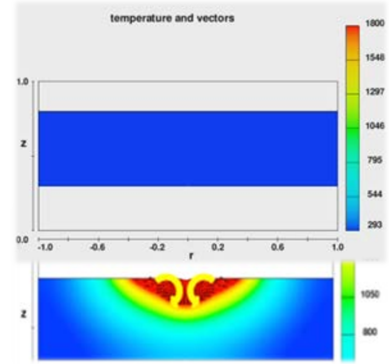

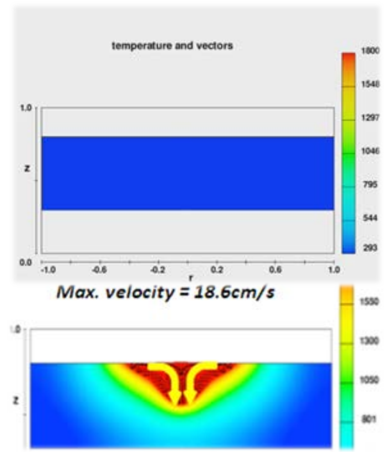

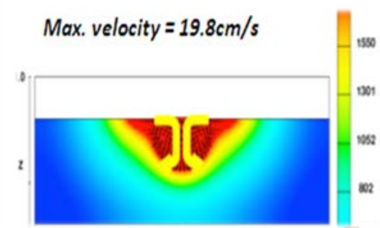

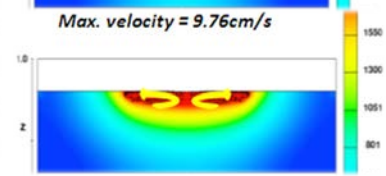

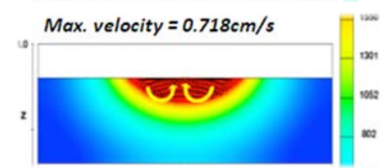

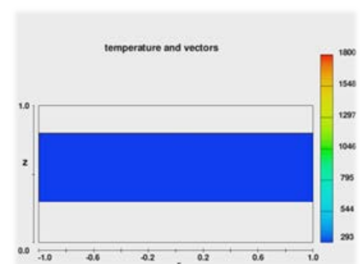

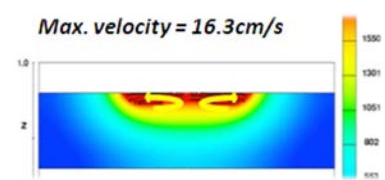

- Workpiece: SS400 steel, 10mm thickness, - Solid Wire: Y308 stainless steel **(20% Cr, 10% Ni)**

Alloying Element Distribution (wt. % Cr)

Alloying Element Distribution (wt. % Ni)

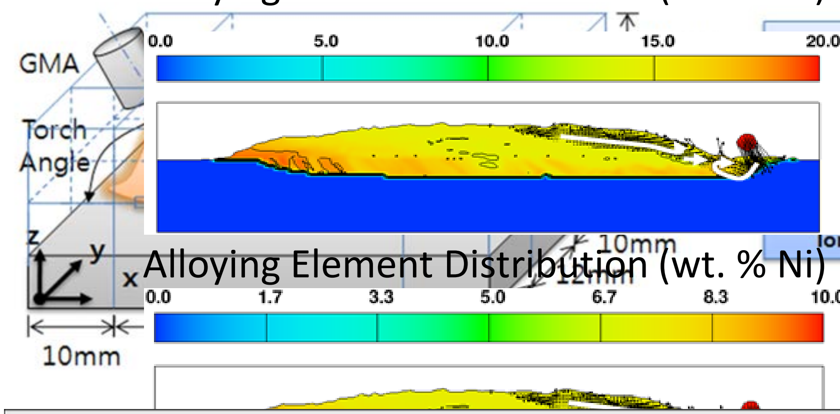

Welding Condition	
: Voltage	28 V
: Current	231 A
'eeding Rate	8 m/min
ling Speed	1 m/min
Torch Angle	61°, 90°

eat input efficiency = 0.54
ution parameter = 3.0mm

- **Boundary Conditions**
  - Top surface, heat flux
    - Arc heat source
    - Air convection, heat radiation

$$K\frac{\partial T}{\partial n} = \eta_A q_A - h_A(T - T_\infty) - \sigma_s \varepsilon_r (T^4 - T_\infty^4) - q_{vap}$$

  - Top surface, pressure
    - Arc pressure, surface tension

$$-p + 2\mu\frac{\partial V_n}{\partial n} = -p_A + \frac{\gamma}{R_c}$$

  - For other five surfaces
    - Continuative boundary condition
    - Normal derivatives of all quantities at the boundary are zero
    - Smooth continuation of the flow through boundary
    - No influence of boundary to the internal region

h_A = convection coefficient, T_∞ = ambient temperature
σ_s = Stefan-Boltzmann constant, ε_r = emissivity, μ = viscosity,
γ = surface tension, R_c = local curvature, n = normal component

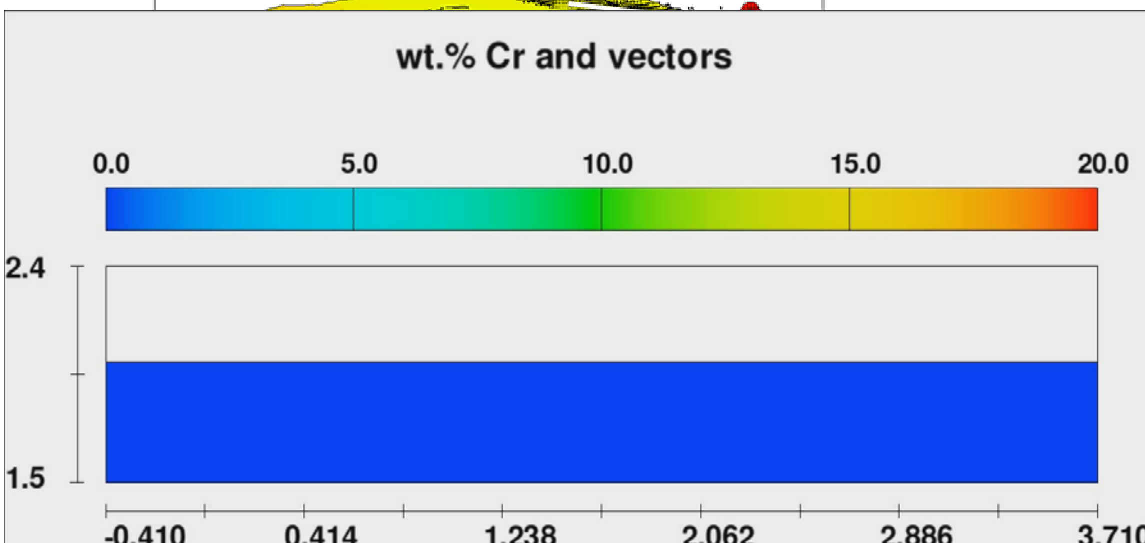

ibution in weld bead

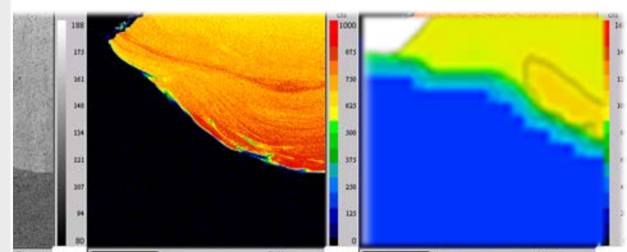

EPMA measurement **Simulation**

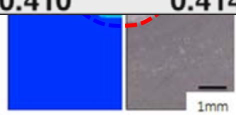

Bead height: 0.23cm
Bead width: 0.62cm
Penetration depth: 0.16cm

- ➢Well mixed in the entire weld bead
- ➢ Relatively high Cr concentration in the center part of lower bead region

CFD-FEM Coupling: Temperature Data Transfer from CFD to FEM

Computational Fluid Dynamics (CFD) vs. Finite Element Method (FEM) Configuration

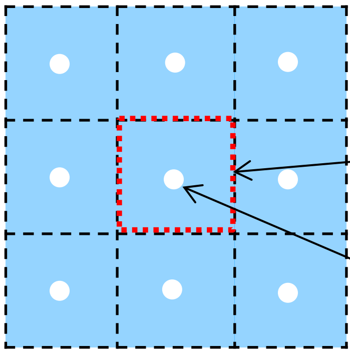

CFD	Method	FEM
Control Volume (CV) Fixed Shape	Volume	Element Deformable Shape
Control Volume Center (CVC) Center of CV	Data Point	Node Vertex of Element

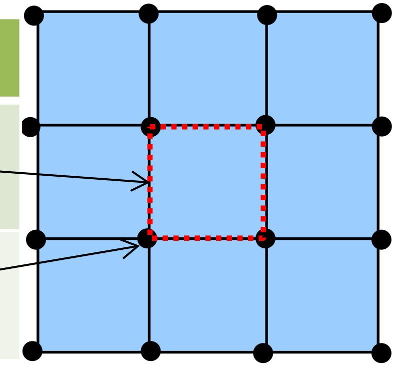

The position of data point between CFD and FEM: different ➔ Proper data implantation scheme needed

- Spatial Interpolation (Binary Search Algorithm)

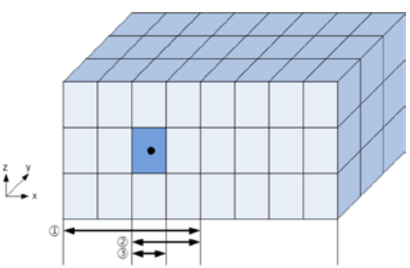

①Compare mid point CVC and target node

②Compare ±¼ point CVC and target node

③Compare ±⅛ point CVC and target node

⋮

➔Interpolation by surrounding 8 CVC

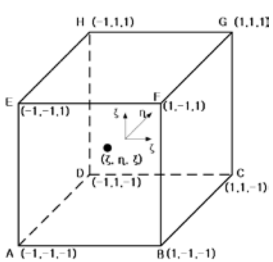

$$
\begin{aligned}
T(\zeta,\eta,\xi) = & \frac{1}{8}(1-\zeta)(1-\eta)(1-\xi)T_A + \frac{1}{8}(1+\zeta)(1-\eta)(1-\xi)T_B \\
& + \frac{1}{8}(1+\zeta)(1+\eta)(1-\xi)T_C + \frac{1}{8}(1-\zeta)(1+\eta)(1-\xi)T_D \\
& + \frac{1}{8}(1-\zeta)(1-\eta)(1+\xi)T_E + \frac{1}{8}(1+\zeta)(1-\eta)(1+\xi)T_F \\
& + \frac{1}{8}(1+\zeta)(1+\eta)(1+\xi)T_G + \frac{1}{8}(1-\zeta)(1+\eta)(1+\xi)T_H
\end{aligned}
$$

- Temporal Interpolation

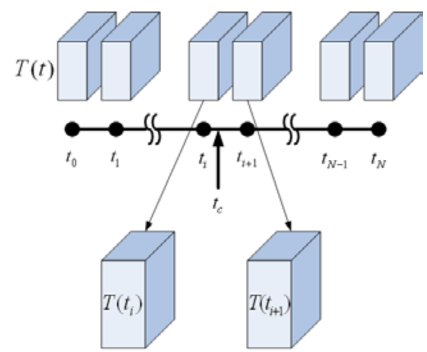

$T(t)$: Array [x,y,z,T] at time t

①CFD data requisition 10Hz

②Set current FEM time step t_c

③Set the one CFD step earlier t_i

④Set the one CFD step later t_{i+1}

➔Interpolation by t_i and t_{i+1}

$$
T(t_c) = \frac{(t_{i+1}-t_c)T(t_i) + (t_c - t_i)T(t_{i+1})}{t_{i+1}-t_i}
$$

CFD-FEM Coupling for Long Temperature History

Temporal Boundary

Temp. history at last time step of CFD analysis

Period 1 (in CFD) → Period 2 (in FEM)

Energy equation

$$\frac{\partial h}{\partial t} + \cancel{V \cdot \nabla h} = \frac{1}{\rho}\nabla \cdot (k\nabla T) + h_s$$

Temperature discontinuity

- Thermal properties
- Surface and volume calculation

Simulation for Period 2 *(10.9~ 3,000s)*

Temperature measured at 4 points

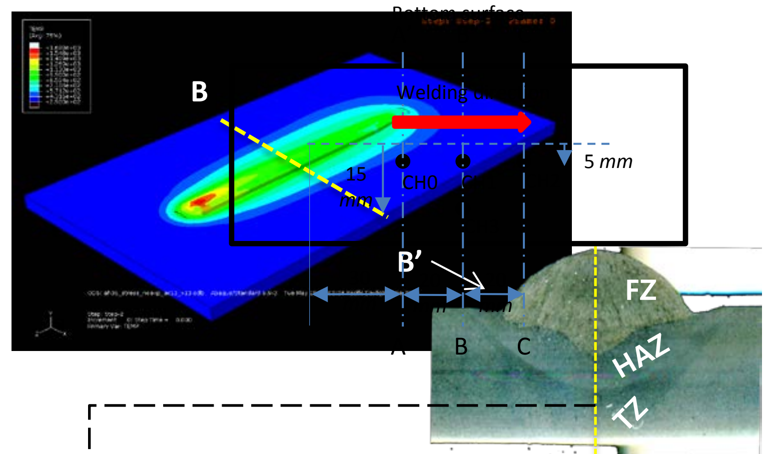

Temporal Boundary Effect (@10.9 s)

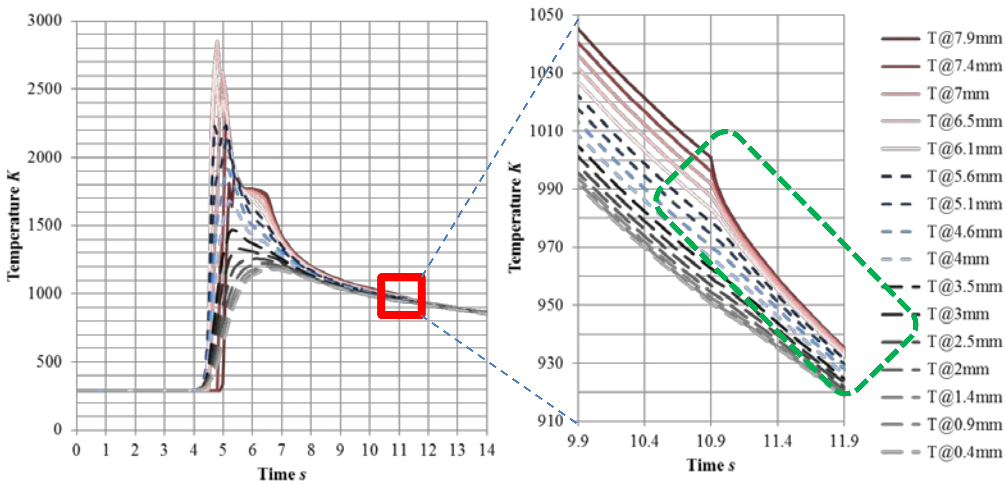

Temperature drop on temporal boundary

FZ >> HAZ >TZ

Bottom Surface Temperature History

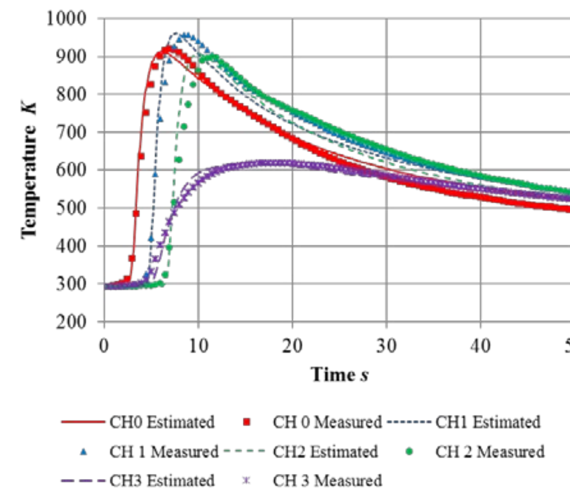

6.8K maximum error between Sim. and Exp.

Thermal-Metallurgical Analysis: Phase Transformation

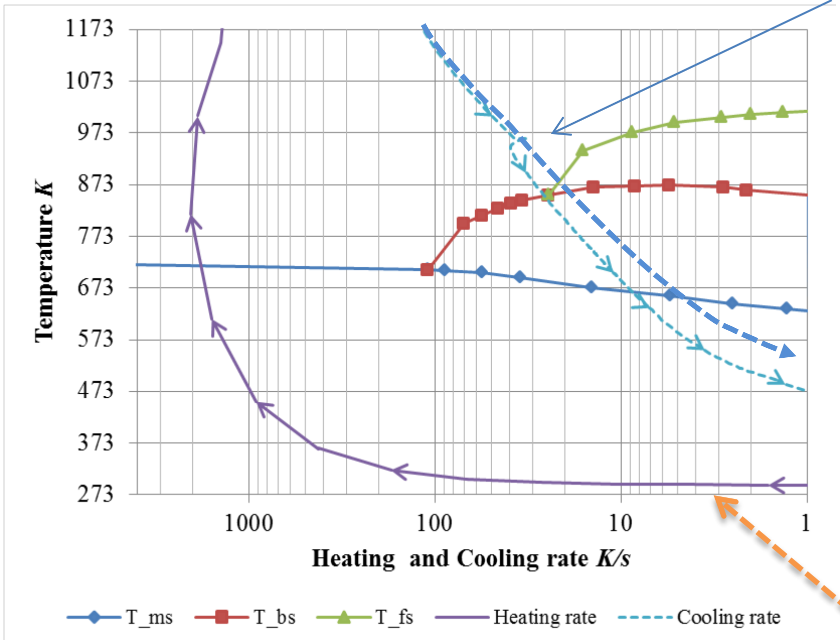

CR fluctuation by **temporal boundary** leads to **overestimated martensite** fraction

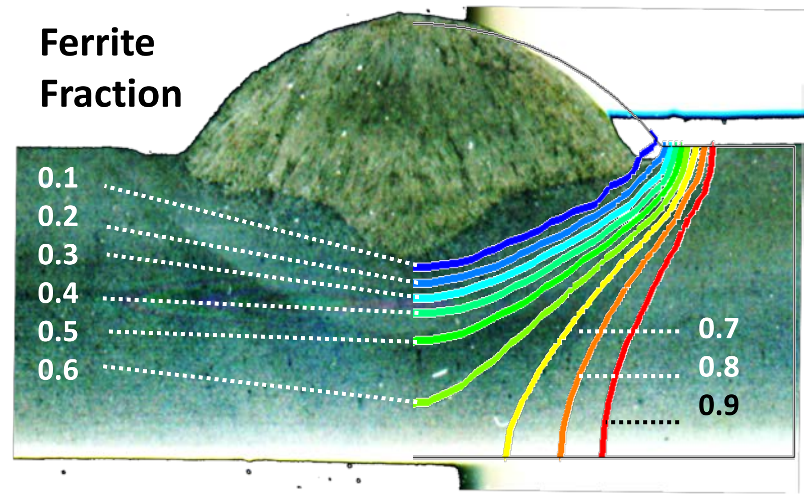

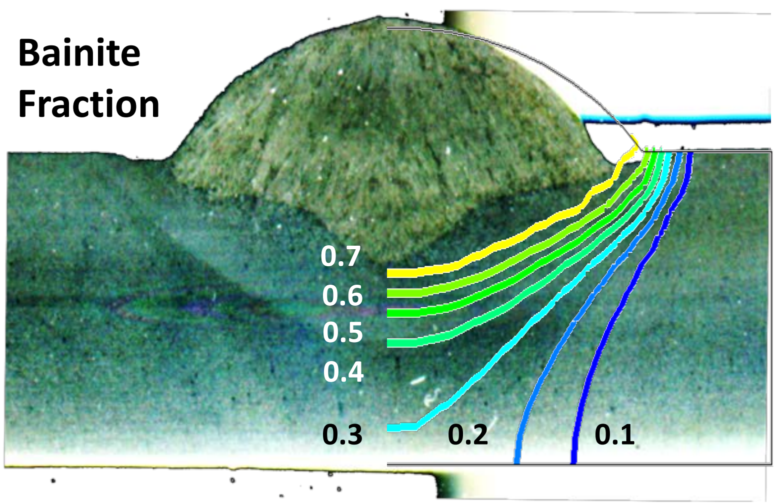

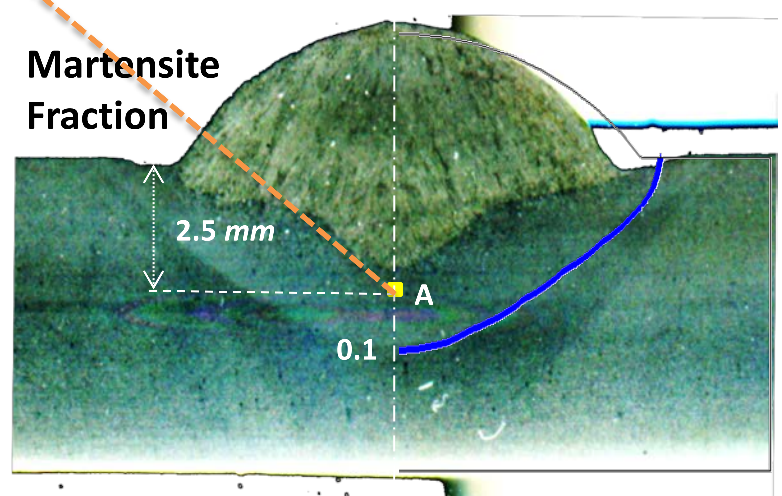

Heating Rate vs. Austenization Temperature

Fe-C Equilibrium Phase Diagram

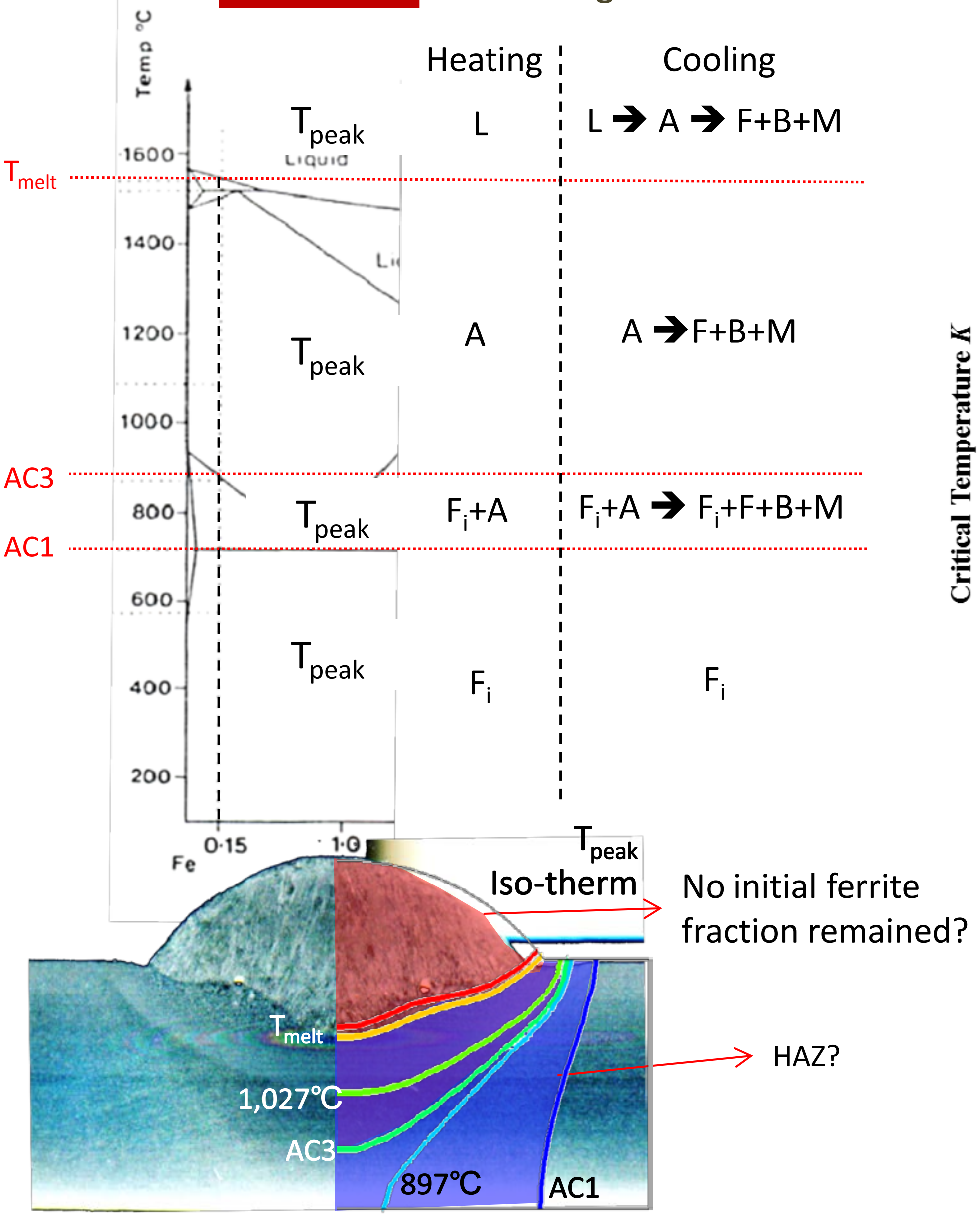

Dilatometric Analysis

….austenite is a solid solution of iron and carbon. The solubility of carbon mainly depends on the "diffusion" process.

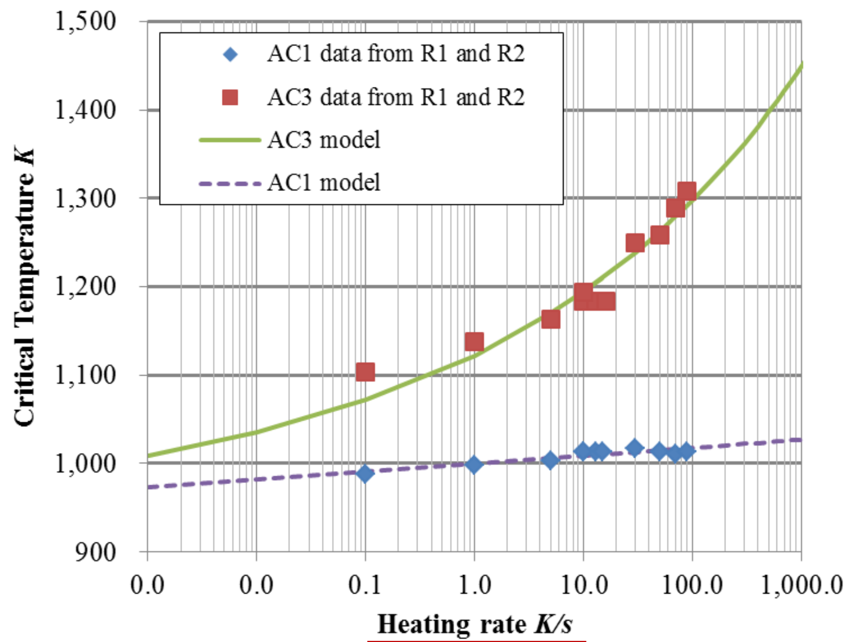

Model of Austenization Temperature

$$total\ austenite\ formation\ time = Q\left(\frac{dT}{dt}\right)^{-g}$$

(Macedo, M Q., et. al (2011))

$$AC1 = Q_1\left(\frac{dT}{dt}\right)^{-g_1+1} + R_1$$

$$AC3 = Q_3\left(\frac{dT}{dt}\right)^{-g_3+1} + AC1$$

Phase Prediction vs. AC1 and AC3

Constant AC1 and AC3

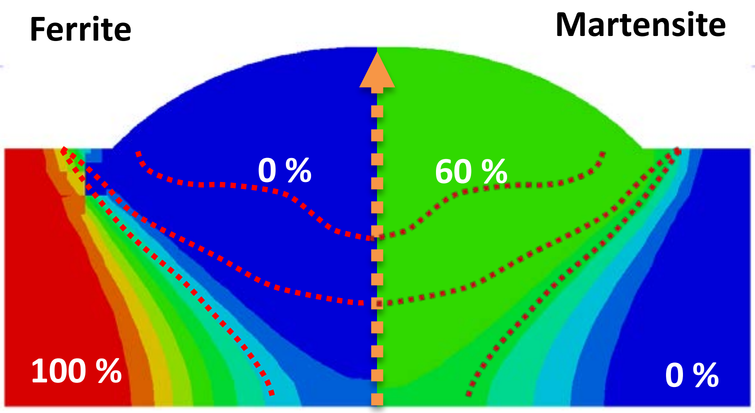

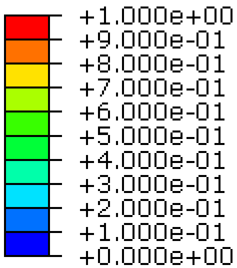

Variable AC1 and AC3

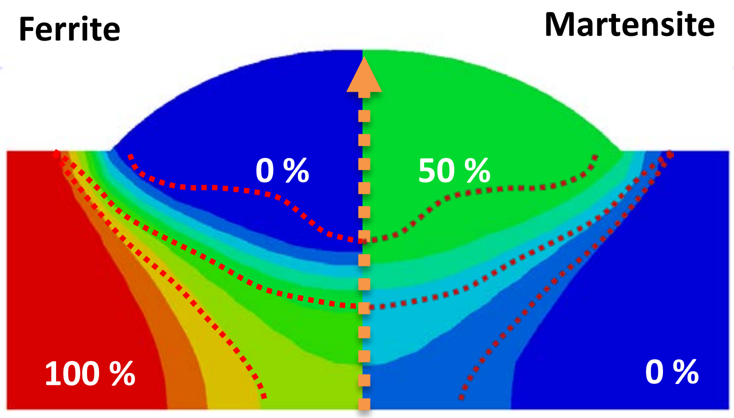

Prediction of phase fraction & hardness in vertical direction

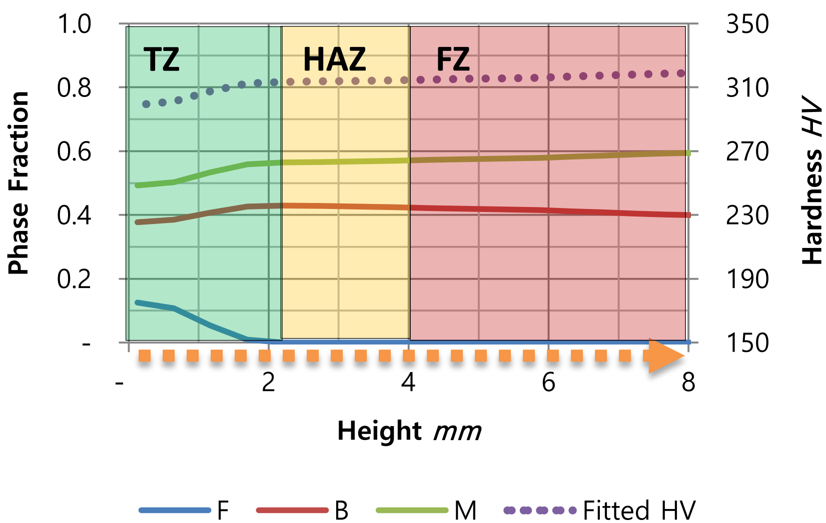

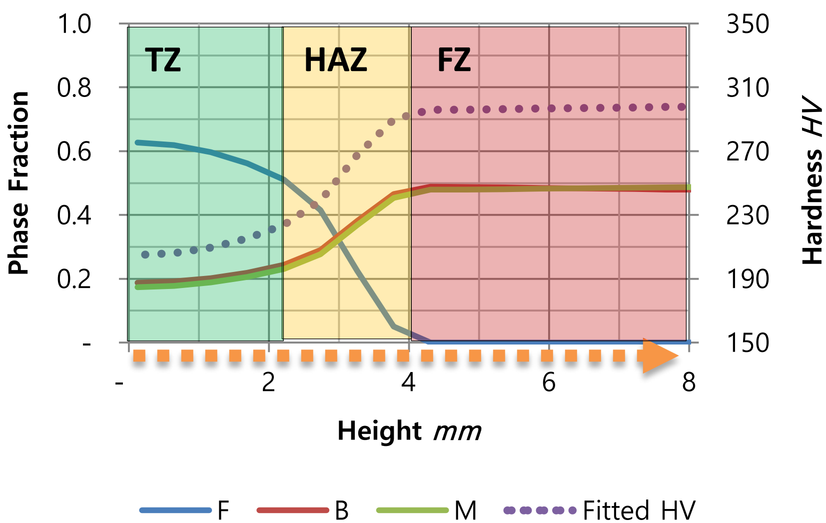

Cooling Rate: Conventional vs. Instant

Conventional Cooling Rate

The welding constant ($\Delta t_{8\text{-}5}$) based

$$w\ CR = -\frac{T_{reference} - T}{t_{@reference\ T} - t}$$

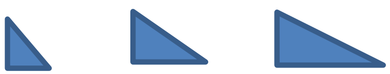

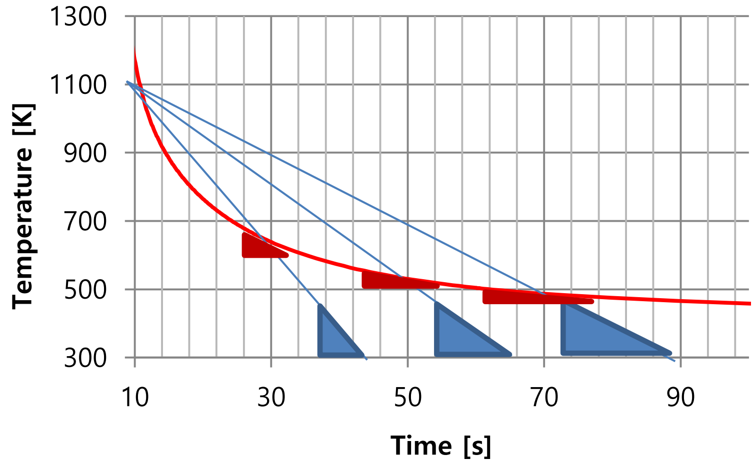

Instant Cooling Rate

Time & temperature delta in step

$$Inst.CR = -\frac{T_{step\ start} - T_{step\ end}}{t_{step\ start} - t_{step\ end}}$$

w CR > Inst. CR ➔ w CR leads to a higher martensite fraction

Cooling Rates in Temp. History

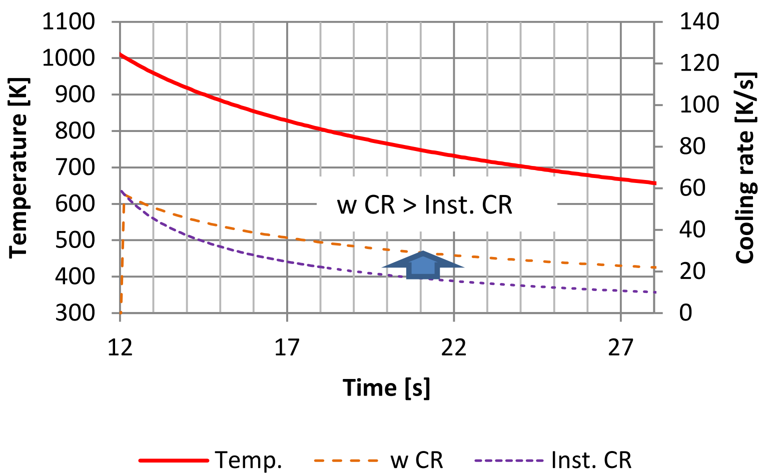

Cooling Rates in CCT

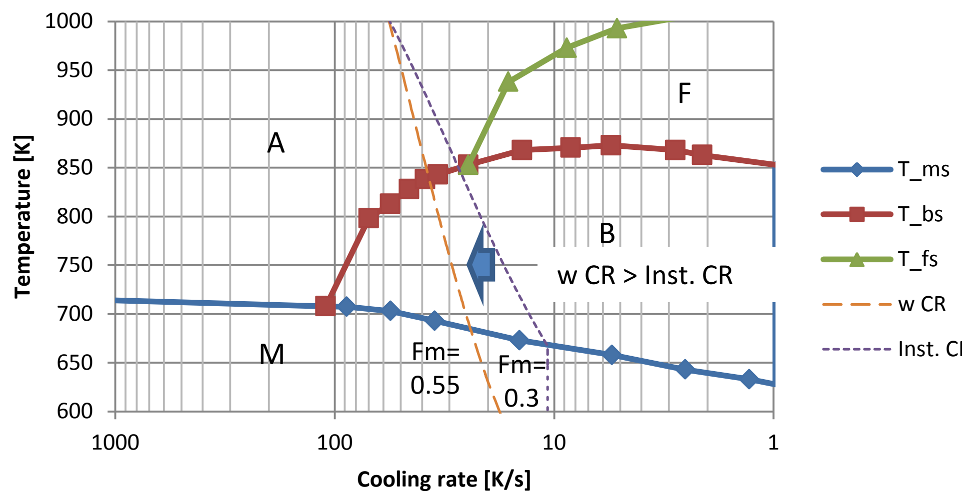

Phase Prediction vs. Cooling Rate

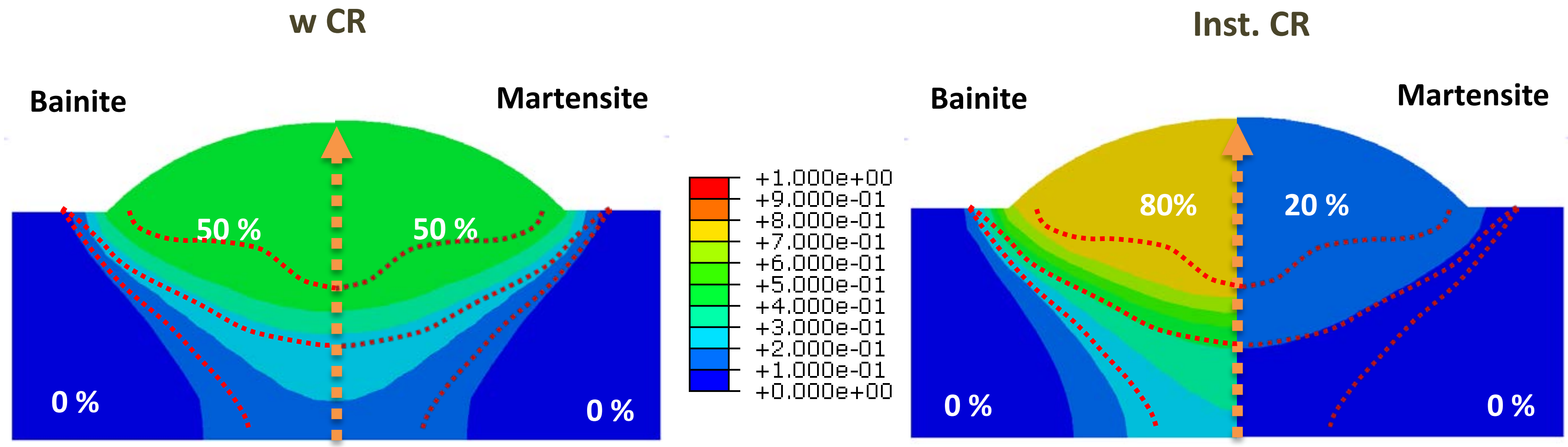

Prediction of phase fraction & hardness in vertical direction

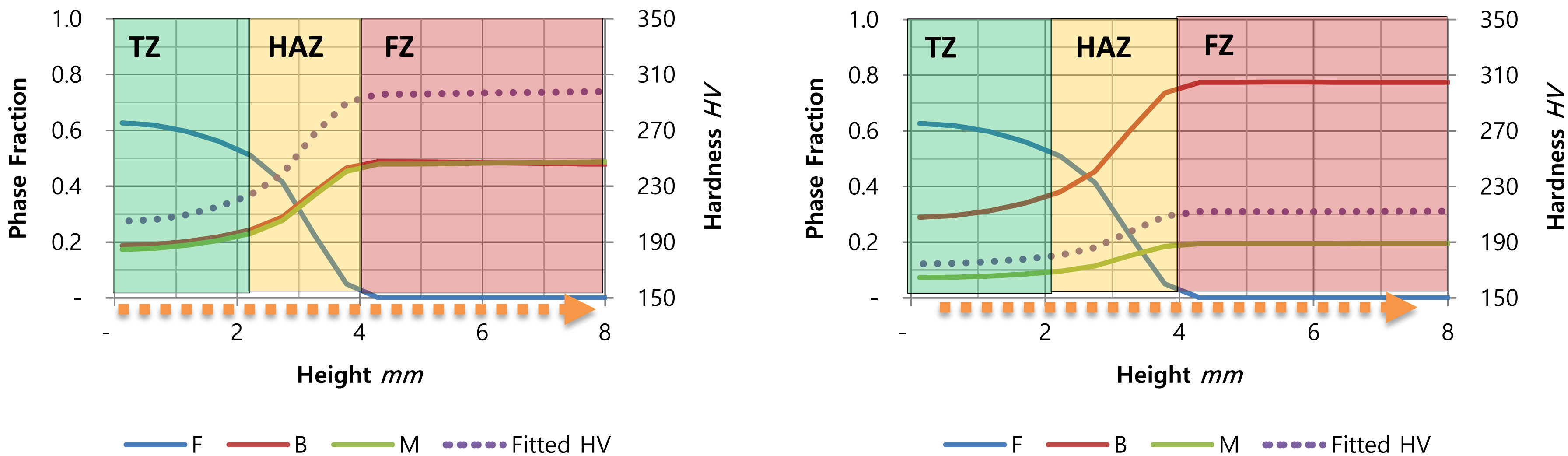

Validation: Prediction and Measurement of Bainite+Martensite

Micro etching condition

Vilella's etchant (1 g Picric acid + 5 ml HCl + 100 ml Ethanol)

(ASTM E407-99, Scott(1991), Beraha(1992), Lee(2014)...)

Area fraction measurement

Window : 200 um x 200 um

Brightness threshold by Initial fraction (F : P = 0.3 : 0.7)

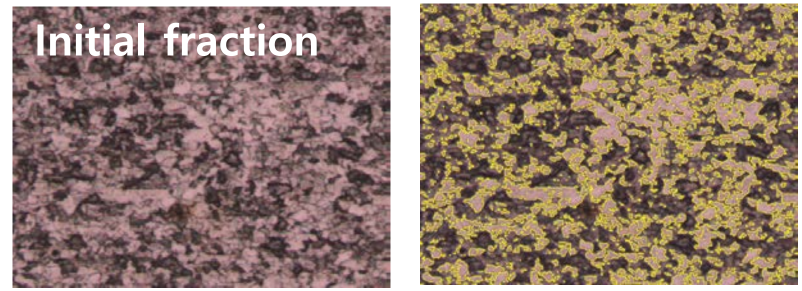

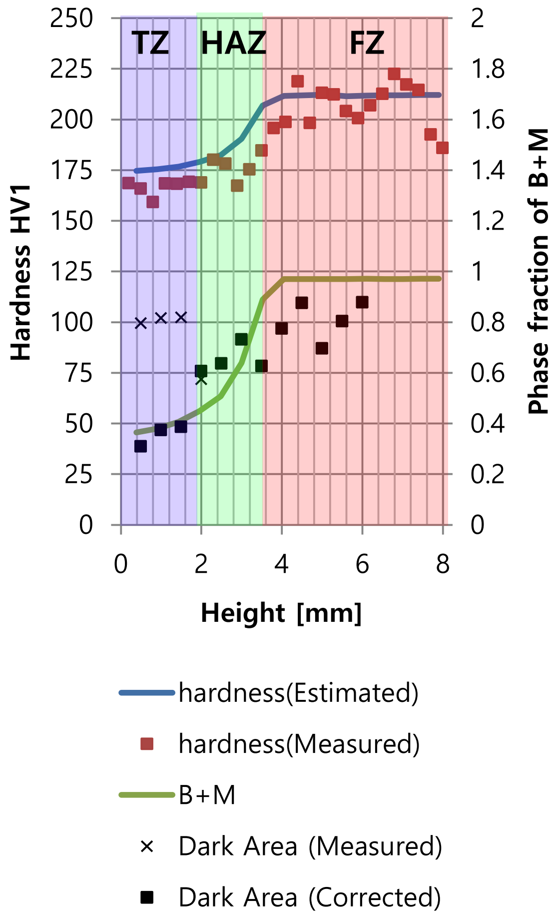

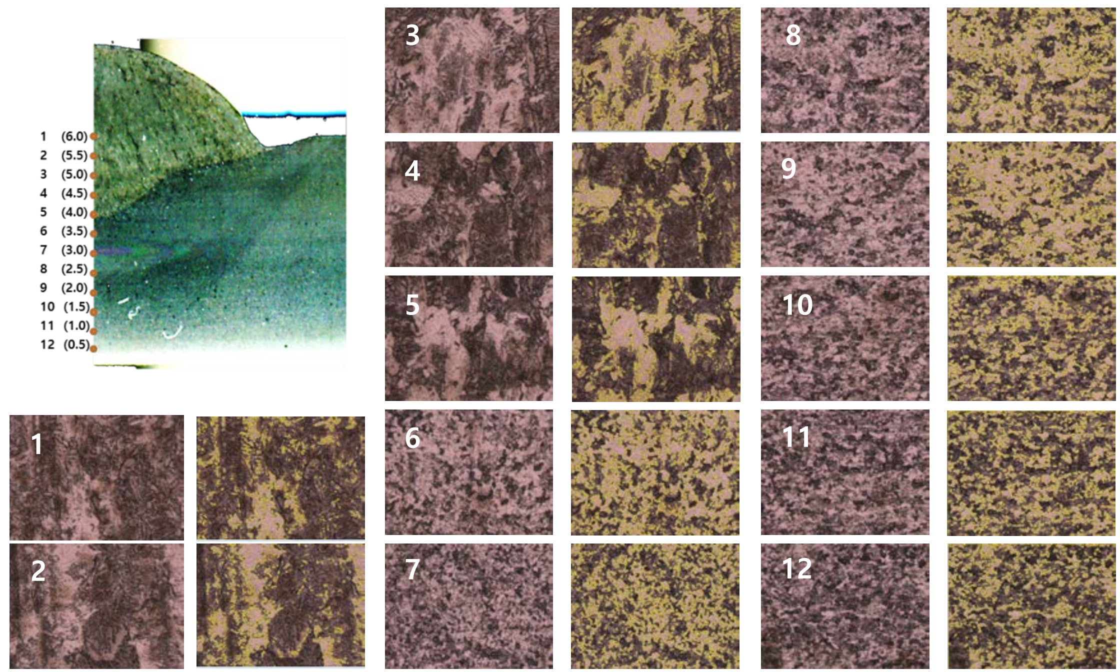

*correction equation for TZ region

$$F_i + P_i = 1$$

$$F_i \times (1 - F_{BM}) + F_i \times F_{BM} + P_i \times (1 - F_{BM}) + P_i \times F_{BM} = 1$$

$$F_i \times F_{BM} + P_i \times (1 - F_{BM}) + P_i \times F_{BM} = B$$

$$F_{BM} = \frac{B - P_i}{1 - P_i}$$

F_i=Initial ferrite fraction

P_i=Initial pearlite fraction

F_{BM}=Sum of bainite and martensite fraction

B=Dark area fraction

Phase Distribution vs. Micro Hardness

CCT Diagram

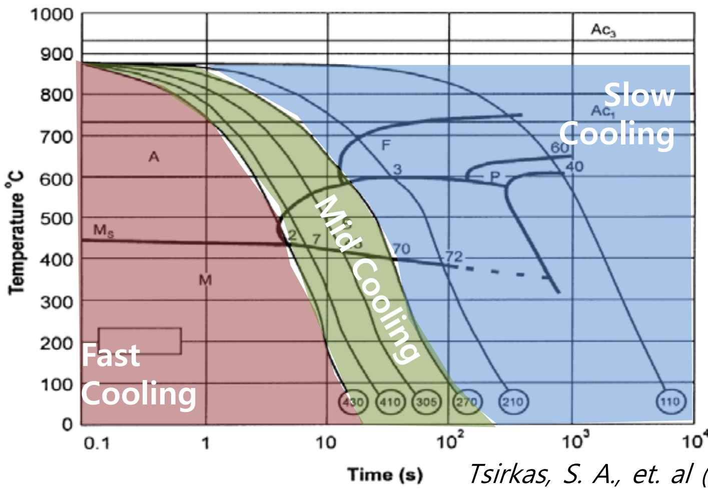

Tsirkas, S. A., et. al (2003)..

$$Hardness = \sum_{i=0}^{4}(\alpha_i F_m{}^i) + \beta$$

Fitted Vickers Hardness

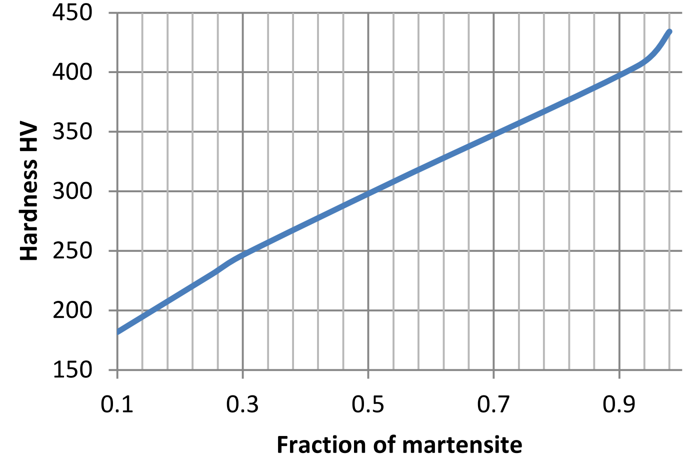

Phase Starting / Finishing Temperature

Fast Cooling $T_{xs} = \sum_{i=0}^{l}(A_i CR^i) + B$

Mid Cooling $T_{xs} = \sum_{i=0}^{m}(C_i CR^i) + D$

Slow Cooling $T_{xs} = \sum_{i=0}^{n}(E_i CR^i) + F$

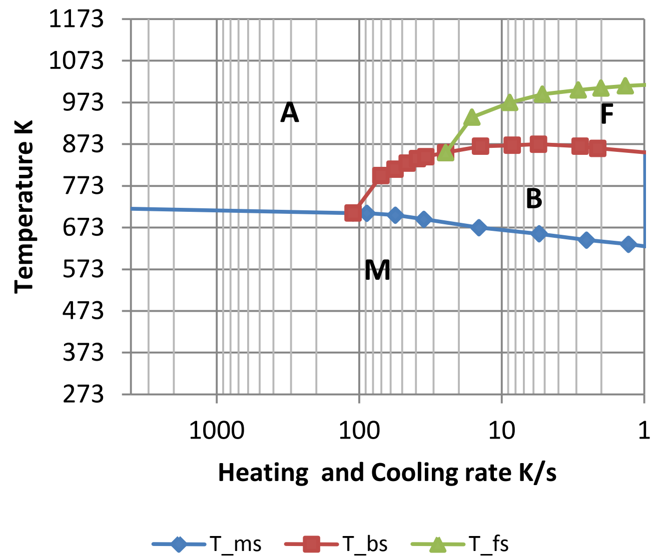

Indirect validation of phase distribution via hardness distribution

$$F_{sum} = 1 = F_f + F_a + F_b + F_m + F_l$$

Validation: Horizontal Hardness Distribution

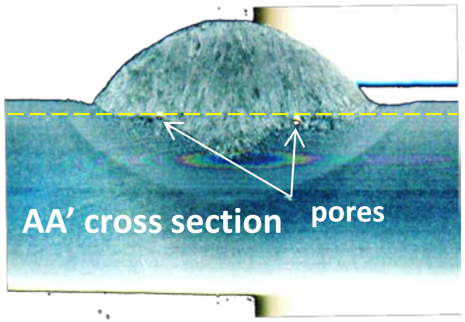

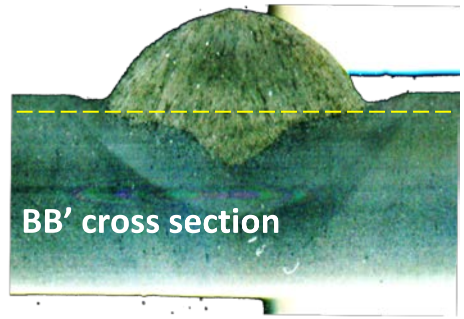

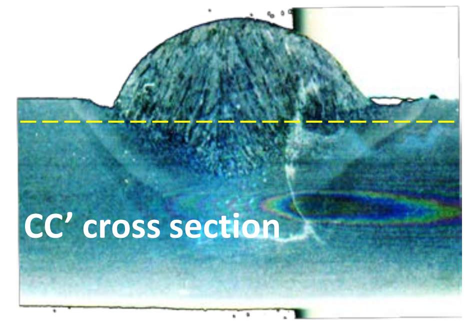

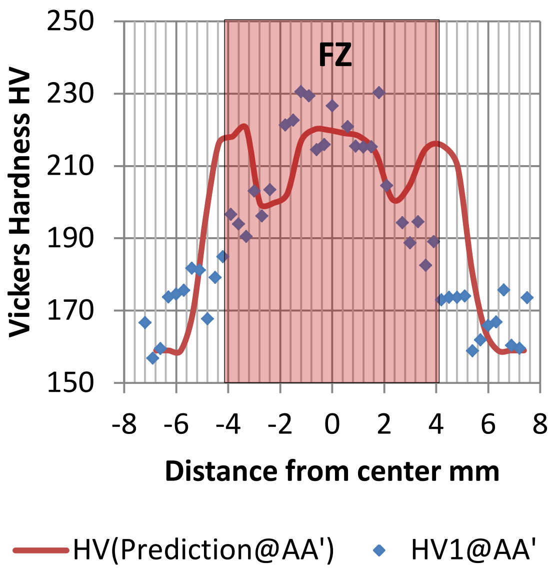

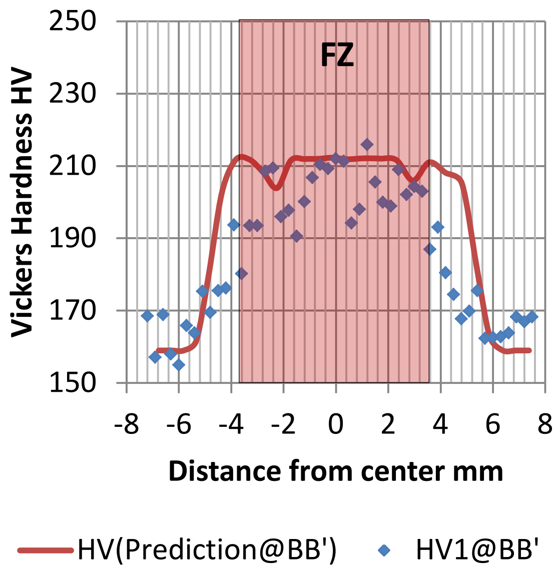

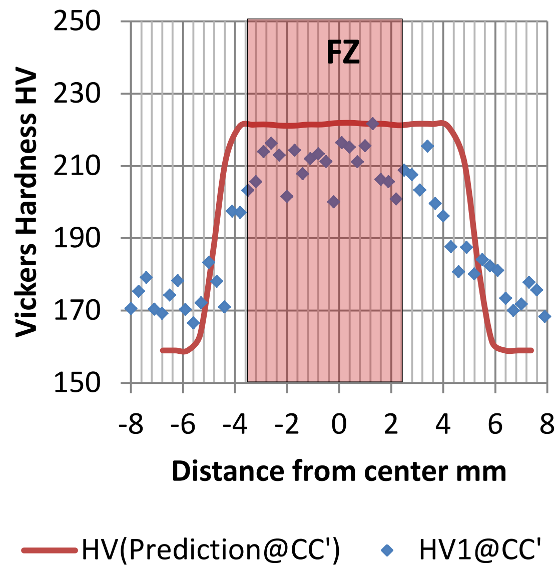

The hardness trend of near to the pore (ASTM standard violated) was fluctuated

The **hardness distribution** was **slightly overestimated** by **temporal boundary effect**

Hardness **steep decrease location** was **expanded out** by **FZ width estimation error**

Thermal-Metallurgical-Mechanical Analysis of Weldment

Dilatometric curves

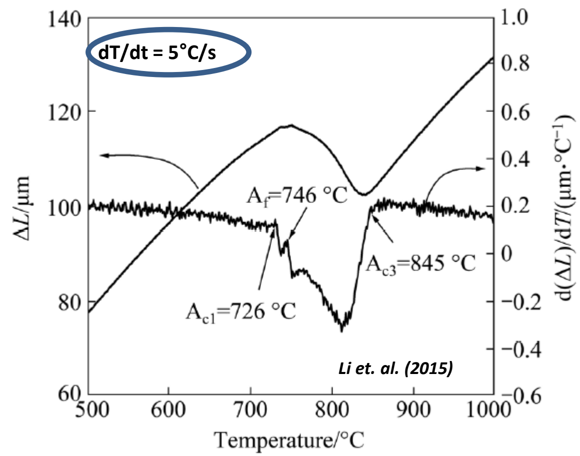

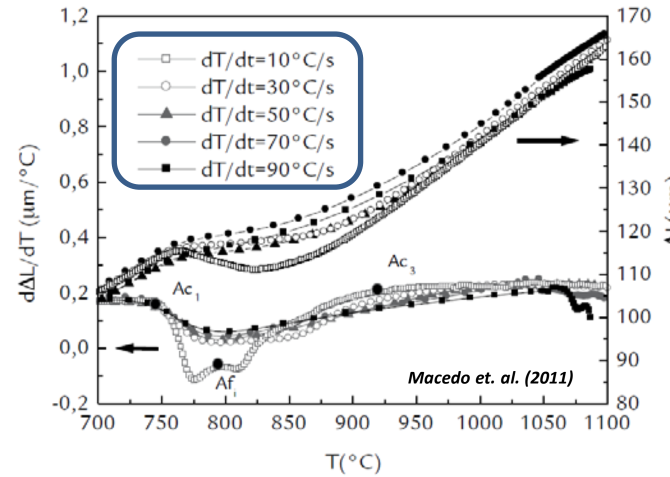

Thermal strain with phase transformation-induced volumetric strain

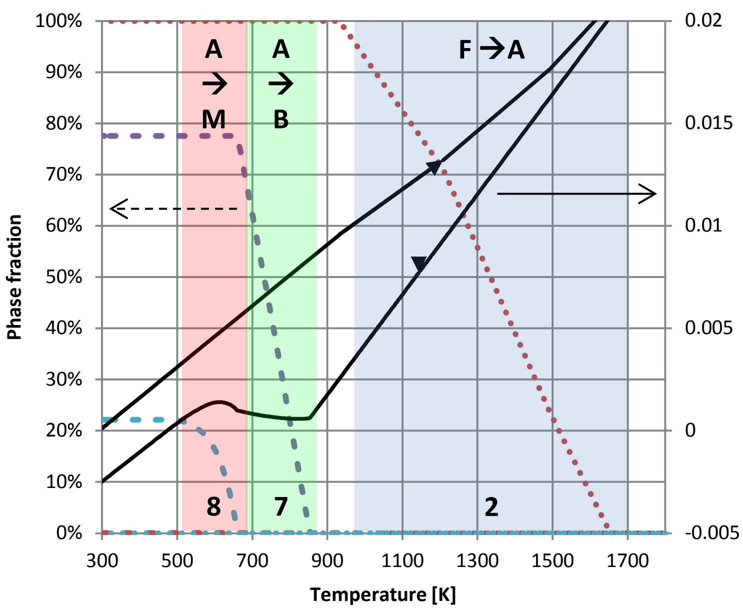

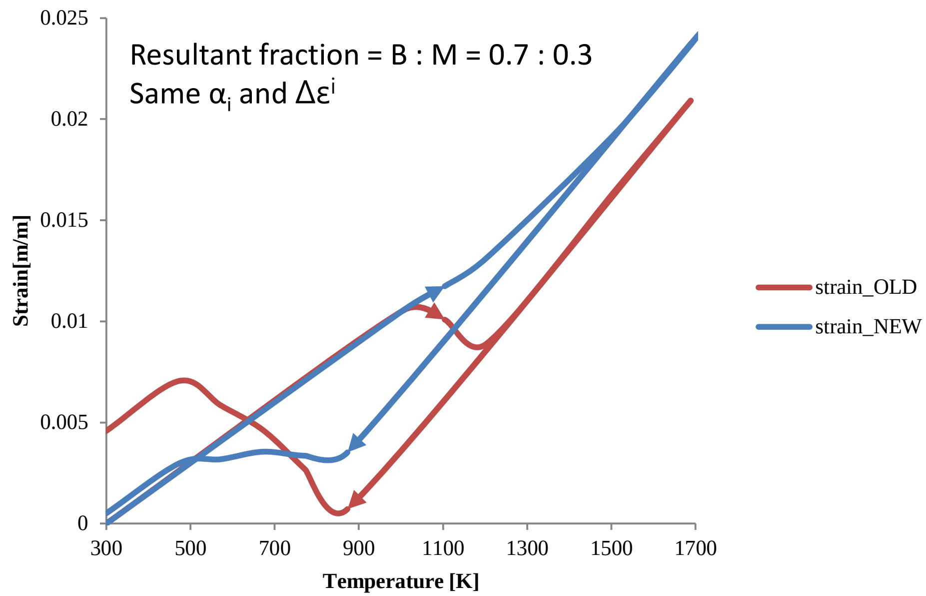

Phase-dependent Material Properties

Phase fraction of weldment

Phase (source)	Yield strength @ Tamb [MPa]
Initial (Certificate AH36)	**430**
Ferrite (JMATpro)	**146**
Austenite (JMATpro)	155
Pearlite / Bainite (JMATpro)	563
Martensite (JMATpro)	1153

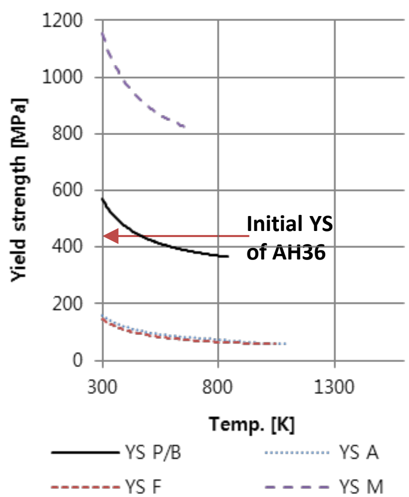

Initial 100 % ferrite fraction condition is invalid
No DP steel ➔ no martensite

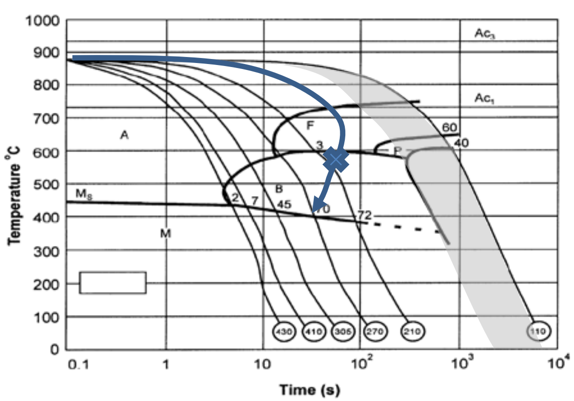

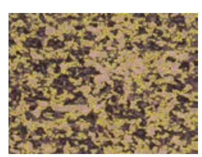

$$F_F + F_P = 1$$

$$YS_{Initial} = YS_{F@Tamb} \cdot F_F + YS_{P@Tamb} \cdot F_P$$

$$YS_{Initial}(T) = 0.3 \cdot YS_F(T) + 0.7 \cdot YS_P(T)$$

Young's modulus, Poisson's ratio, Yield strength

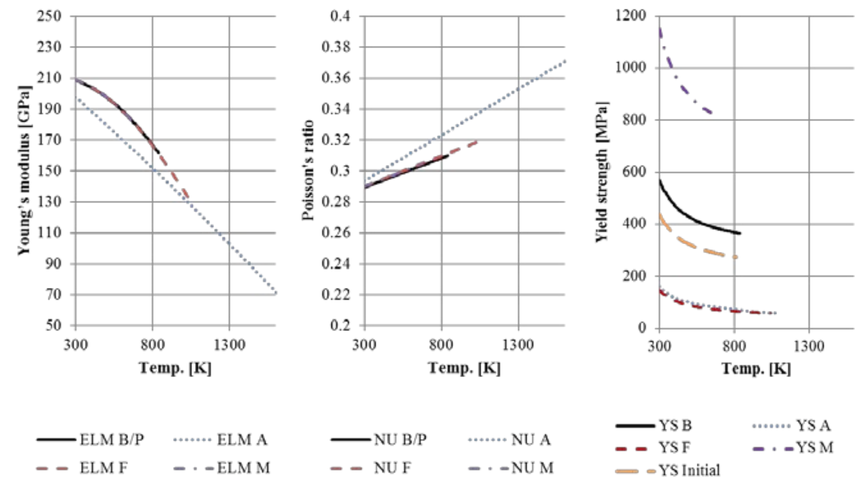

$$ELM = \sum F_i E_i \qquad YS = \sum F_i YS_i$$

Heating process - 100 % austenization
Cooling process - 80 % bainite + 20 % martensite

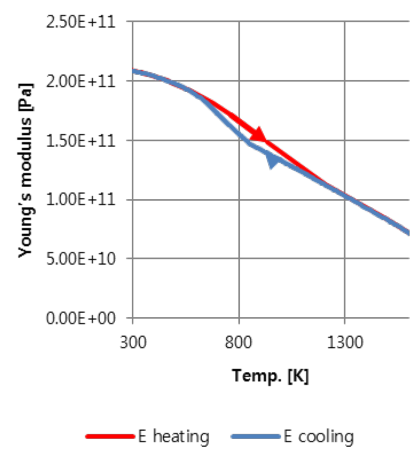

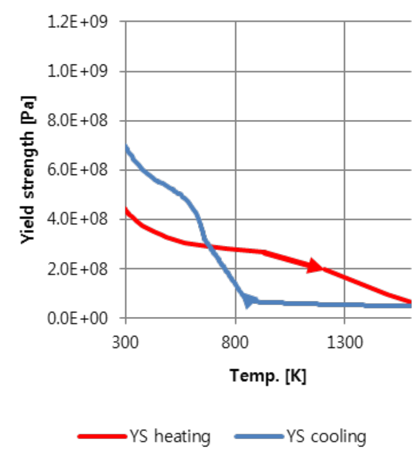

Liquid State Treatment and its Effect

Liquid state treatment

Liquid state : Temp. > ZST

Zero strength ➔ Young's Modulus (ELM) & YS becomes zero

➔ Zero stress / infinite strain ➔ Diverging condition

$$\sigma_{ij} = 3\frac{E}{3(1-2\nu)}\left(\frac{1}{3}\varepsilon_{kk}\delta_{ij}\right) + 2\frac{E}{2(1+\nu)}\left(\varepsilon_{ij} - \frac{1}{3}\varepsilon_{kk}\delta_{ij}\right)$$

$$\varepsilon_{ij} = \frac{1}{E}\left(\sigma_{ij} - \nu[\sigma_{kk}\delta_{ij} - \sigma_{ij}]\right)$$

****ZST : Zero Strength Temperature near to melting temperature***

Author	Cut-off Temperature (′C)	Remedy	Solver
Ueda, 1971	600	Temp. restraint	House
Fujita, 1972	500	Temp. restraint	↑
Hepworth, 1980	800	Thermal dilatation restraint	↑
Ueda, 1985	700	E=zero, YS=zero	↑
Free, 1989	900	E=const. no yielding	↑
Tekriwal, 1991	600~Melting Temp.	No residual stress calculation	ABAQUS

Model change scheme (element activation & deactivation, EAD)

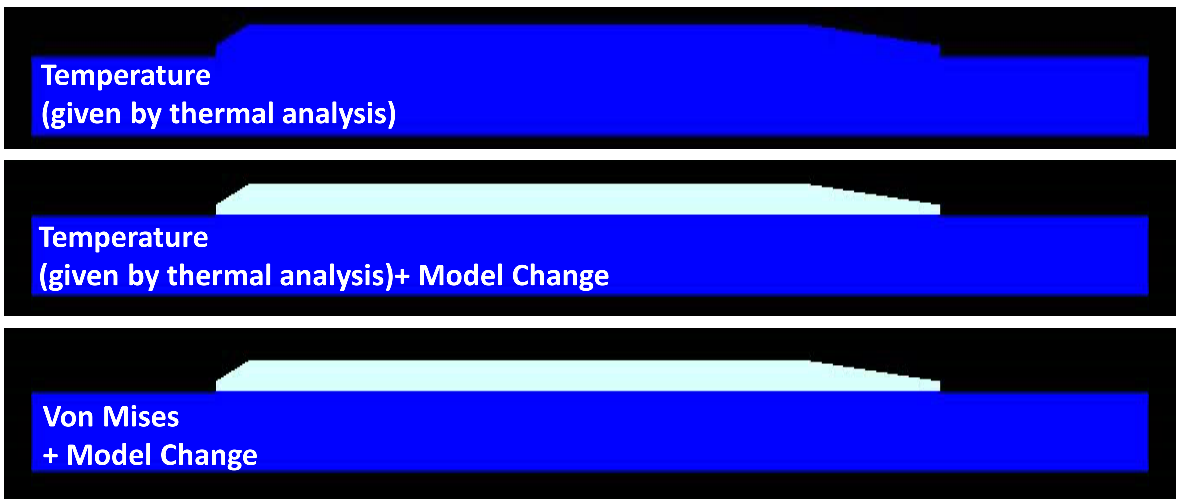

Bead set
Deact. → Act. → Calc.
Ceasing strain propagation
to coming bead

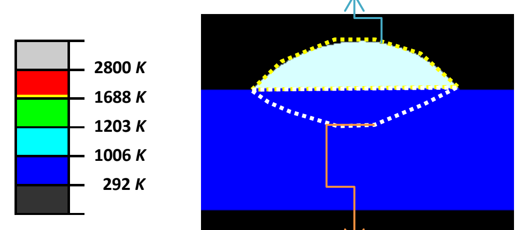

FZ set
Calc. ➔ Deact. ➔ Act. ➔ Calc.
Resetting mechanical history
on liquid state

Deactivation losing all history of
- **Temperature**
- **Phase fraction**
- **Strains (e, p, th)**
- **Stress and displacement**

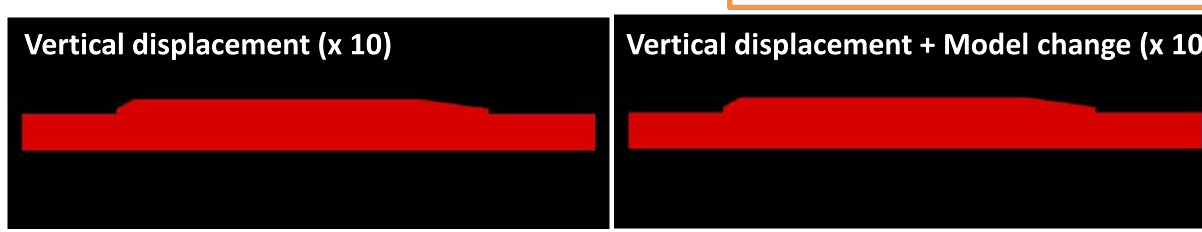

Procedure of Thermal-Metallurgical-Mechanical Analysis

Volumetric Expansion Behavior

Phase fraction Calc.
[UEXPAN]

Heating phase
(Ferrite ➔ Austenite ➔Liquid)

Heating rate ➔ AC1 & AC3

Cooling phase
(liquid ➔ Austenite)

Cooling rate ➔ phase transformation starting, finishing temperature and Max. fraction

Fast cooling
(Austenite ➔ Martensite)

Mid cooling
(Austenite ➔ Ferrite ➔ Martensite)

Slow cooling
(Austenite ➔ Ferrite ➔ Bainite ➔ Martensite)

Phase fraction, F
(SDVINI)

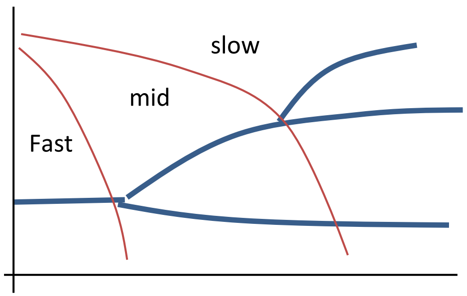

$\Delta\varepsilon^{TH}$=f(F, CTE)

$\Delta\varepsilon^{\Delta V}$ =f(F, ΔF, TRIV strain)

$\Delta\varepsilon^{TRIP}$=f(F, ΔF, deviatoric stress, TRIP coefficient)

Material Mechanical Behavior

Deformation Calc.
[UMAT]

Jacobian Matrix
(Δσ/Δε, stiffness matrix)
f(ELM, NU)

Stress predictor
(stress for no plastic)

Effective stress
(von Mises)

Deviatoric stress

Yield condition
f(YS, Effective stress)

Plastic flow

Equivalent plastic strain rate
f(hardening coefficient)

Shift stress

Jacobian Matrix update
(Δσ/Δε, stiffness matrix)

Residual Stress and Displacement: Prediction and Measurement

Transversal stress

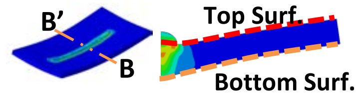

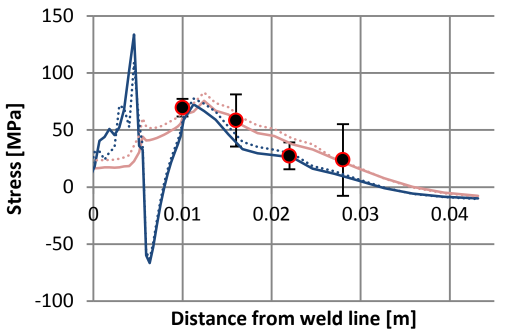

Longitudinal stress

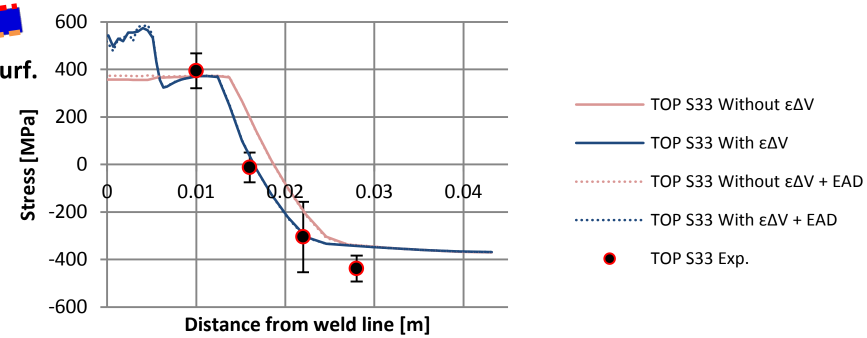

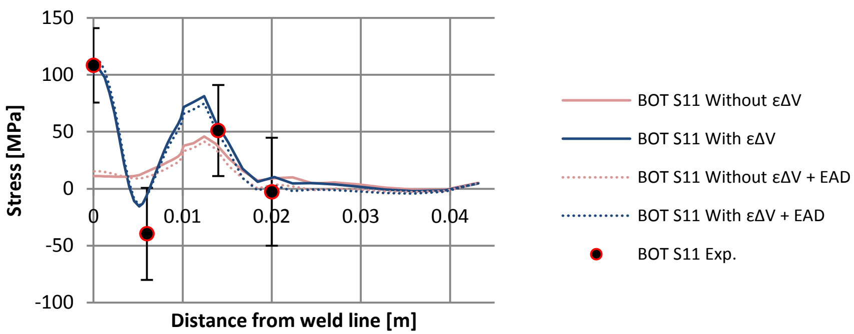

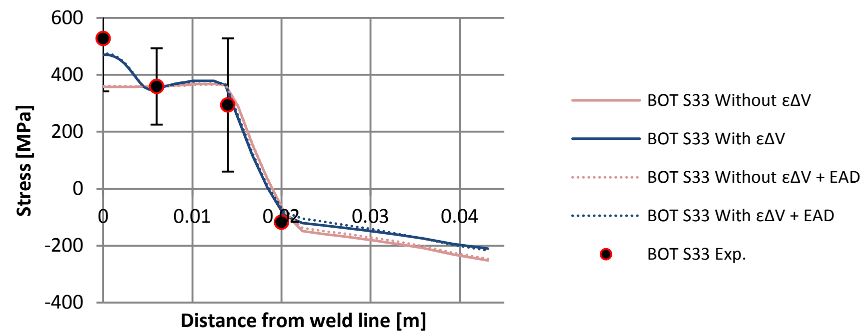

Displacement on bottom surface

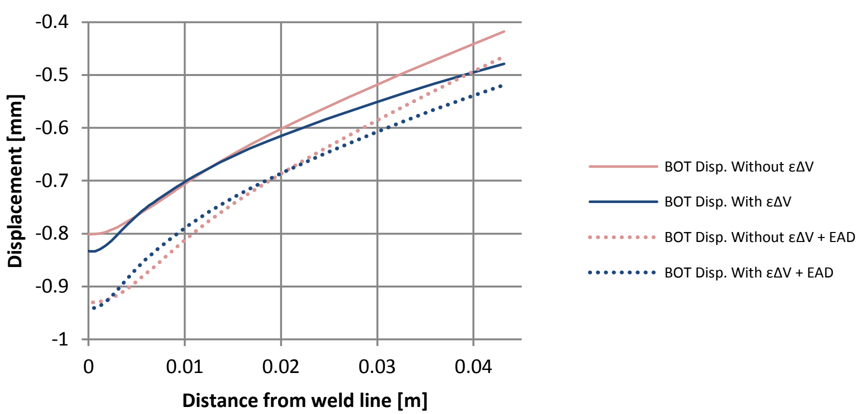

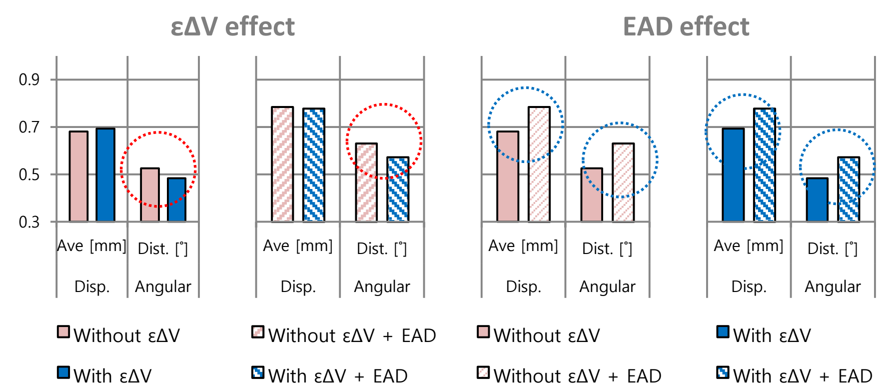

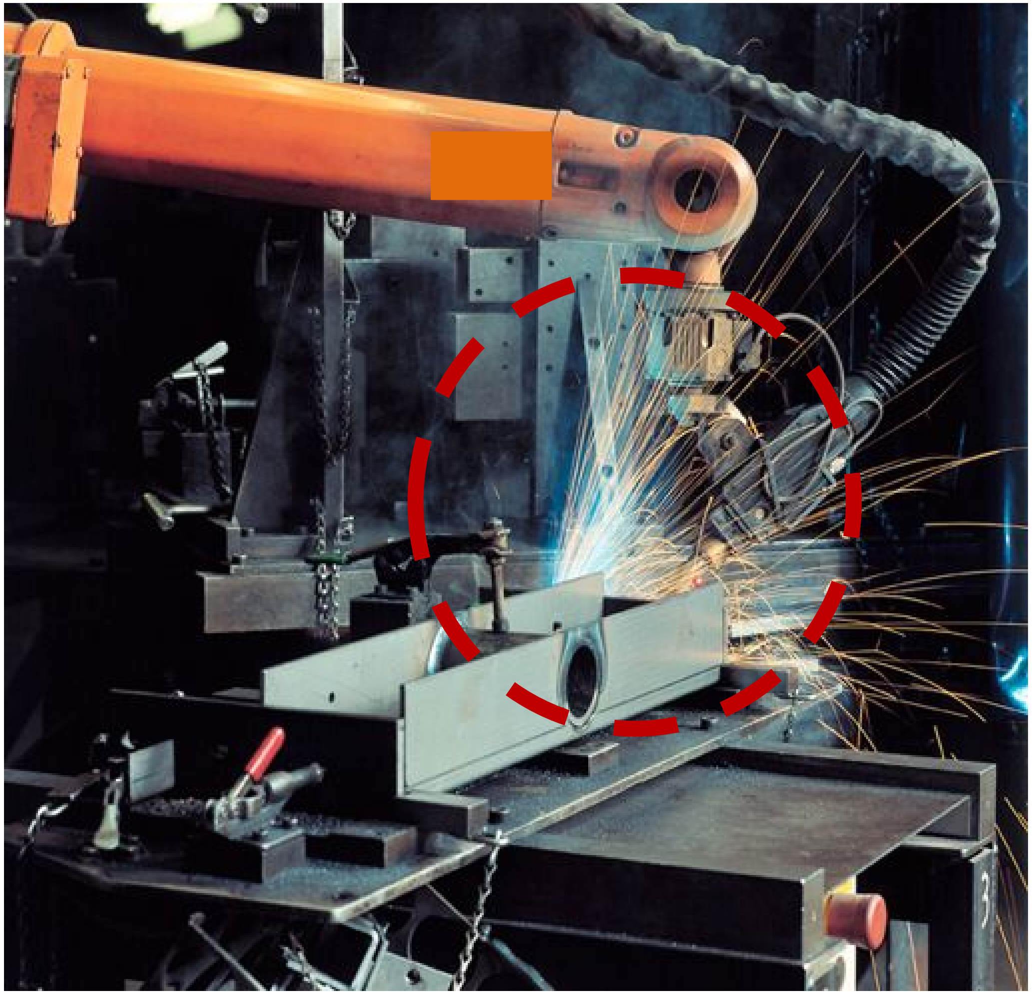

Arc Welding Models

- Arc Heat Source Model: Gaussian Axisymmetric ?

$$\eta_A q_A(x,y) = \eta_A \frac{VI}{2\pi r_A^2}\exp\left(-\frac{x^2+y^2}{2r_A^2}\right)$$

η_A: Heat input efficiency(0.54),
V: Voltage, I: Arc current,
r_A: Heat distribution parameter(2.4mm)

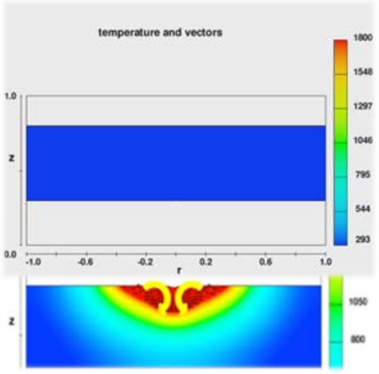

- Arc Pressure Model Axisymmetric ?

$$p_A \cong \frac{\mu_0 I^2}{4\pi^2 {r_A}^2}\exp\left(-\frac{r^2}{2{r_A}^2}\right)$$

μ_0: vacuum permeability

Z. Cao, Z. Yang and X. L. Chen: *Weld. J.*, 2004, **83**, 169s-176s

- Electromagnetic Force Model Axisymmetric ?

$$J_z = \frac{I}{2\pi}\int_0^\infty \lambda J_0(\lambda r)\exp(-\lambda^2 {r_A}^2/12)\frac{\sinh[\lambda(c-z)]}{\sinh(\lambda c)}d\lambda$$

$$J_r = \frac{I}{2\pi}\int_0^\infty \lambda J_1(\lambda r)\exp(-\lambda^2 {r_A}^2/12)\frac{\cosh[\lambda(c-z)]}{\sinh(\lambda c)}d\lambda$$

$$B_\theta = \frac{\mu_m I}{2\pi}\int_0^\infty J_1(\lambda r)\exp(-\lambda^2 {r_A}^2/12)\frac{\sinh[\lambda(c-z)]}{\sinh(\lambda c)}d\lambda$$

S. Kou and D. K. Sun: Metall. Trans. A, 1985, **16A**, 203

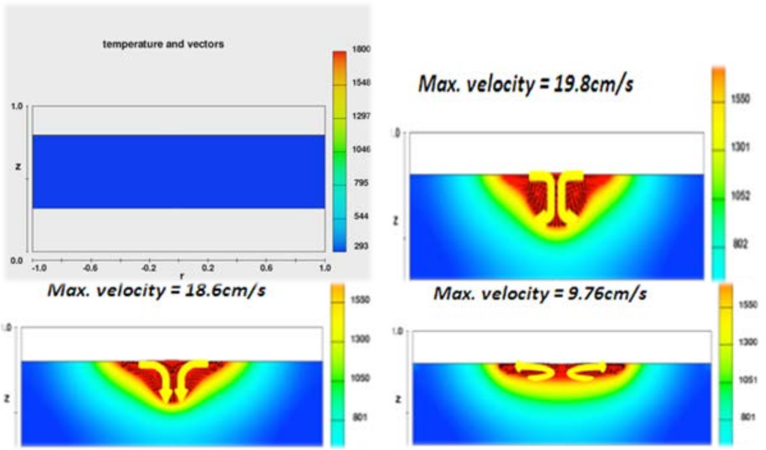

- Surface Tension Model

$$\mu\frac{\partial v_t}{\partial n} = -\frac{\partial \gamma}{\partial T}\frac{\partial T}{\partial r}$$

μ: dynamic viscosity, v_t : tangential velocity, n: normal to the free surface, r: tangential direction

- Buoyancy Model

$$F_b = \rho g \beta (T - T_0)$$

ρ: density, g: gravity, β: thermal expansion rate, T: temperature, T_0: reference temperature

- Drag Force Model

$$\frac{\tau}{\rho_p u_0^2}\mathrm{Re}_0^{1/2}\left(\frac{H}{D}\right)^2 = g_2\left(\frac{r}{H}\right)$$

τ: shear stress, ρ_p: density, u_0: initial plasma velocity, Re_0: Reynolds number, H: nozzle height, D: nozzle diameter, r: radius from the center, g_2: universal function

D. J. Phares, G. T. Smedley and R. C. Flagan: *J. Fluid Mech.*, 2000, **418**, 351-375

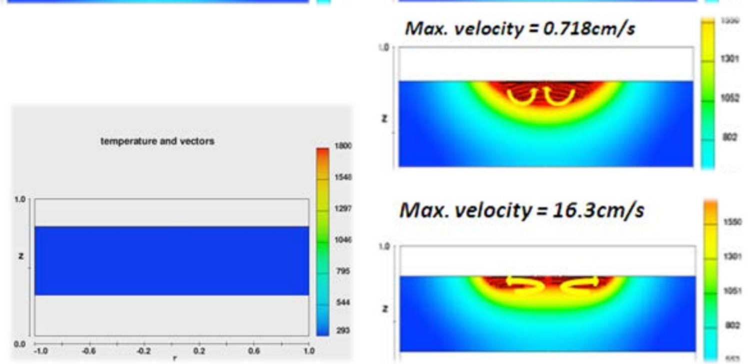

(Hypothetical) Heat Source Model for Arc Welding

: Conductive Heat Transfer Analysis

GA.SHS: Gaussian Axisymmetric Surface Heat Source
($\sigma_x = \sigma_y$)

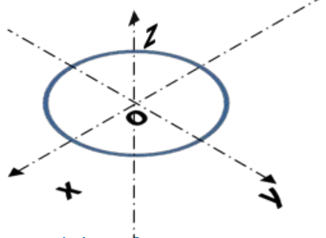

GE.SHS: Gaussian Ellipsoidal Surface Heat Source
($\sigma_x \neq \sigma_y$, $\sigma_{xF} = \sigma_{xR}$)

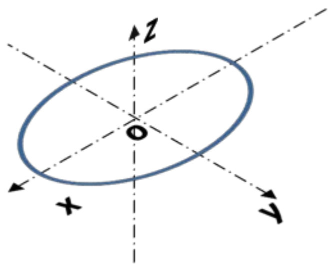

GDE.SHS: Gaussian Double Ellipsoidal Surface Heat Source
($\sigma_x \neq \sigma_y$, $\sigma_{xF} \neq \sigma_{xR}$)

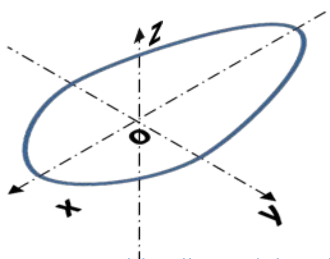

DGDE.SHS: Dual Gaussian Double Ellipsoidal Surface Heat Source

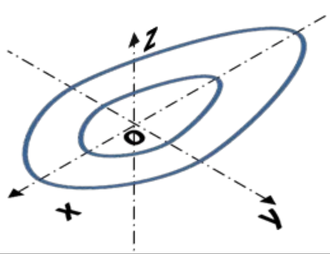

GDE.VHS: Gaussian Double Ellipsoidal Volumetric Heat Source

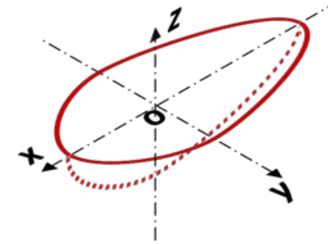

DGDE.VHS: Dual Gaussian Double Ellipsoidal Volumetric Heat Source

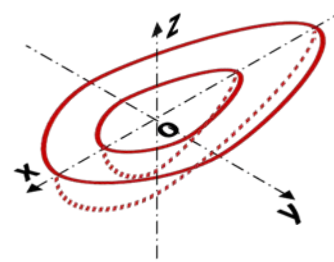

GDE.SHS + **GDE.VHS**: Gaussian Double Ellipsoidal Surface Heat Source +
Gaussian Double Ellipsoidal Volumetric Heat Source

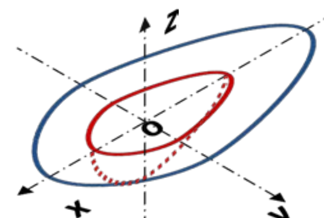

GDE.SHS + **C.VHS**: Gaussian Double Ellipsoidal Surface Heat Source +
Cylindrical Volumetric Heat Source

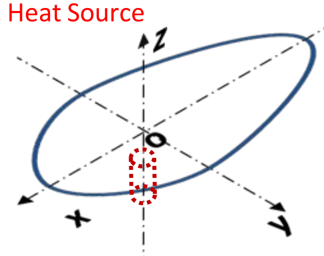

Theoretical-Experimental Method for Arc Models

Energy transfer from arc plasma root to material

$$Q_{cathode} = Q_{cond} + Q_{conv} + Q_{rad}$$

$$Q_{cathode} = \frac{k_{eff}(T_{cb} - T_{ca})}{\delta} + \frac{0.515}{\mathrm{Pr}_{ca}}\left(\frac{\mu_{cb}\rho_{cb}}{\mu_{ca}\rho_{ca}}\right)^{0.11}\left(\mu_{ca}\rho_{ca}\frac{u_{cb}}{r}\right)^{0.5}\bar{C}_p(T_{cb} - T_{ca})$$

$$Q_{cathode} \approx J_a(2.76 + \varphi_a) + k_g\frac{T_{cb} - T_{ca}}{\delta}$$

Current-density vs. Irradiance of arc plasma root (ε)

$$\varepsilon = C_2 J_a \rightarrow J_a = C_3\varepsilon$$

Temperature vs. Irradiance of arc plasma (ε)

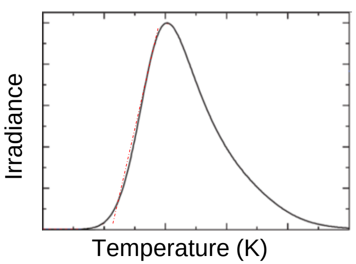

Fowler-Milne method

If 10000K< Temperature < 15000K
➔ Temperature (K) ∝ Irradiance(ε)

If 15000K < Temperature
➔ It will follow Fowler-Milner method

Temperature of arc plasma root
←→ Irradiance of arc plasma root

Current Density: $J_a = \frac{\varepsilon}{C_4}$

Arc heat flux: $Q_{cathode} = \varepsilon\left(\frac{2.76 + \varphi_a}{C_5} + \frac{k_g}{\delta C_6}\right) + C_9$

Arc pressure: $p_{arc} = \frac{1}{2}\rho v^2 = \frac{\mu_o IJ}{4\pi} \equiv C_{10}\varepsilon$

Irradiance distribution of arc on workpiece

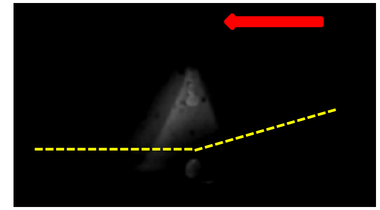

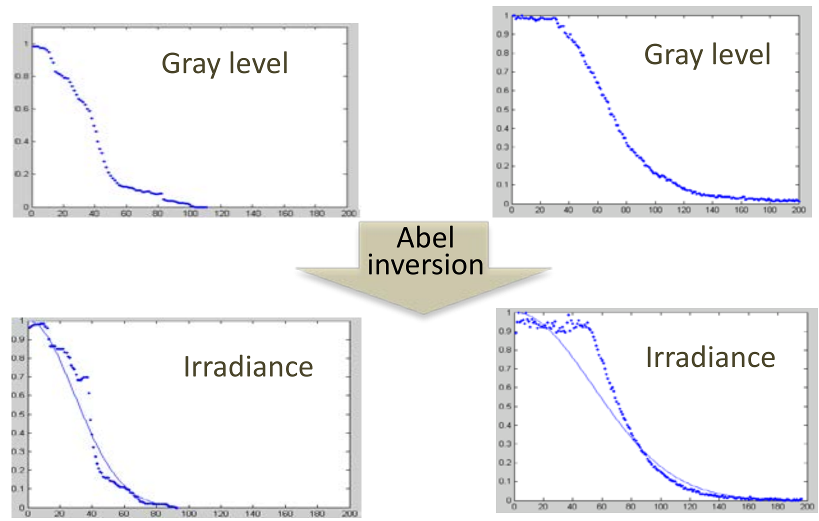

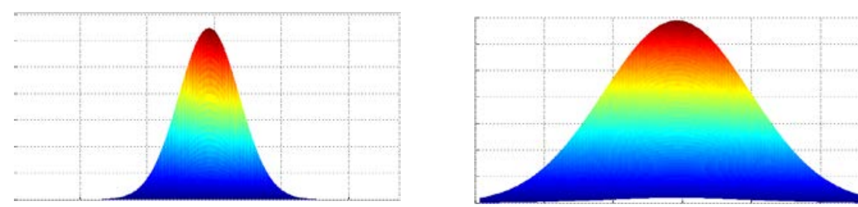

Elliptic arc characteristics

GMAW of V-groove Pipelines

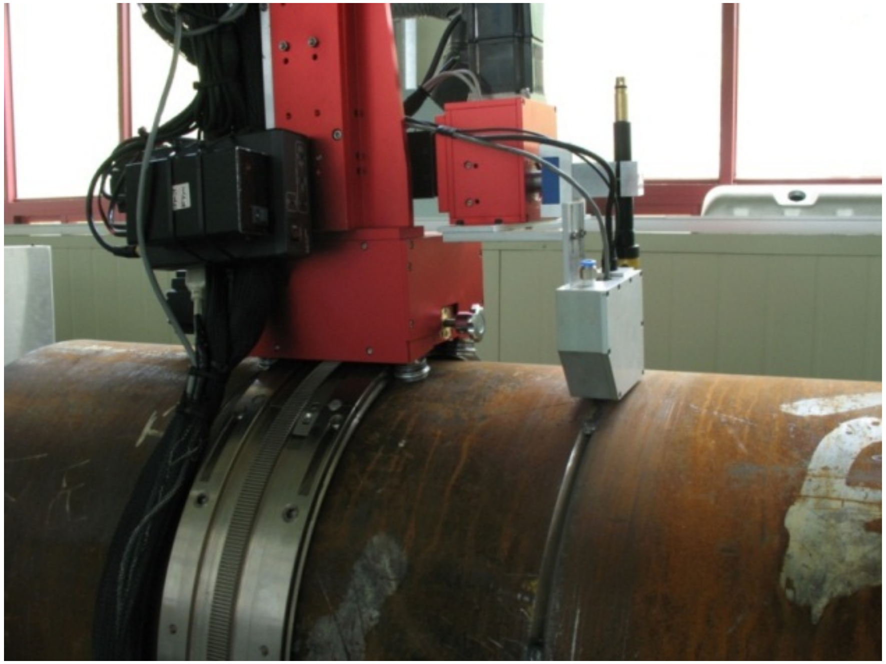

For better lifestyle, the people are connected with infrastructures using lifelines

Distribution of Arc Plasma in V-groove GMAW by Abel Inversion

Arc plasma shape in V-groove

Front

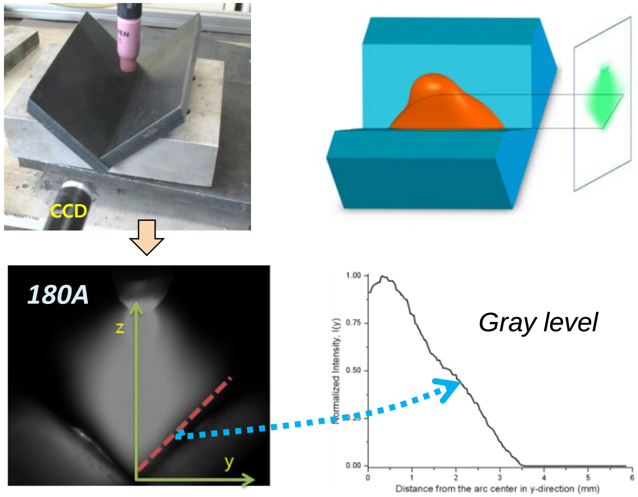

Side

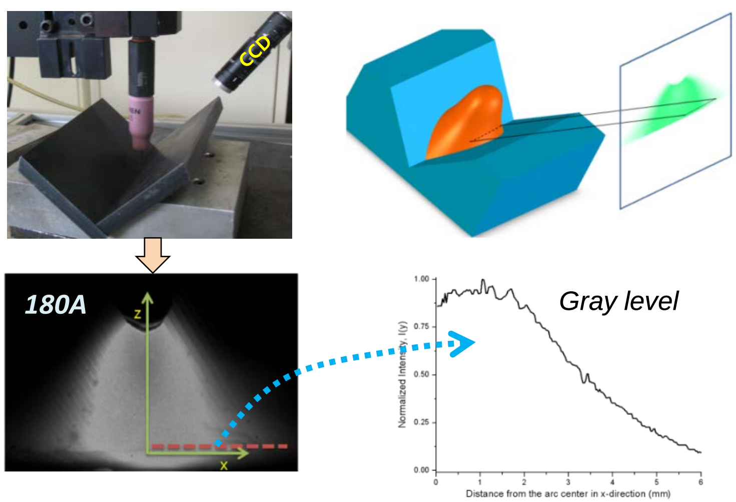

The arc plasma cannot maintain an **axisymmetric** shape

The **elliptically symmetric** arc model is better in V-groove arc welding

V-groove pipe welding

Flat position

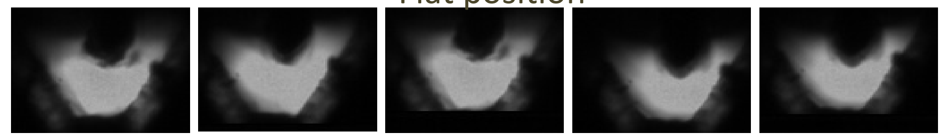

Vertical position

Overhead position

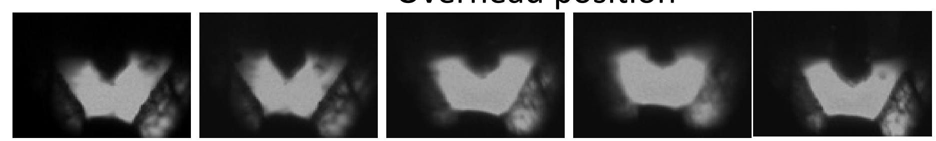

Arc shape rarely changes along the welding position

Average effective arc radius: $\sigma_x = 1.54mm$ $\sigma_y = 0.90mm$

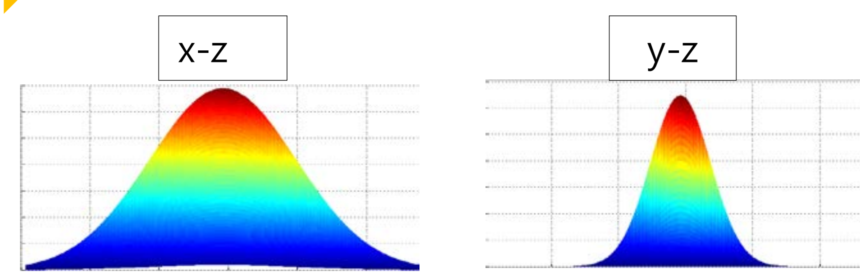

GMA V-groove Welding at Flat and Overhead Position

Welding speed: 10mm/s

Flat Position

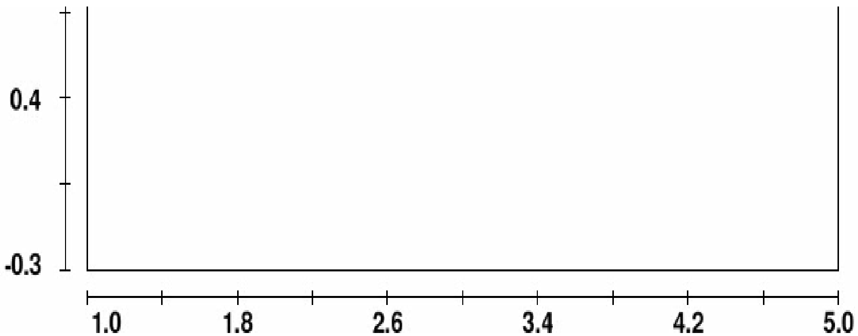

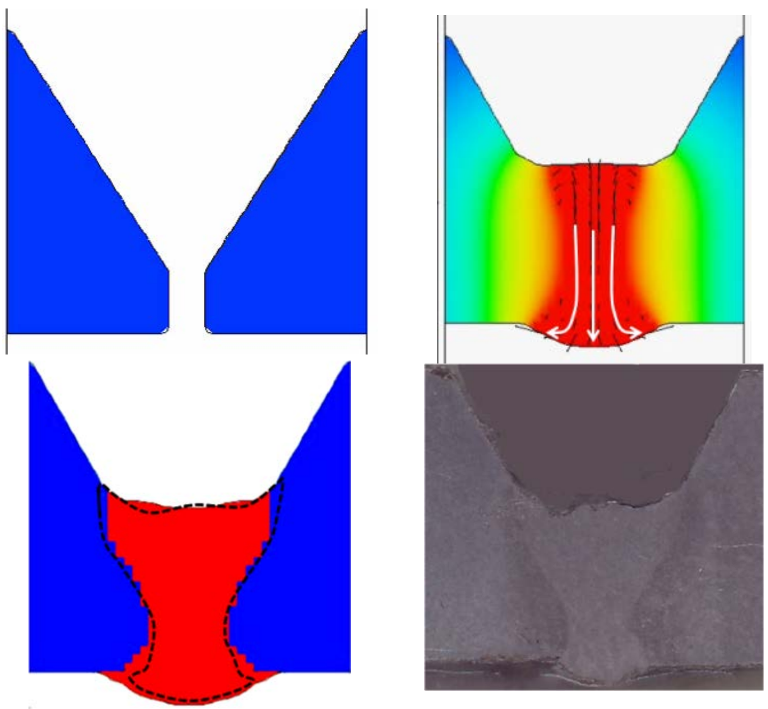

Overhead Position

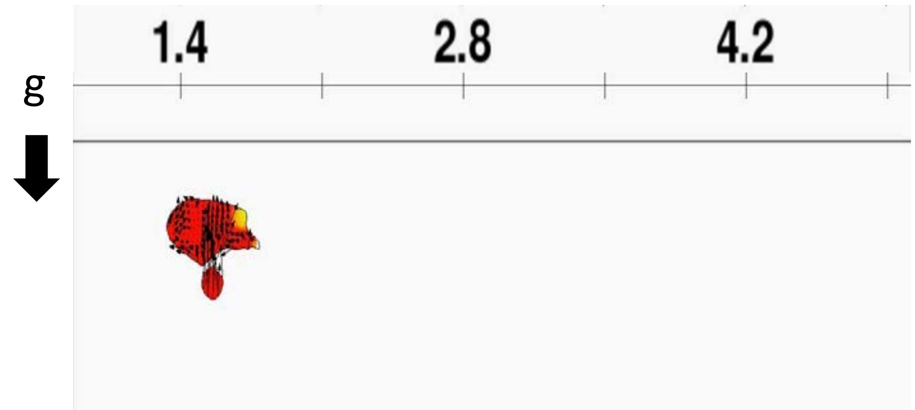

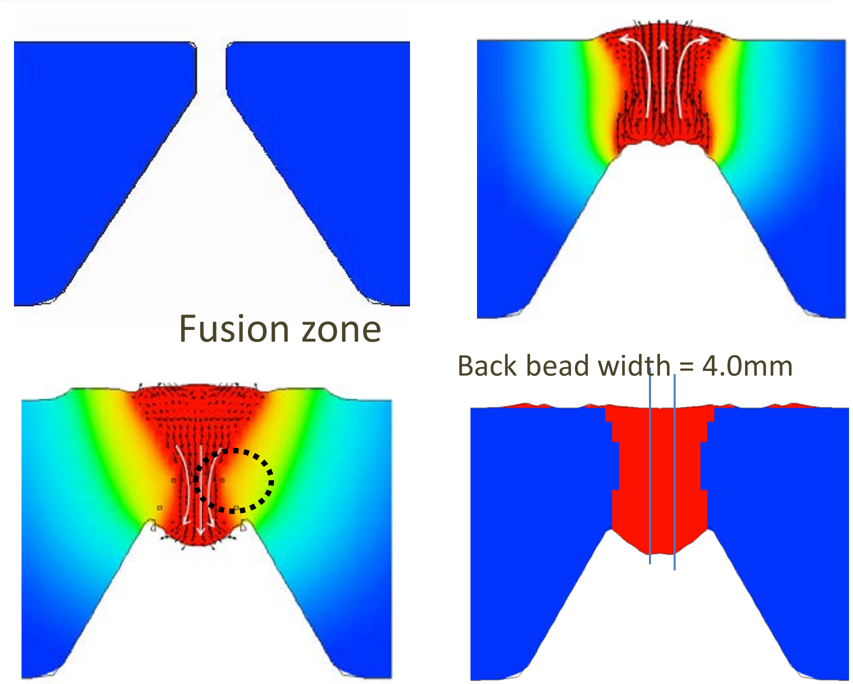

GMA V-groove Welding at Vertical Down Position

Welding speed: 10mm/s

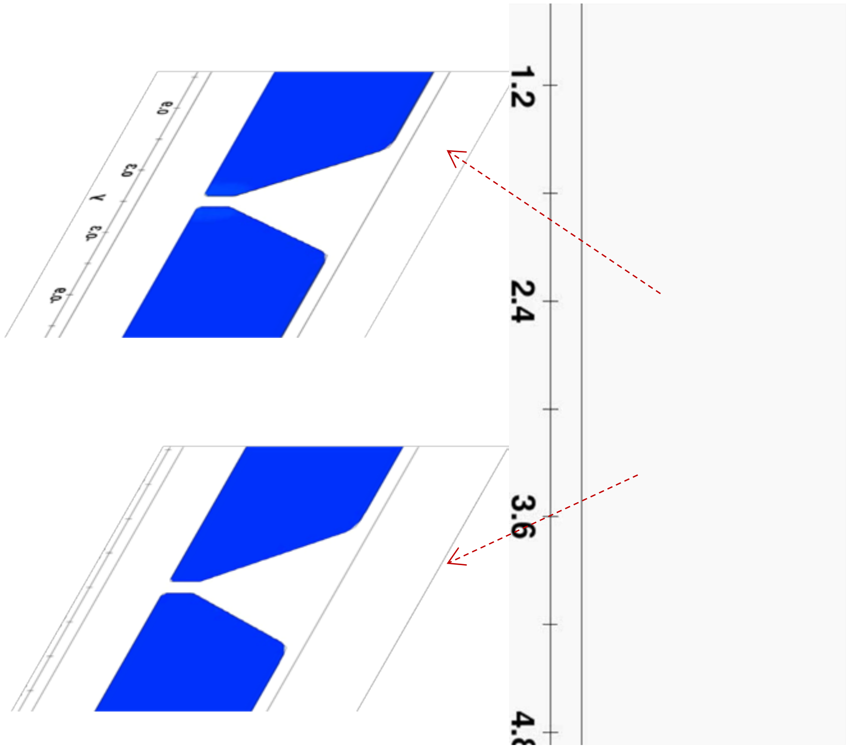

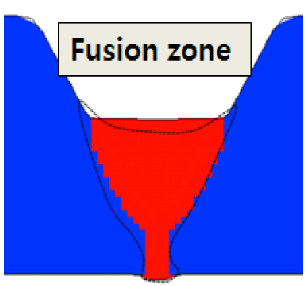

Flow of liquid metal into the front of arc

Melting of groove, but not root face

Lack of fusion on the root face

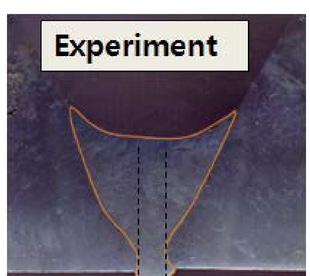

Welding speed: 20mm/s

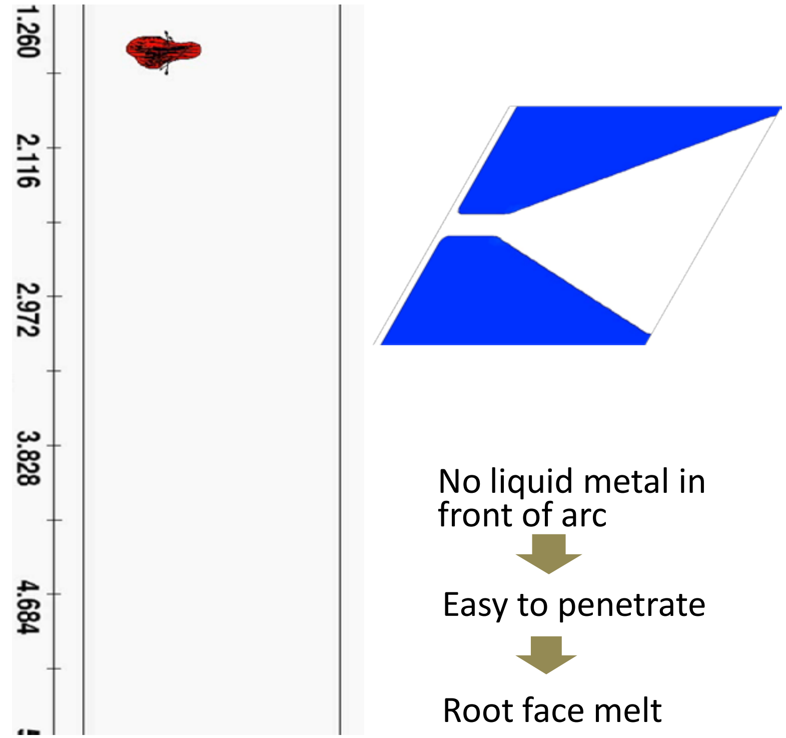

No liquid metal in front of arc

Easy to penetrate

Root face melt

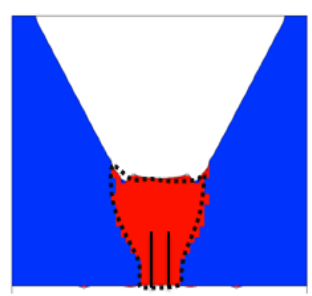

Back bead width = 2.1mm

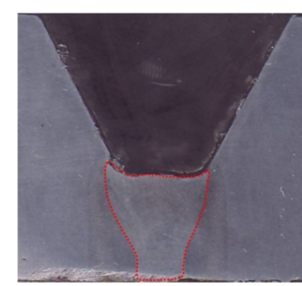

2^{nd} Pass Welding in V-groove GMAW at Different Positions

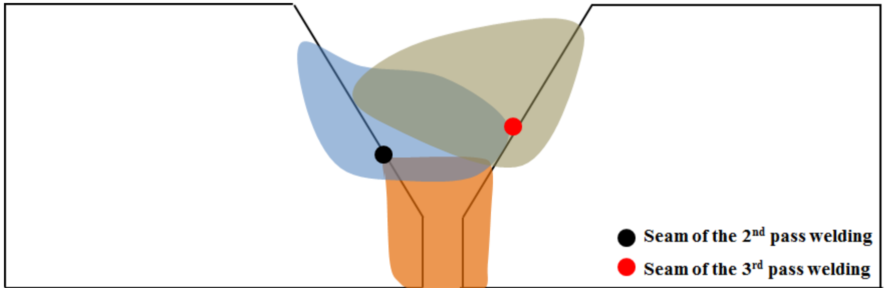

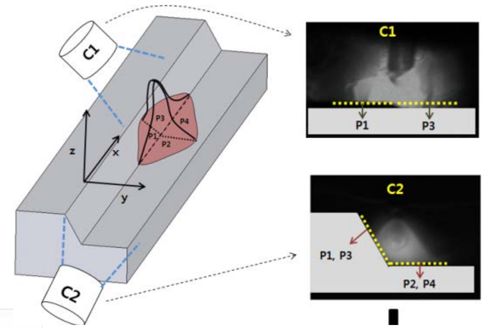

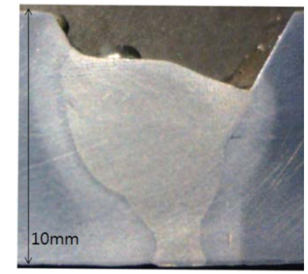

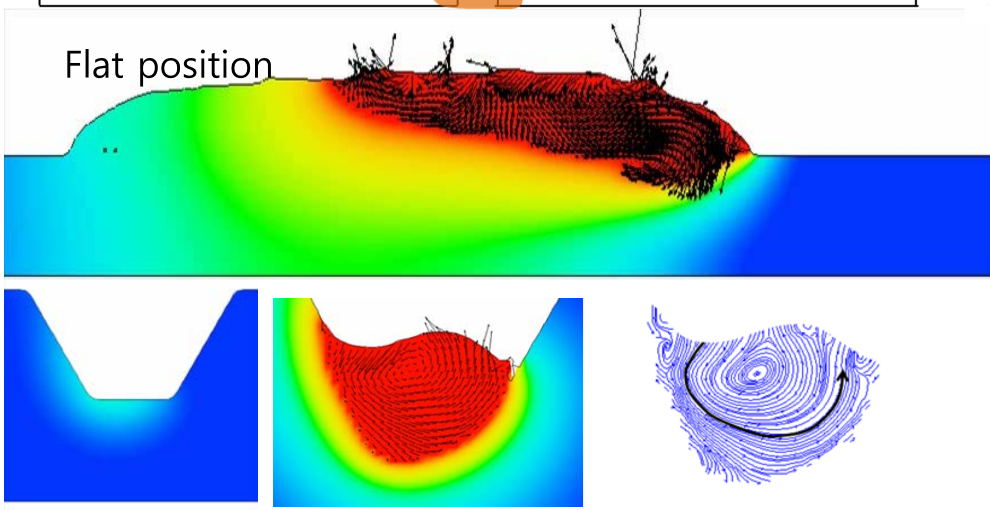

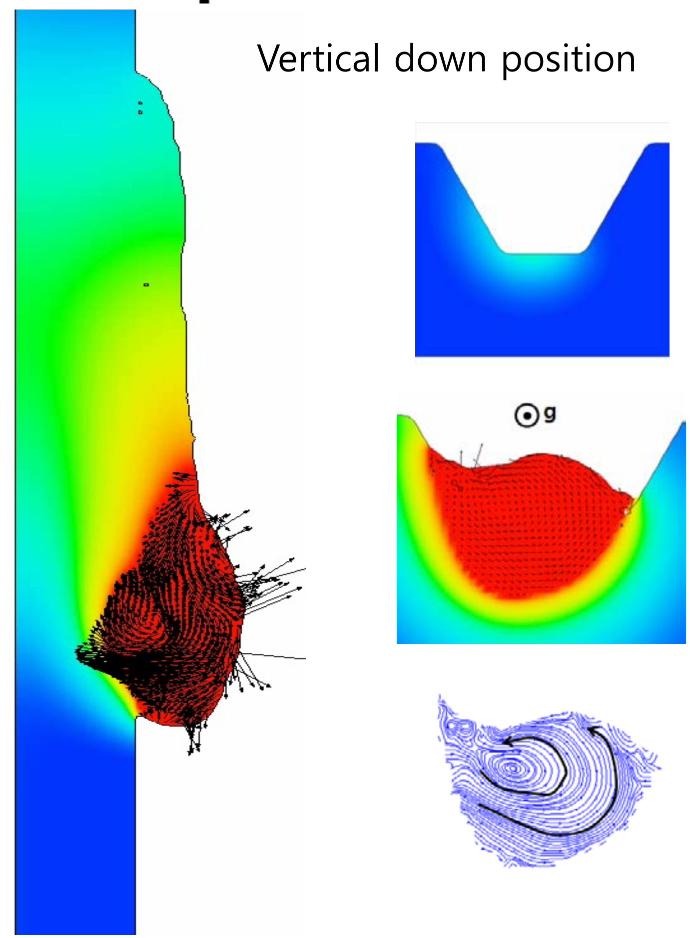

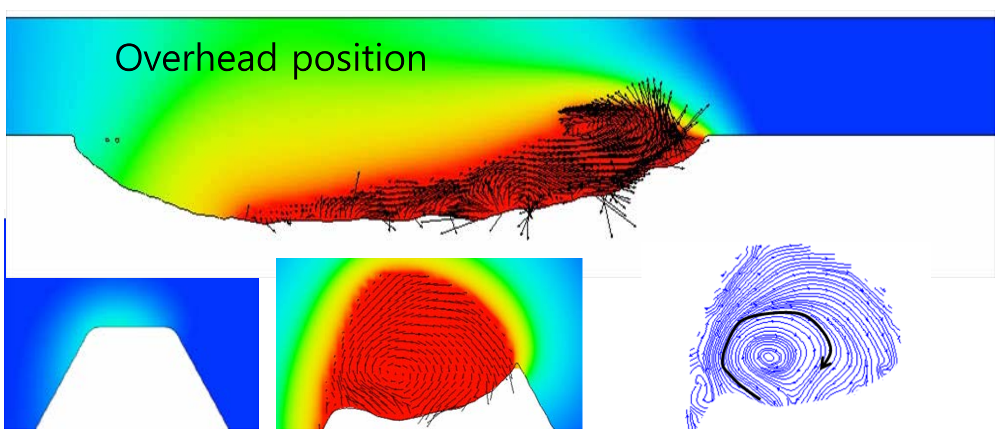

GMA Stiffener Welding in Ship Building

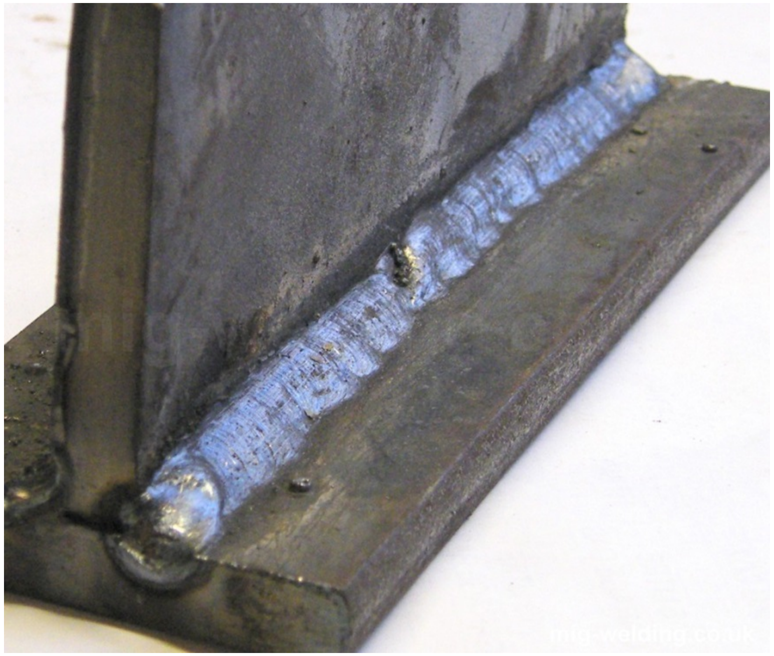

Stiffener welding is required to improve the stiffness of large structures such as ships

Arc Image Processing for Effective Arc Radius

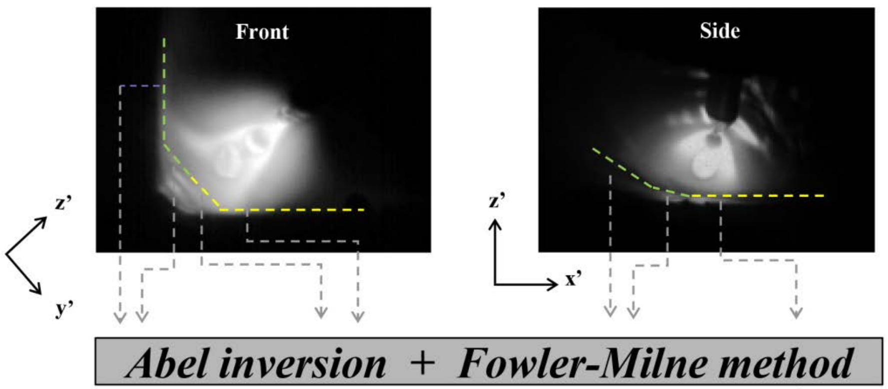

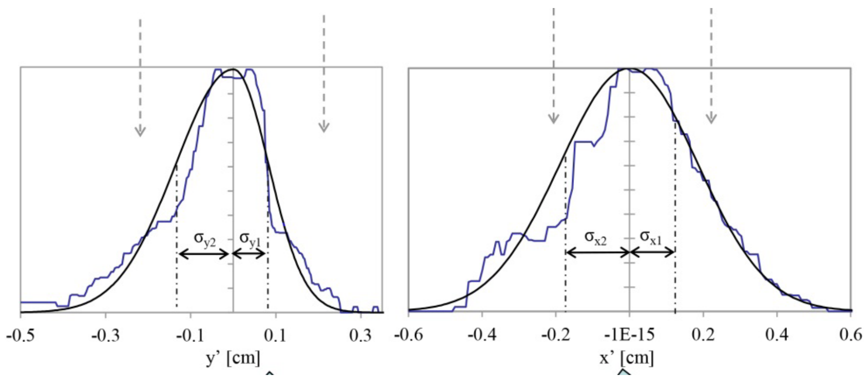

Asymmetric surface heat flux model and arc pressure model

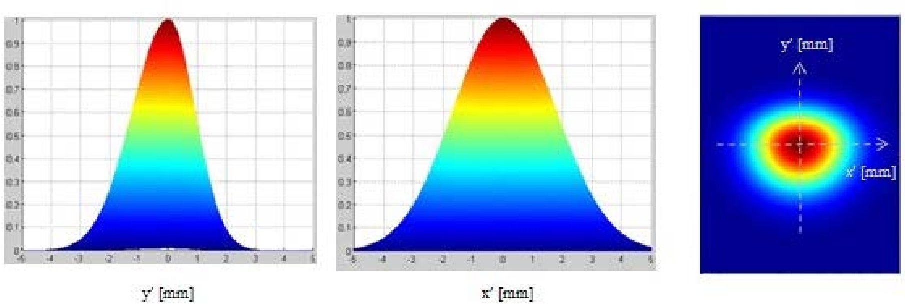

	Current [A]	Voltage [V]	Welding speed [cm/s]	WFR [m/min]
Case 1	25.8	255.4	0.4	7.5
Case 2	25.4	249.0	0.7	7.5
Case 3	25.6	258.5	1.0	7.5
Case 4	25.8	266.3	0.7	8.5
Case 5	26.2	298.8	0.7	9.5

	σ_{x1} (cm)	σ_{x2} (cm)	σ_{y1} (cm)	σ_{y2} (cm)
Case 1	0.176	0.168	0.091	0.123
Case 2	0.160	0.146	0.104	0.107
Case 3	0.153	0.142	0.130	0.148
Case 4	0.162	0.148	0.096	0.160
Case 5	0.153	0.137	0.092	0.143

CFD Simulations of Horizontal Fillet Welding

- Simulation parameters
  - Droplet radius: 0.06cm
  - Droplet velocity: 120cm/s
  - Droplet temperature: 2400 K
  - Torch angle: 51degree
  - Total arc efficiency: 0.8
  - Mesh size: 0.25mm/mesh
  - Effective arc radius: 2.854mm
  - Shift distance: 0.0 mm

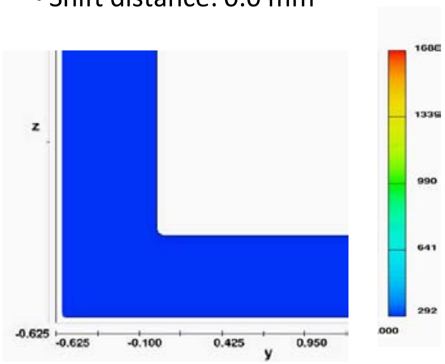

- Material properties used in simulation

	Phase	Value	Unit
density	sol	7.9	g/cm3
density	liq	6.9	g/cm3
latent heat	-	2.47E+09	erg/gK
thermal conductivity	sol	3.70E+06	erg/cmK
thermal conductivity	liq	2.60E+06	erg/cmK
specific heat	sol	4.70E+06	erg/gK
specific heat	liq	6.97E+06	erg/gK
viscosity		0.1	g/cm s
surface tension coefficient		1.90E+03	dyne/cm
surface tension gradient		-0.3	dyne/cmK
liquidus temperature		1791	K
solidus temepeerature		1688	K
CTE		1.20E-05	1/k
drag coefficient		1.0	-
coherent solid fraction		0.5	-
critical solid fraction		0.6	-

t= 3.3s

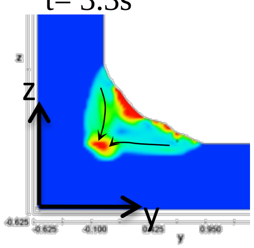

t=3.70s

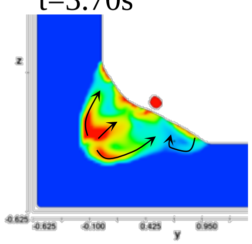

t=3.90s

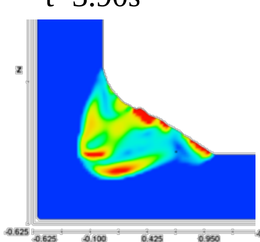

t=4.1s

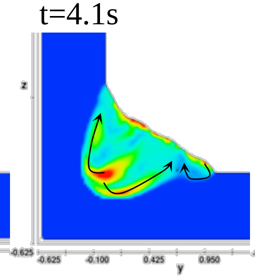

t=4.3s

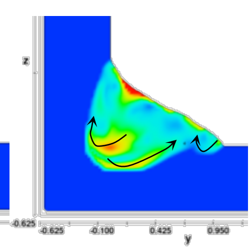

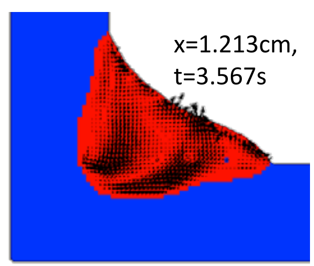

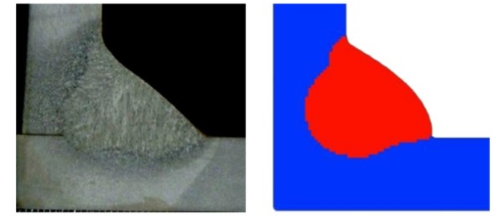

(a) Case 1 : v=0.4 cm/s and WFR=7.5 m/min

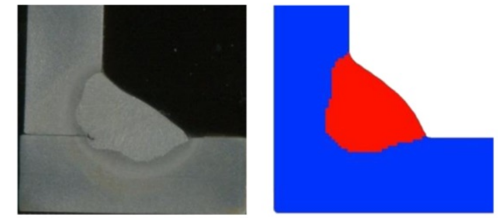

(b) Case 2 : v=0.7 cm/s and WFR=7.5 m/min

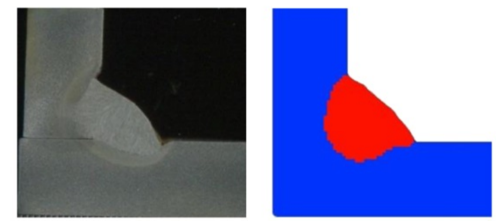

(c) Case 3 : v=1.0 cm/s and WFR=7.5 m/min

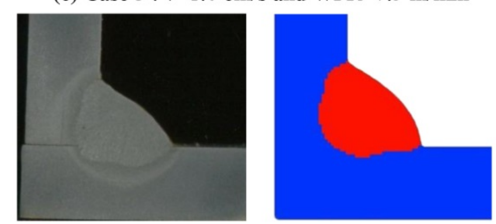

(d) Case 4 : v=0.7 cm/s and WFR=8.5 m/min

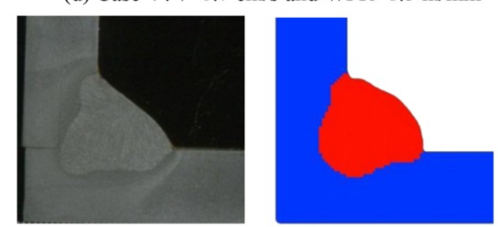

(e) Case 5 : v=0.7 cm/s and WFR=9.5 m/min

Multi-electrode Submerged Arc Welding

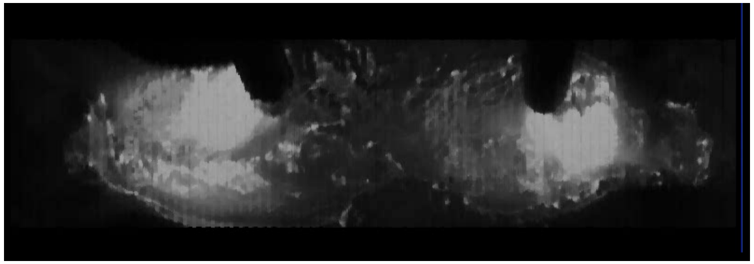

Arc observation in the air

Models

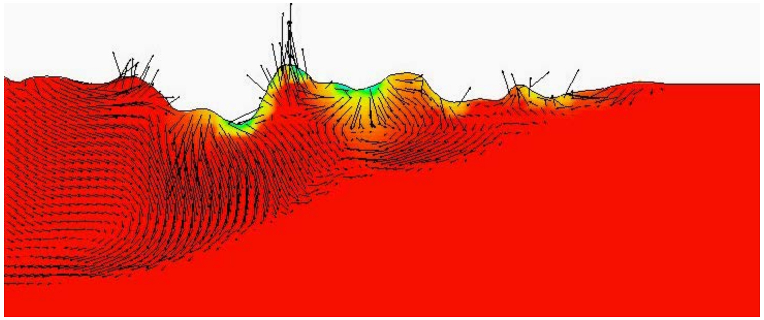

Weld pool behavior under the flux

Arc Root Dimension Models in Multi-electrode SAW Process

Single wire SAW

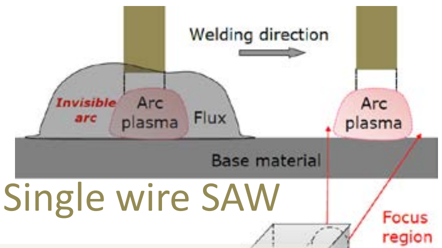

Assumption:
The arc plasma just outside the flux is very similar to the arc plasma in the flux cavity

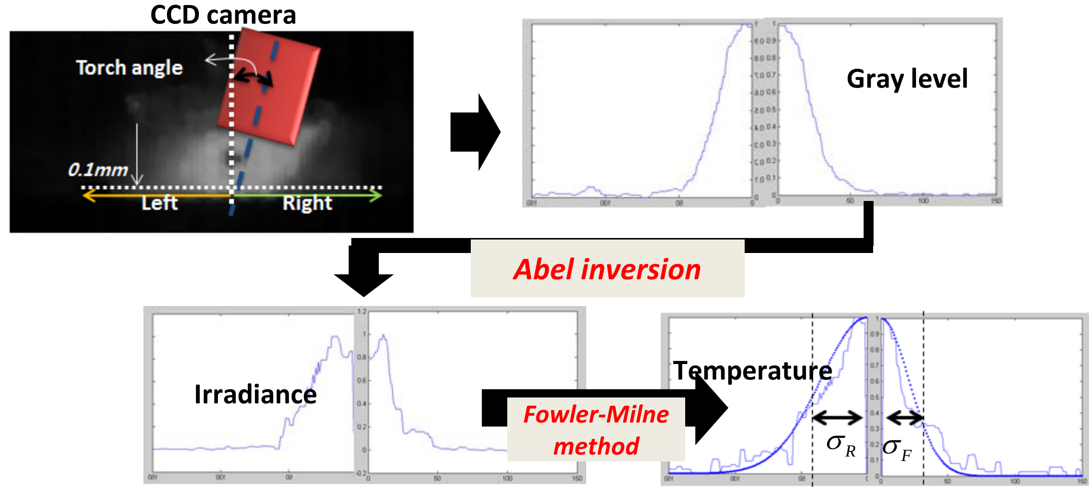

Tandem SAW

→ Arc interaction model

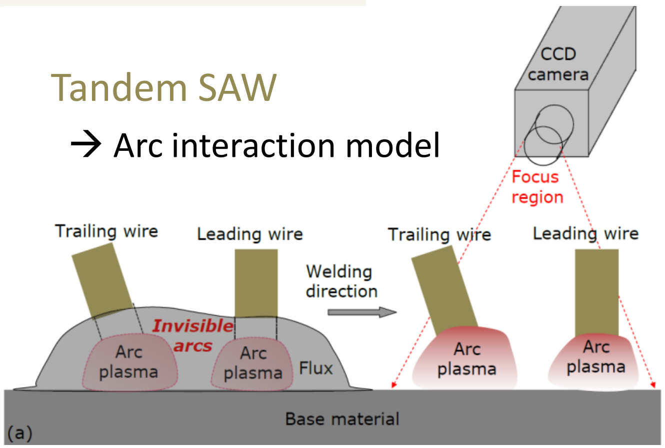

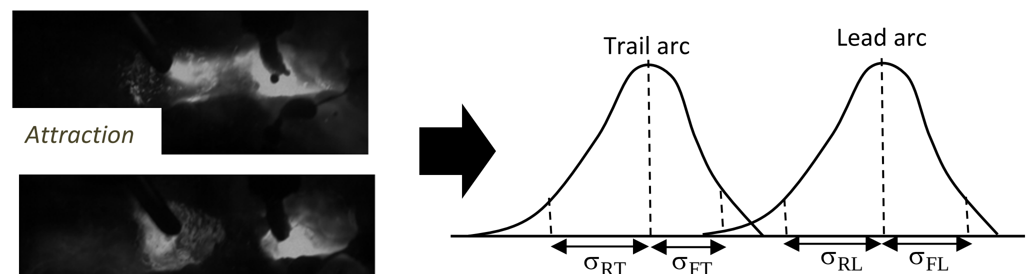

Development of the regression model

Three wire SAW

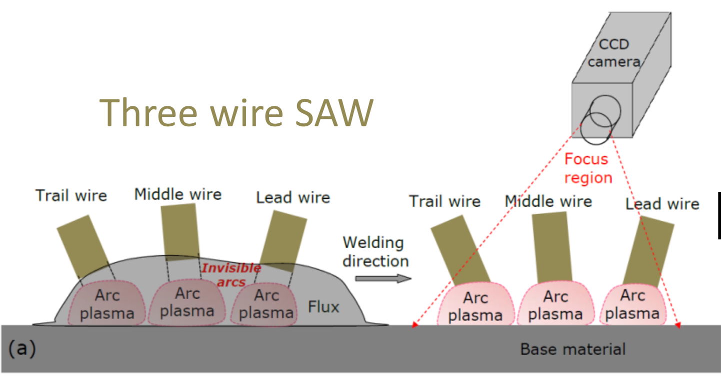

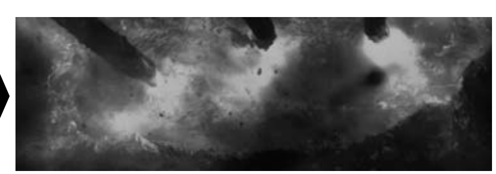

Arc images are not clear

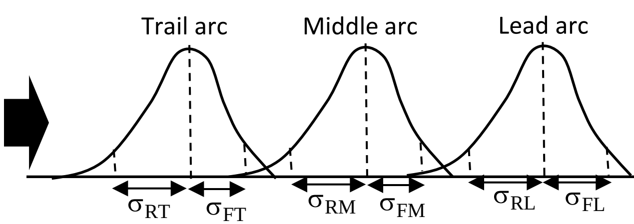

→ Tandem SAW arc root dimensions for three wire case

Weld Pool Behavior of Single Wire DC SAW

	Cur (A)	Vol (V)	Angle (deg)	(mm)	(mm)	Ratio	Wire feed rate (m/min)	Welding speed (m/min)	Heat input (KJ/cm)
Case 1	1000	32	-20 (backward)	2.43	2.21	1.10	2.24	140	13.7
Case 2	1000	32	+20 (forward)	2.18	2.41	0.90	2.24	140	13.7

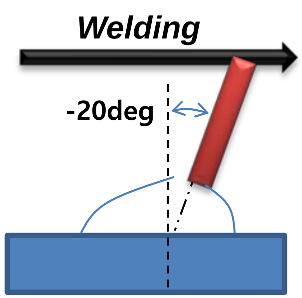

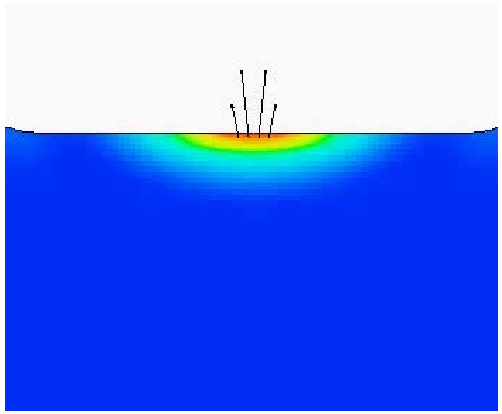

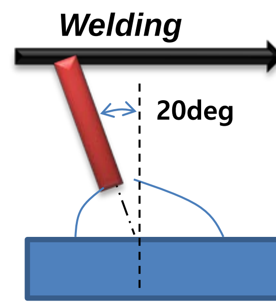

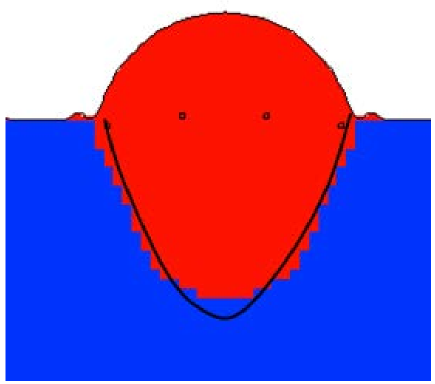

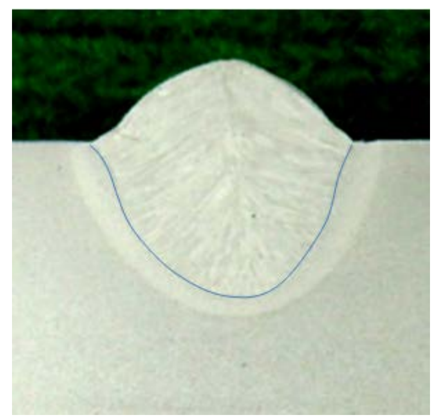

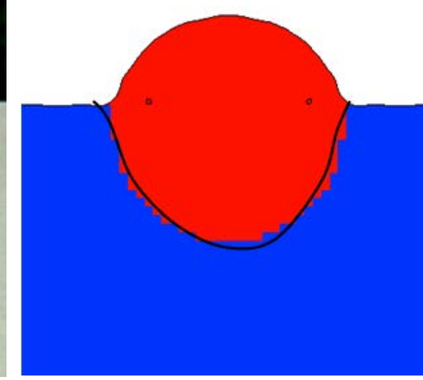

Deeper and narrower weld bead

Shallower and wider weld bead

Tandem SAW on V-groove

EX) Case 1 (Leading: 1000A, Trailing: 700A)

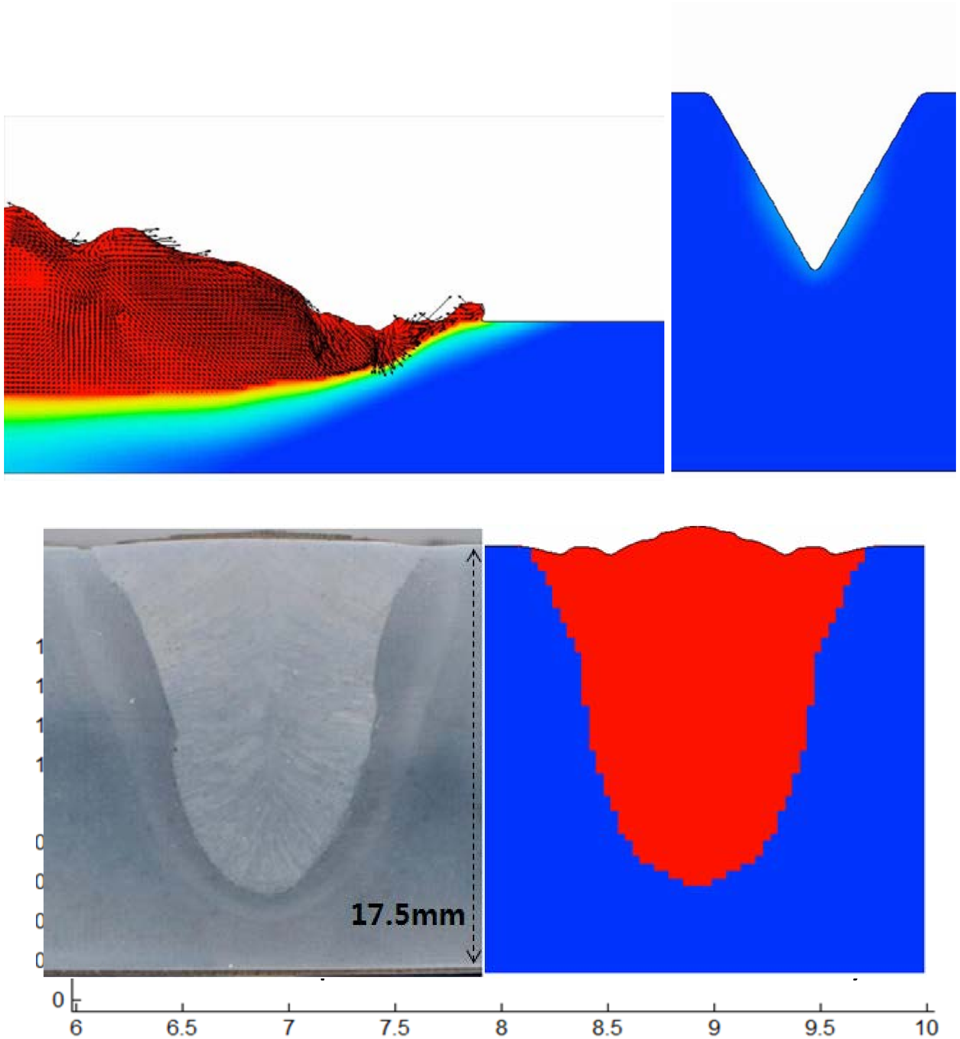

Deeper and narrower weld bead

Case 2 (Leading: 700A, Trailing: 1000A)

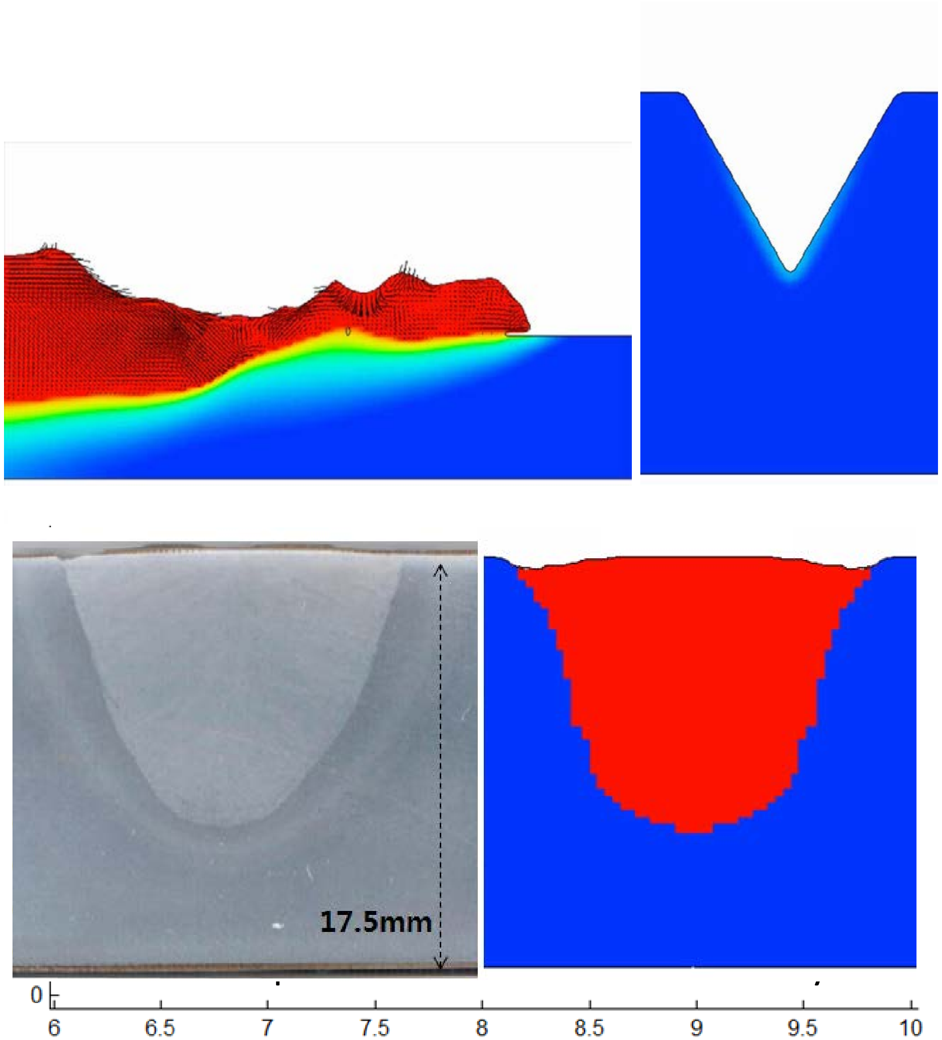

Shallower and wider weld bead

Fairly good agreement between simulations and experiments

Three-electrode Submerged Arc Welding

Case 1: Sine waveform

$I_L = 1200\,A;\ I_M = 900\,A;\ I_T = 800\,A;\ S = 36.4\,mm/s$

$V_L = 32\,V;\ V_M = 35\,V;\ V_T = 36\,V$

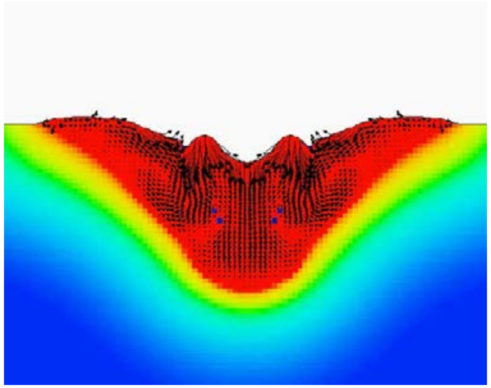

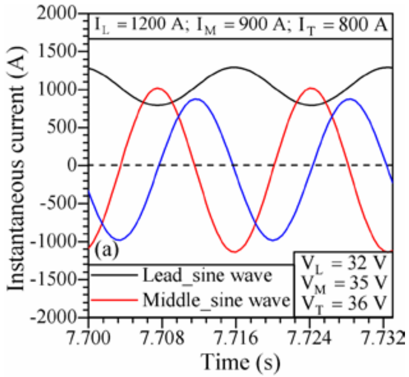

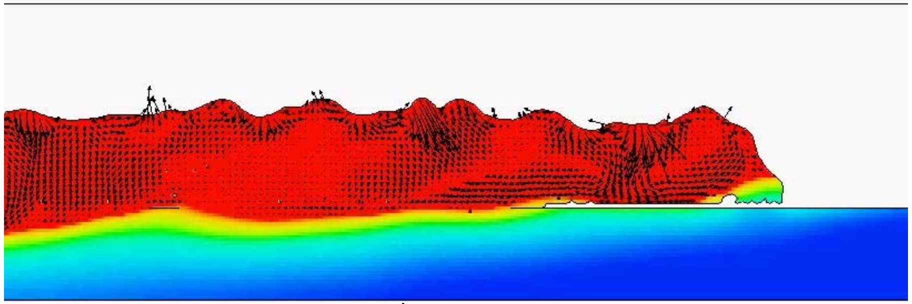

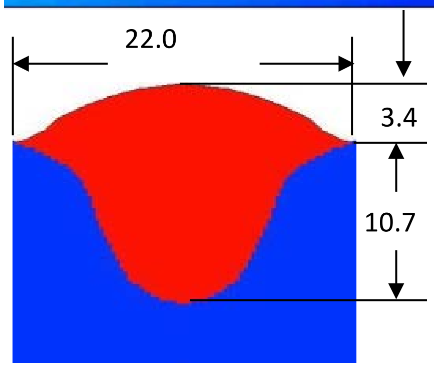

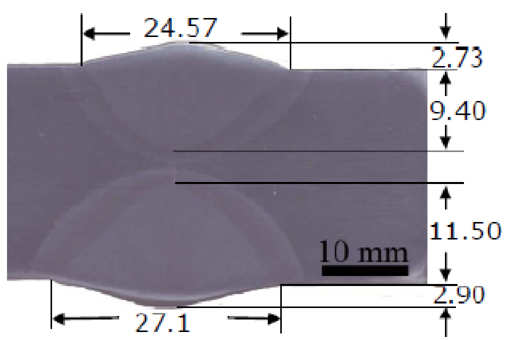

Case 3: Trapezoidal waveform

$I_L = 1200\,A;\ I_M = 900\,A;\ I_T = 800\,A;\ S = 36.4\,mm/s$

$V_L = 32\,V;\ V_M = 35\,V;\ V_T = 36\,V$

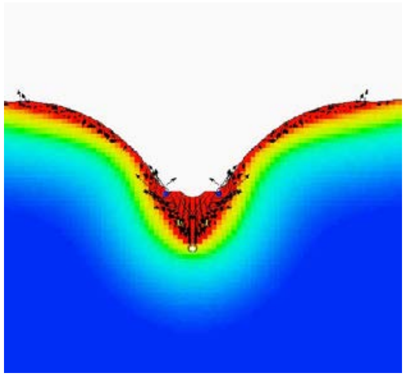

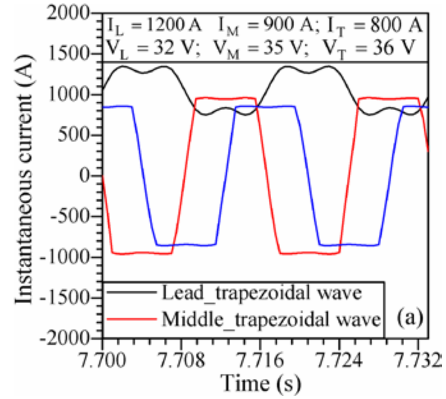

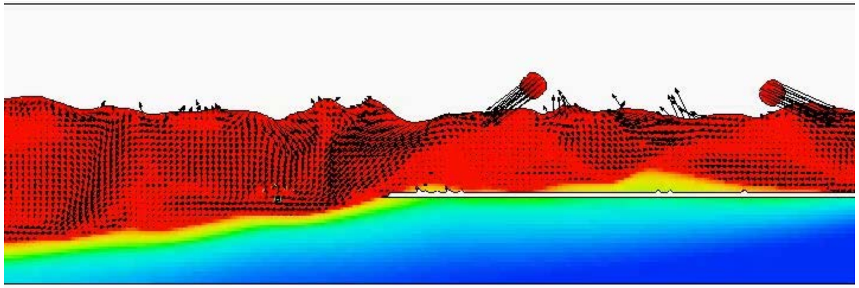

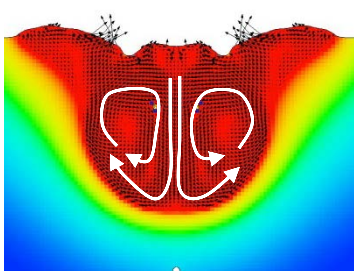

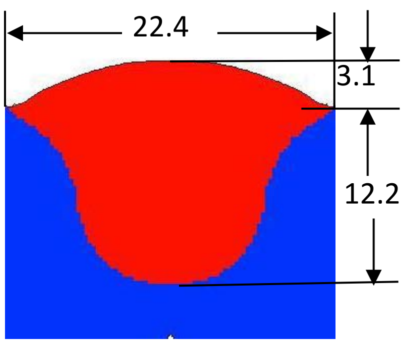

Laser Beam Welding (LBW)

Selective Laser Melting (SLM)

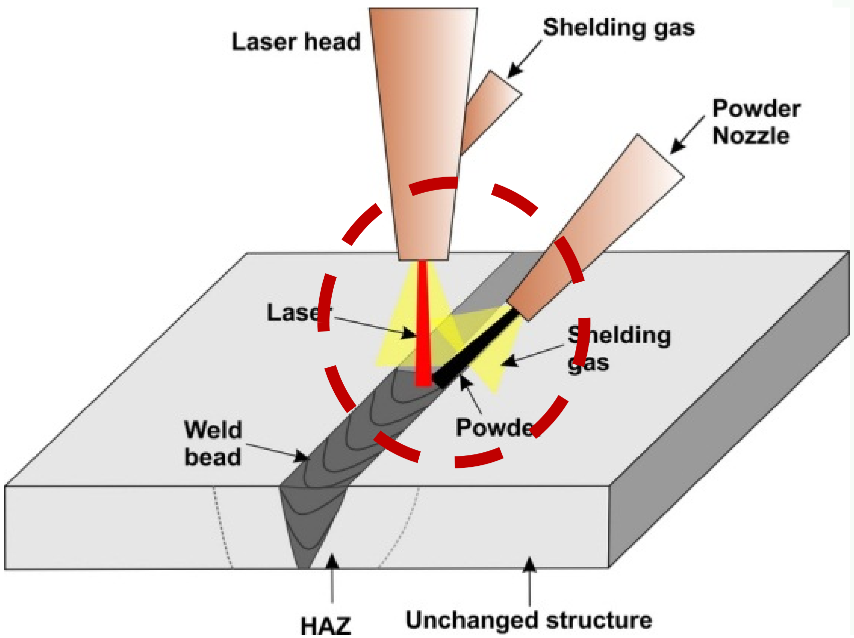

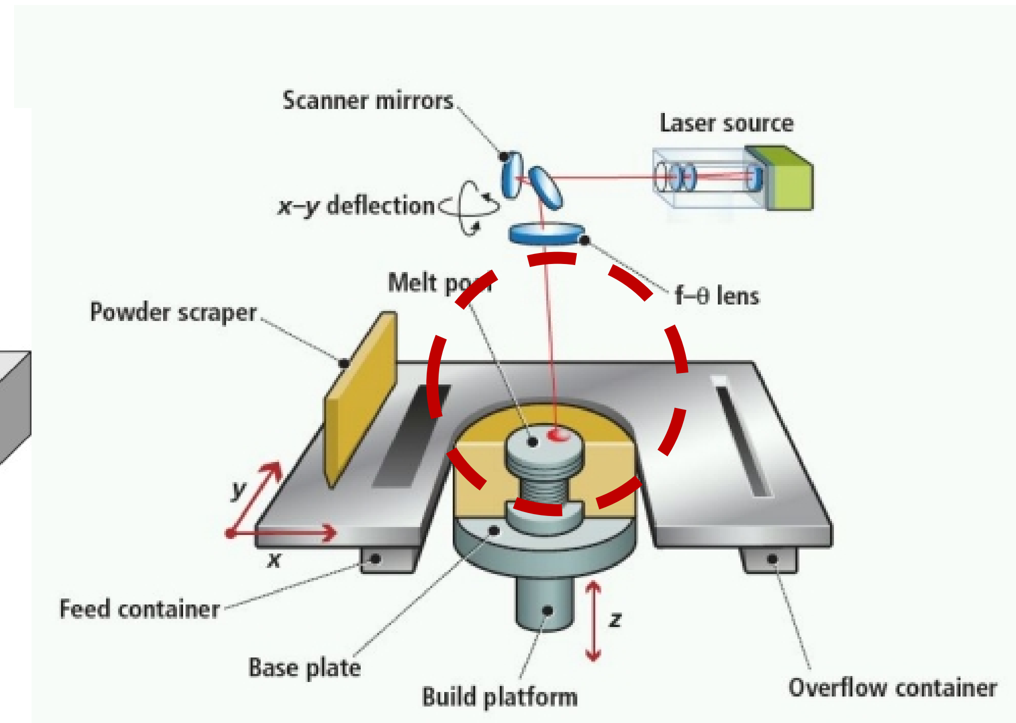

Models for Laser Welding Process

- Laser → multiple reflections by ray-tracing, scattering
- Laser-matter interaction → absorption/reflection/transmission
- Vaporization → recoil pressure
- Vapor-induced heat source
- Vapor-induced shear stress
- Bubble formation → internal pressure

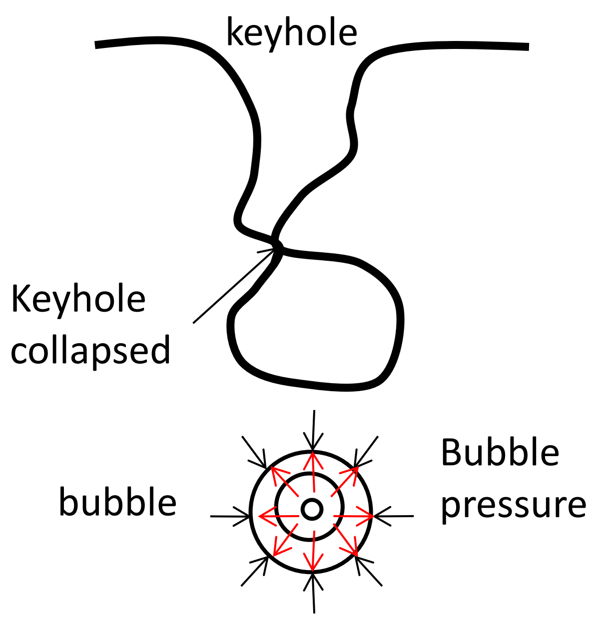

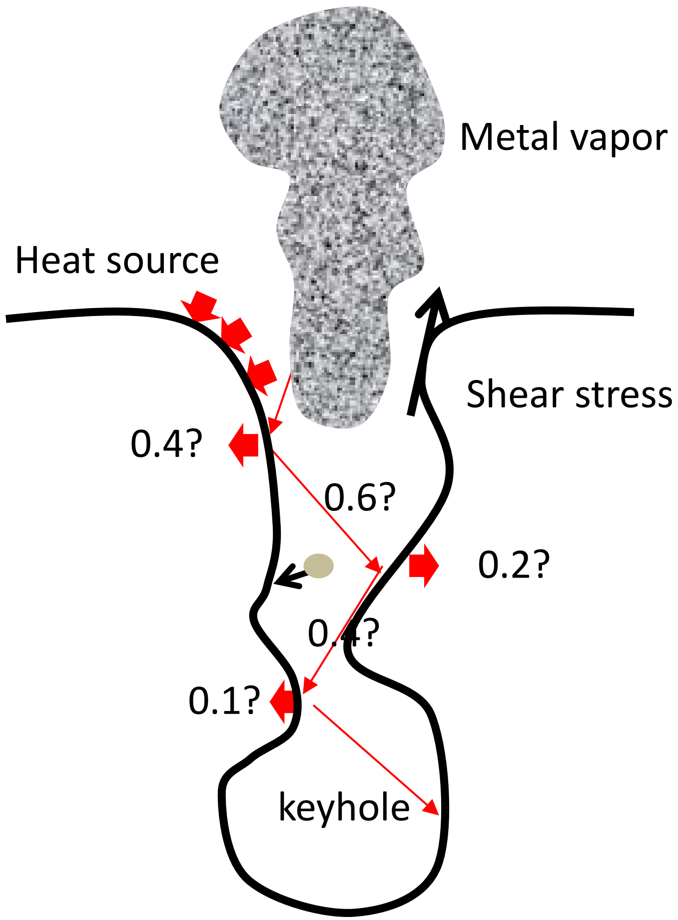

Cell-based Ray Tracing (CRT)

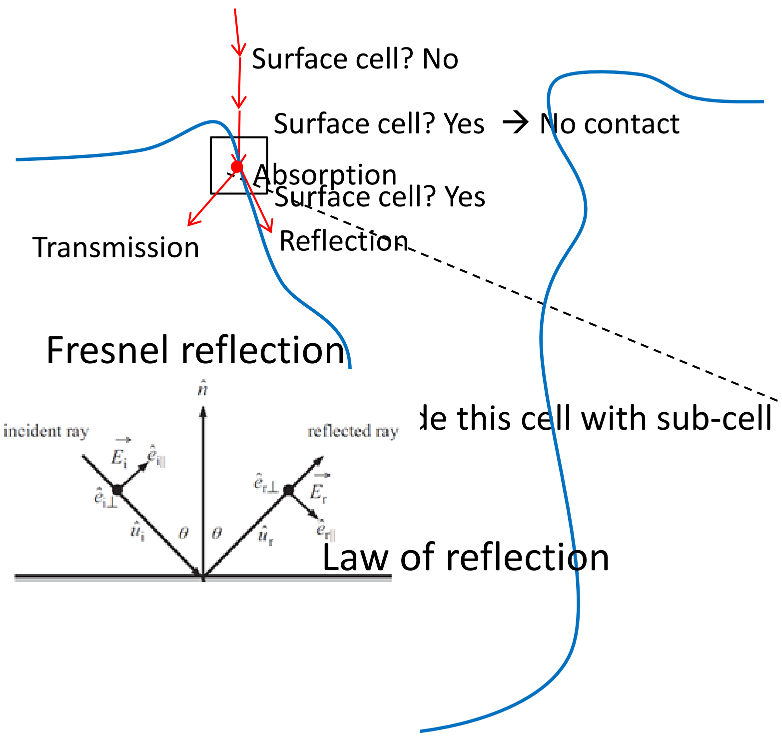

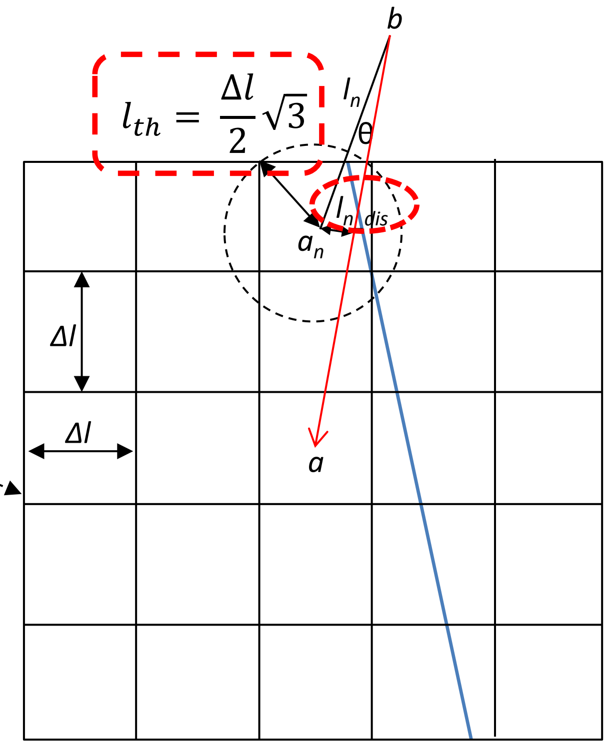

l_n : distance between center of n^{th} sub-cell and ray starting point b

l_{th} : radius of smallest sphere which can include sub-cell

l_{n_dis} : smallest distance between center of n^{th} sub-cell and ray direction vector $\vec{r} = \overrightarrow{a-b}$

Ray is moved from b to a

a_n : Center point of n^{th} sub-cell

Ray contacts the surface in cell when $l_{n\_dis} \leq l_{th}$

$$l_{n\_dis} = l_n \times sin\left[arccos\left(\frac{|\overrightarrow{a_n-b}|\cdot|\overrightarrow{a-b}|}{|\overrightarrow{a_n-b}||\overrightarrow{a-b}|}\right)\right]$$

In this case, the condition is satisfied → Absorption, Reflection , Transmission

Surface-based Ray Tracing (SRT)

New model → Based on real surface

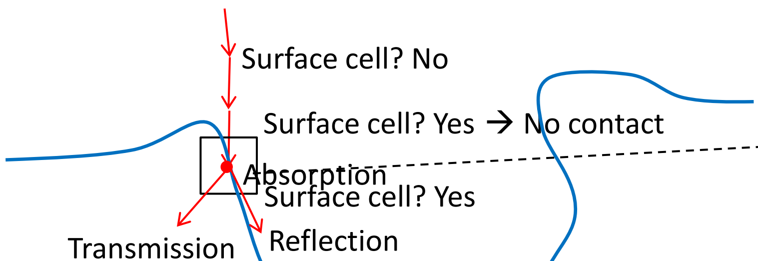

A=1-exp(-αl)

α : absorption coefficient

l : travel distance

(X_1, X_2, X_3) : Ray starting point

$\hat{u} = (u_1, u_2, u_3)$: Direction vector of ray

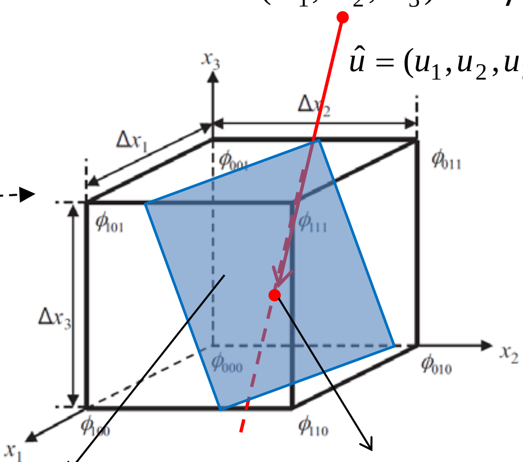

$$\begin{cases} x_1 = X_1 + tu_1 \\ x_2 = X_2 + tu_2 \\ x_3 = X_3 + tu_3 \end{cases}$$

t : distance between (X_1, X_2, X_3) and (x_1, x_2, x_3)

$\phi(x_1, x_2, x_3) = 0$: Surface equation

(x_1, x_2, x_3) : Contact point of surface and ray

Calculate the contact point by a set of equations → $a_3 t^3 + a_2 t^2 + a_1 t + a_0 = 0$

Fresnel reflection

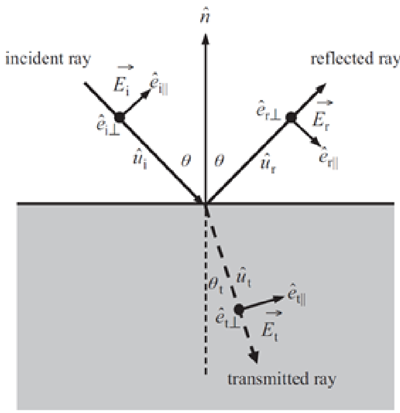

Law of reflection

Snell's law

Condition for contact
- (x_1, x_2, x_3) should exist in a cell
- t should be positive

In this case,
(x_1, x_2, x_3) exist in a cell and t is positive

Contact → Absorption
Reflection
Transmission → Almost zero in metal

Cell-based Ray Tracing vs. Surface-based Ray Tracing

: Case 1 → Cell-based ray tracing (old model)
: Case 2 → Surface-based ray tracing (new model)

[S.-W.Han, J.-S.Ahn, S.-J.Na*, “A study on ray tracing method for CFD simulations of laser keyhole welding: Progressive Search Method”, Welding in the World, Vol.60, P.247-258, March 2016]

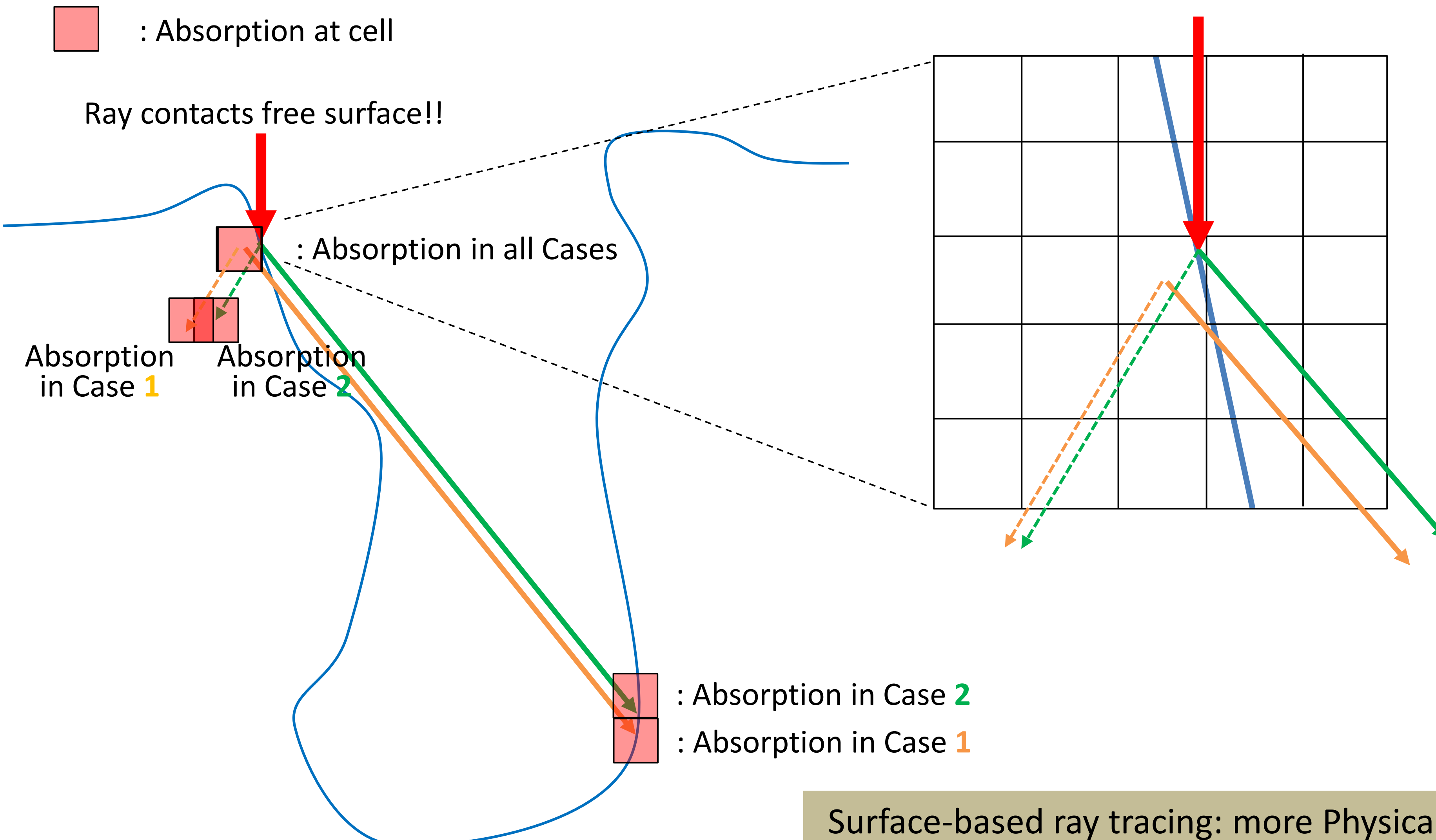

Surface-based ray tracing: more Physical

Fresnel Reflection Model

Absorptivity at each irradiation point ?

1. Experimental investigation - High temperature data is not available!
2. Theoretical model

- General Fresnel reflection model

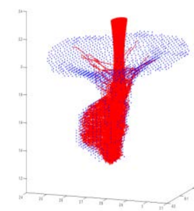

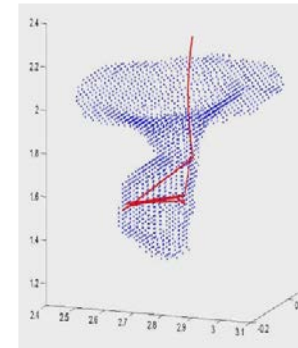

$$E_{r\perp} = E_{i\perp}\frac{\cos\theta - p + qi}{\cos\theta + p - qi}$$

$$E_{r\parallel} = E_{i\parallel}\frac{(p - \sin\theta\tan\theta + qi)(\cos\theta - p + qi)}{(p + \sin\theta\tan\theta - qi)(\cos\theta + p - qi)}$$

where

$$p^2 = \frac{1}{2}\{\sqrt{[n_2{}^2 - k_2{}^2 - (n_1\sin\theta)^2]^2 + 4n_2{}^2k_2{}^2} + [n_2{}^2 - k_2{}^2 - (n_1\sin\theta)^2]\}$$

$$q^2 = \frac{1}{2}\{\sqrt{[n_2{}^2 - k_2{}^2 - (n_1\sin\theta)^2]^2 + 4n_2{}^2k_2{}^2} - [n_2{}^2 - k_2{}^2 - (n_1\sin\theta)^2]\}$$

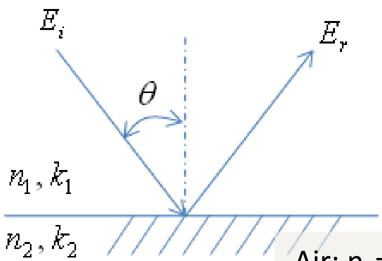

n: refractive index
k: absorptive index

Air: n_1=1, k_1=0 (dielectric)
Metal: complex index of refraction ($m=n_2-ik_2$)

Equation of Fresnel's reflectivity	S-polarization	P-polarization	Circularly polarization
$\rho = \frac{E_{r\parallel}E_{r\parallel}^* + E_{r\perp}E_{r\perp}^*}{E_{i\parallel}E_{i\parallel}^* + E_{i\perp}E_{i\perp}^*}$	$\rho_s = \frac{(n_1\cos\theta - p)^2 + q^2}{(n_1\cos\theta + p)^2 + q^2}$	$\rho_p = \frac{(p - n_1\sin\theta\tan\theta)^2 + q^2}{(p + n_1\sin\theta\tan\theta)^2 + q^2}\rho_s$	$\rho_c = \frac{1}{2}(\rho_s + \rho_p)$

The complex index of refraction ($m=n_2-ik_2$) of a metal

1. Drude theory based on a free electron model; vanishing spring constant in Lorentz model
2. Hagen-Rubens relation – only available for frequency much less than the mean collision rate of the electrons

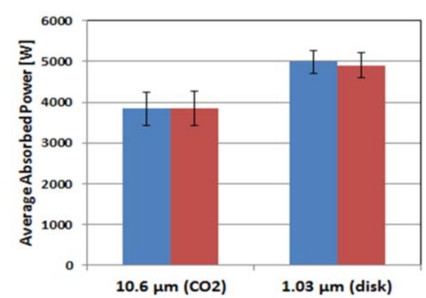

No big difference for multiple reflections in deep keyhole

→ Hagen-Rubens Relation in Further Simulations

Interaction of Laser Beam with Material

[S.-W.Han, J.-S.Ahn, S.-J.Na, "A study on ray tracing method for CFD simulations of laser keyhole welding: Progressive Search Method", Welding in the World, Vol.60, P.247-258, March 2016]

Laser beam : Bundle of rays

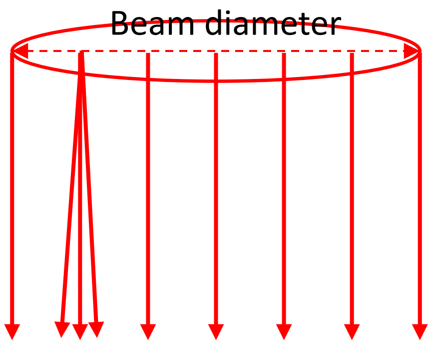

One ray : Single ray **X 777**

[Old model]

Laser beam : Bundle of rays

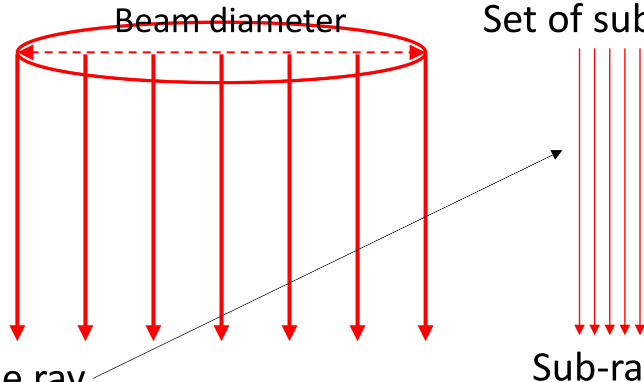

One ray

[New model]

One ray :
Set of sub-rays

Sub-ray :
All sub-rays start at the same point

- Rays in bundle
  : Different starting point
- Sub-rays in one ray
  : Same starting point
  → To depict multi-path

Ray energy = *I*

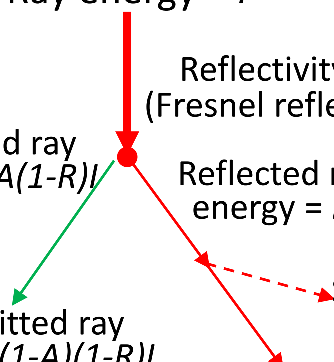

Reflectivity : *R*
(Fresnel reflection)

Absorbed ray energy = *A(1-R)I*

Reflected ray energy = *RI*

Scattered ray energy = *SRI*

Transmitted ray energy = *(1-A)(1-R)I*

Reflected ray energy = (1-S)*RI*

* *A* > *r* → Absorption
* Probability of absorption : *A*
A is related to *refraction index*

Number of absorbed sub-rays ≈ *A(1-R)N*

Number of transmitted sub-rays ≈ *(1-A)(1-R)N*

Number of sub-rays : *N*

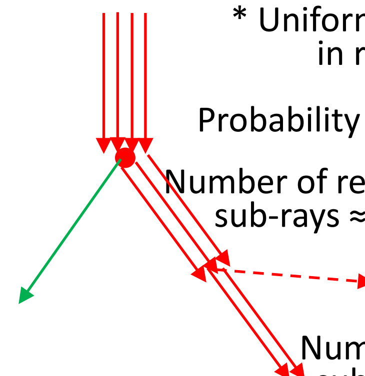

* *R* > *r* → Reflection
* Uniform random number in range 0~1 = *r*

Probability of reflection : *R*

Number of reflected sub-rays ≈ *RN*

Number of scattered sub-rays ≈ *SRN*

Number of reflected sub-rays ≈ (1-S)*RN*

Transmission and scattering: new rays
→ Difficult to trace very many new rays

No change of number of sub-rays
→ More effective for Transmission and/or Scattering

Weld Pool Behavior for Various Powers in Disk Laser

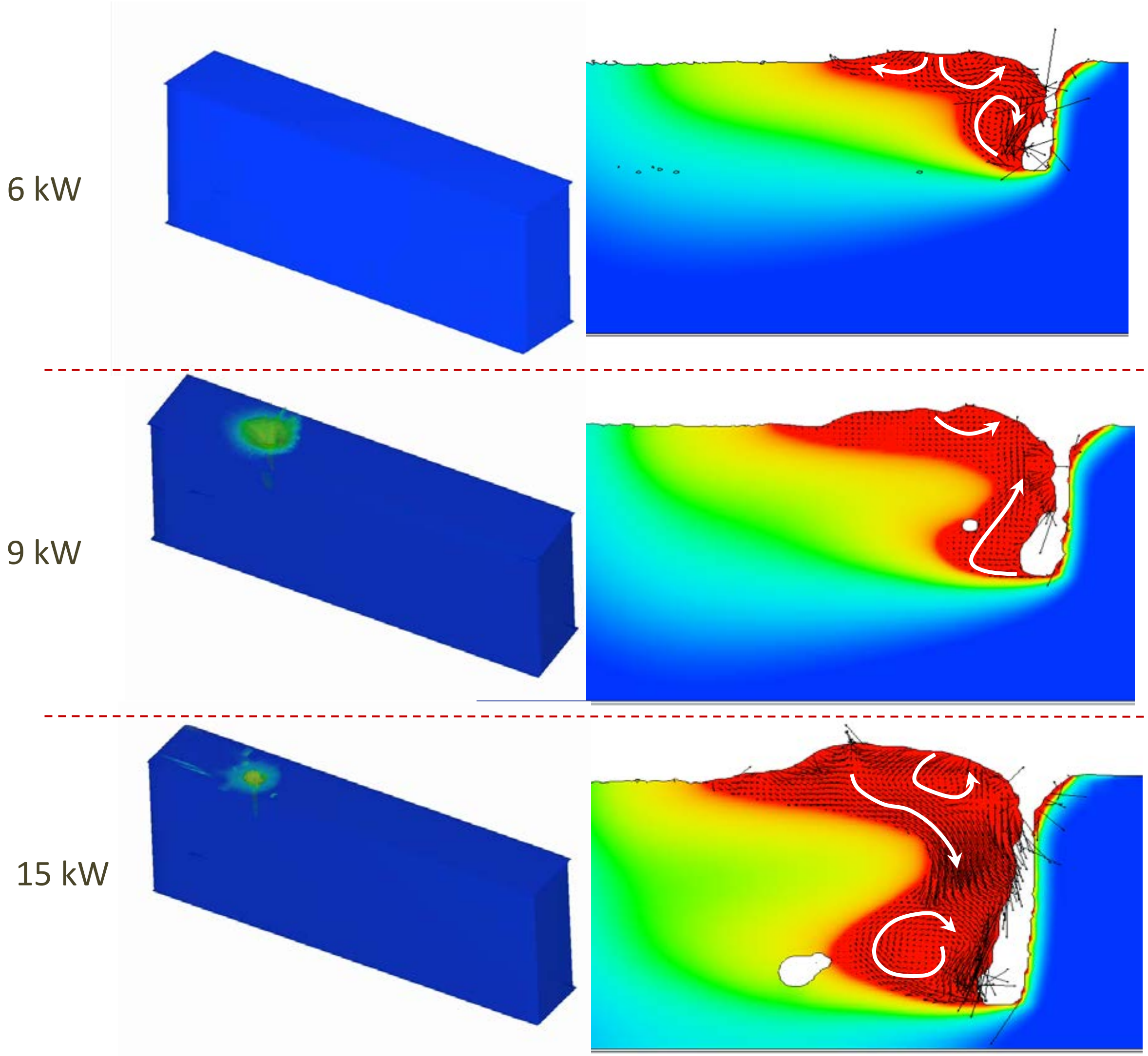

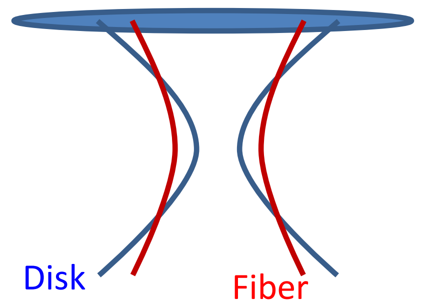

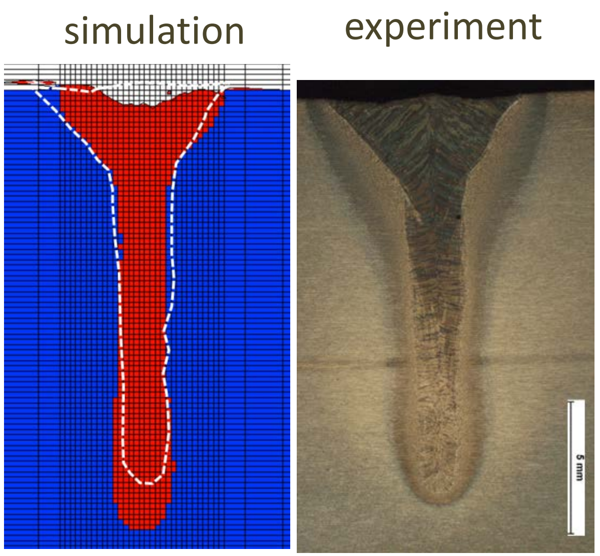

Material A36(ASTM)/SS400(JIS)
Laser power: 15 kW
Thickness 20 mm
Mesh size 0.02cm

- Large keyhole at bottom, Long pool length at top, Short pool length in middle
- Vortex at bottom → Relatively long keyhole

Partial Penetration Laser Welding at Various Positions

Experimental condition

- Laser power : 9kW,
- Welding speed : 1.5m/min
- Workpiece : SS400,
- Workpiece thickness : 20mm

- Similar weld pool shape for all positions
- Necked in the middle of keyhole
- Good agreement in weld bead shape

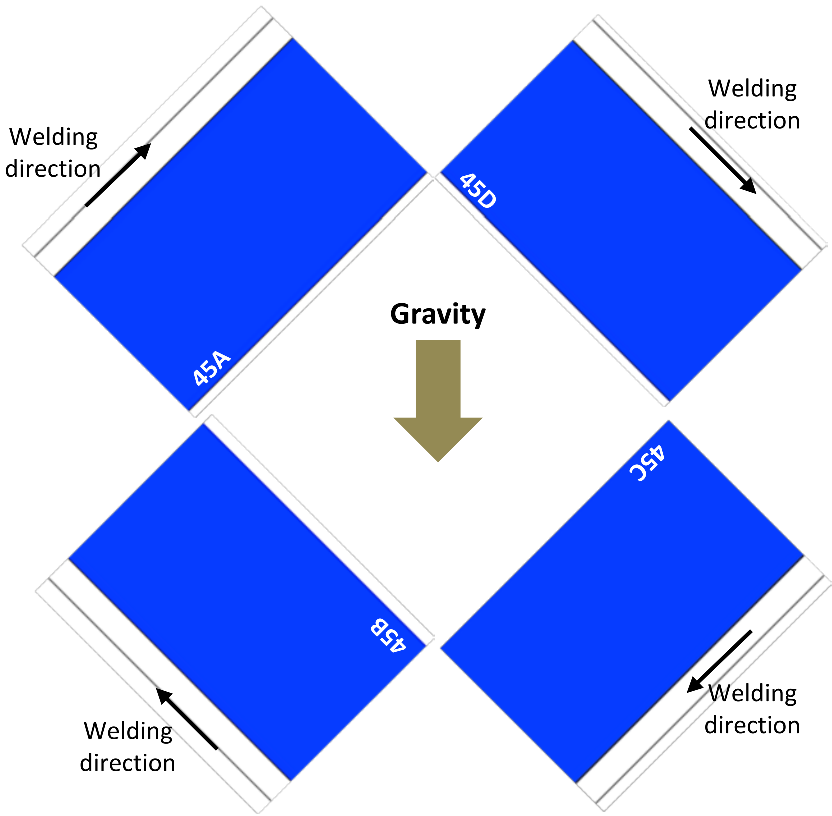

Temperature profile of longitudinal cross section

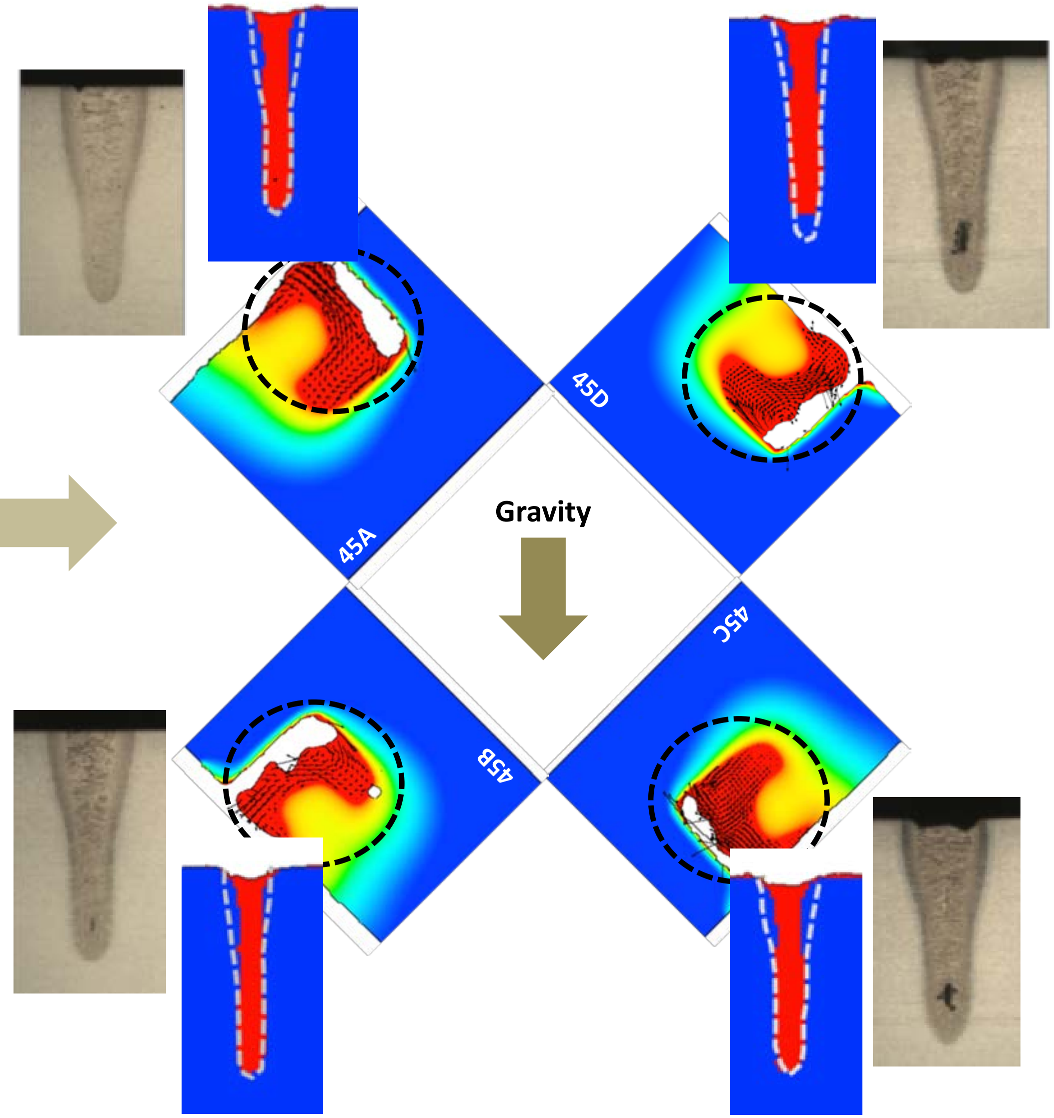

Full Penetration Laser Welding

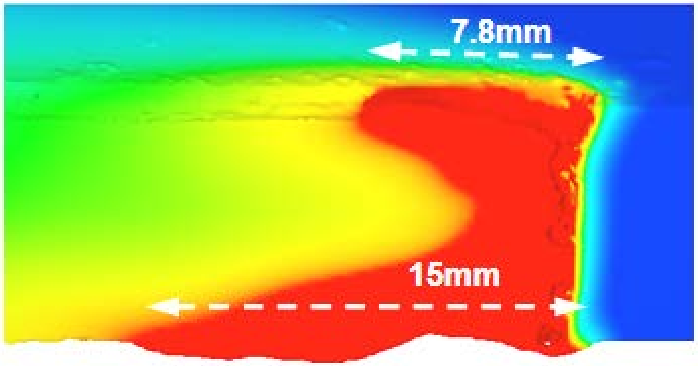

(a) Simulation result

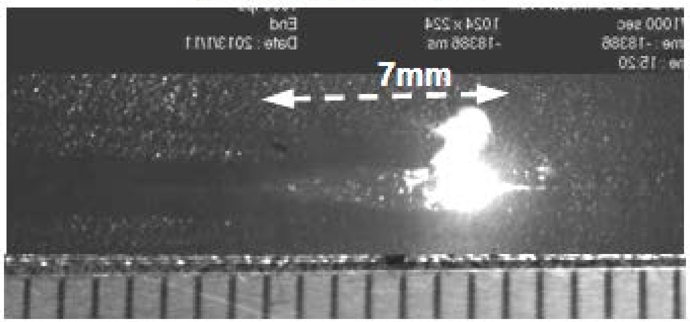

(b) Experiment result: upper surface of molten pool

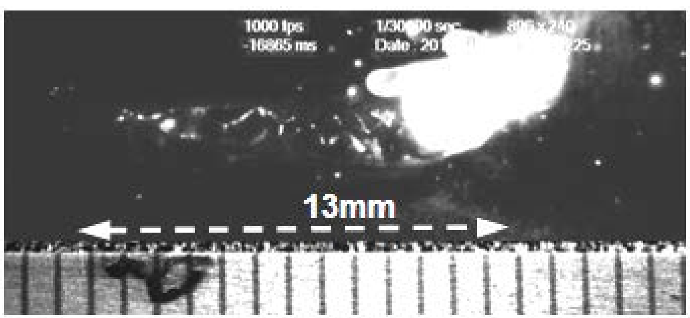

(c) Experiment result: lower surface of molten pool

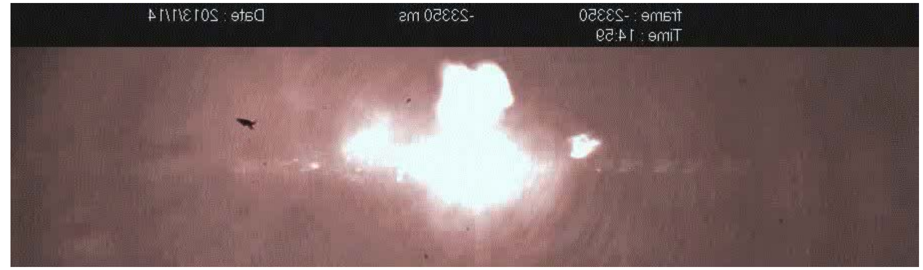

Upper surface of molten pool

Lower surface of molten pool

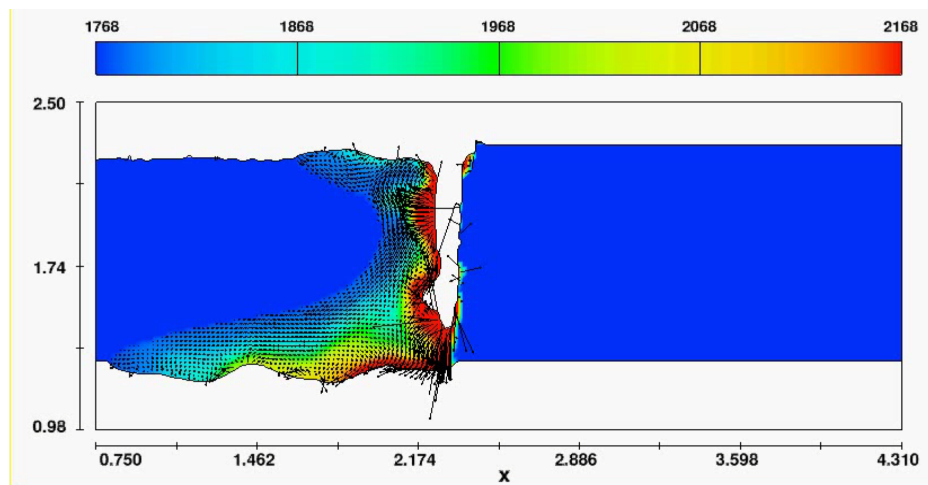

Simulation result of XOZ plane for comparison

Laser-GMA Hybrid Welding

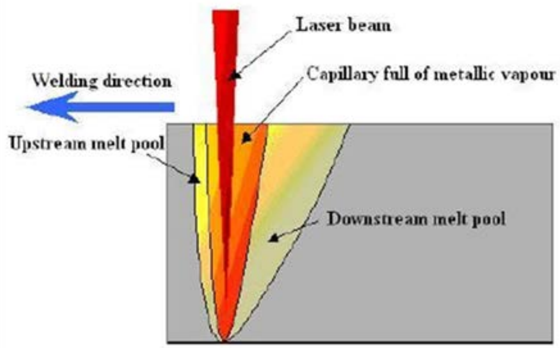

Laser Welding

Advantages
- ✓ High productivity
- ✓ low distortion level
- ✓ Joining of dissimilar materials
- ✓ <u>Narrow, deep weld seam</u>

Disadvantages
- ✓ Poor gap bridging ability
- ✓ High cost
- ✓ metallurgical problems due to the high cooling rates

Keyhole dynamics

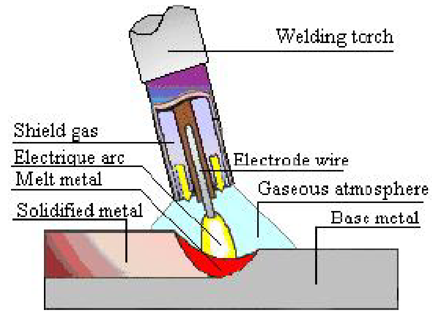

Gas Metal Arc Welding

Advantages
- ✓ Good gap bridging ability
- ✓ Low cost
- ✓ High efficiency (60-80%)
- ✓ <u>Control of metallurgical variables through the addition of filler wire</u>

Disadvantages
- ✓ Low productivity
- ✓ High distortion level

Element mixing

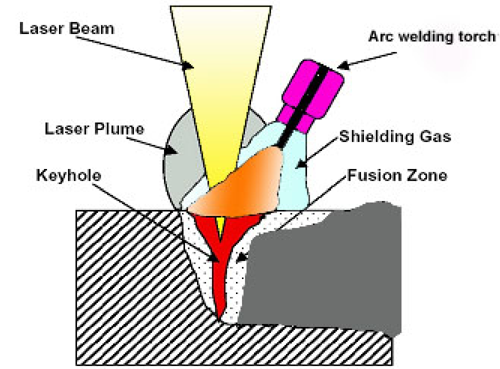

Laser Arc Hybrid Welding

Advantages
- ✓ Advantages of arc and laser welding

Disadvantages
- ✓ Large number of process parameters
- ✓ Process complication

Variations
- ✓ Arc leading
- ✓ Laser leading

Keyhole dynamics
Element mixing

Bead formation and element mixing in experiments and CFD simulations

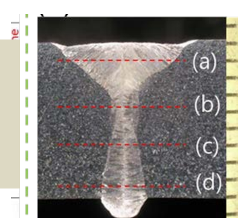

CO_2 Laser-GMA Hybrid Welding with Partial Penetration

Alloying element distribution (wt. % Cr)

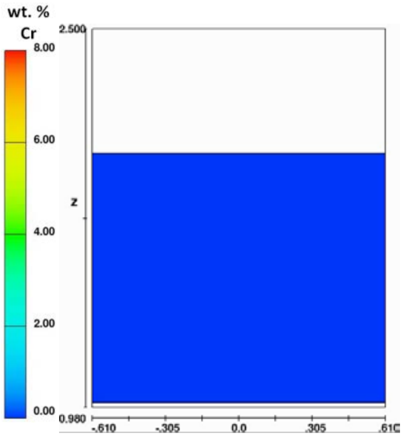

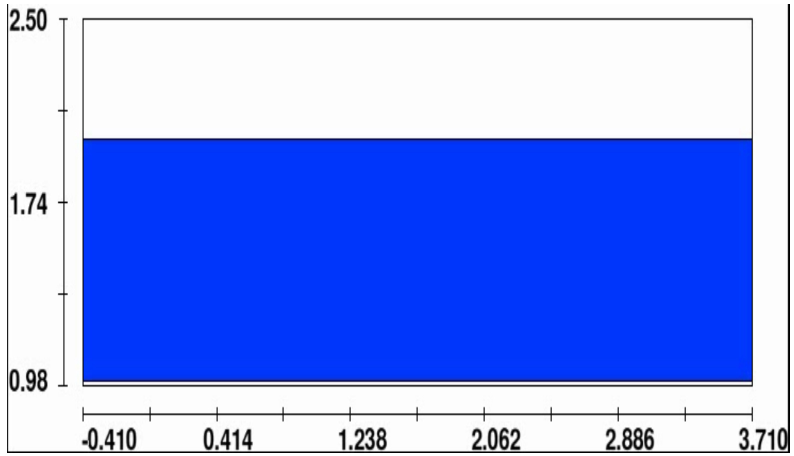

- Simulation:
  Filler metal flows down, but flows back upwards without arriving at the pool bottom → Tendency of periodical variation!

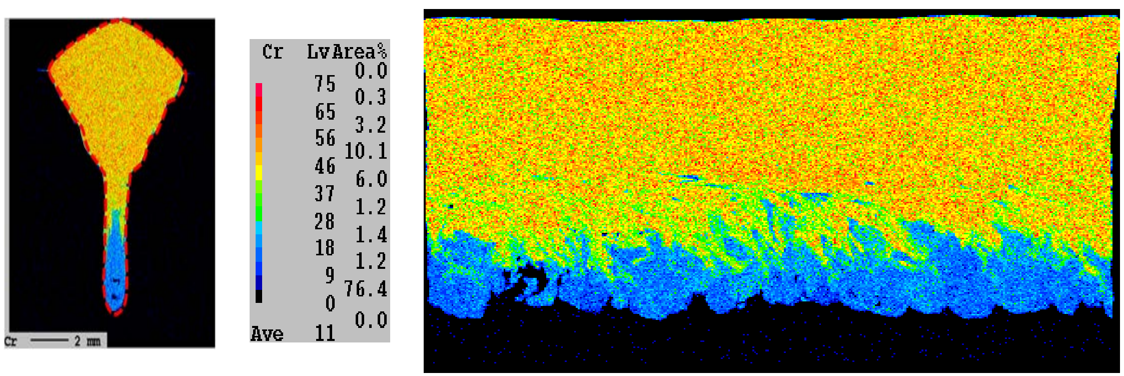

- Experiment:
  Fairly good agreement in weld bead shape and alloy element distribution with simulations!

- Sawtoothlike patterns in bottom bead of simulations and experiments

Models for Laser Welding Process

- Laser → multiple reflections by ray-tracing, scattering
- Laser-matter interaction → absorption/reflection/transmission
- Vaporization → recoil pressure
- Vapor-induced heat source
- Vapor-induced shear stress
- Bubble formation → internal pressure

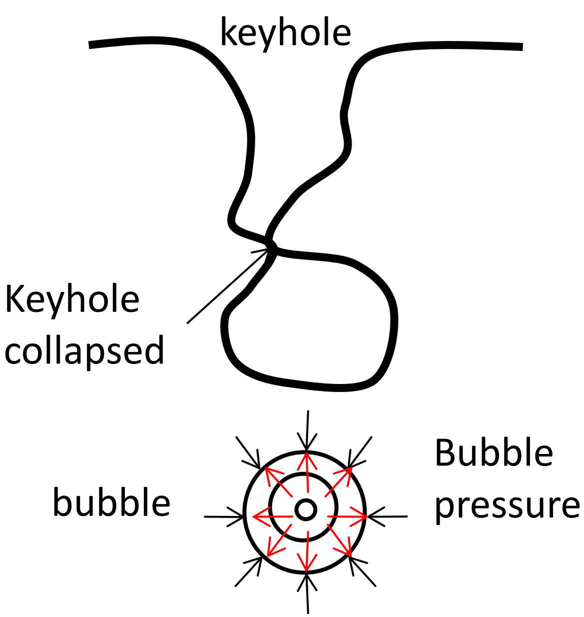

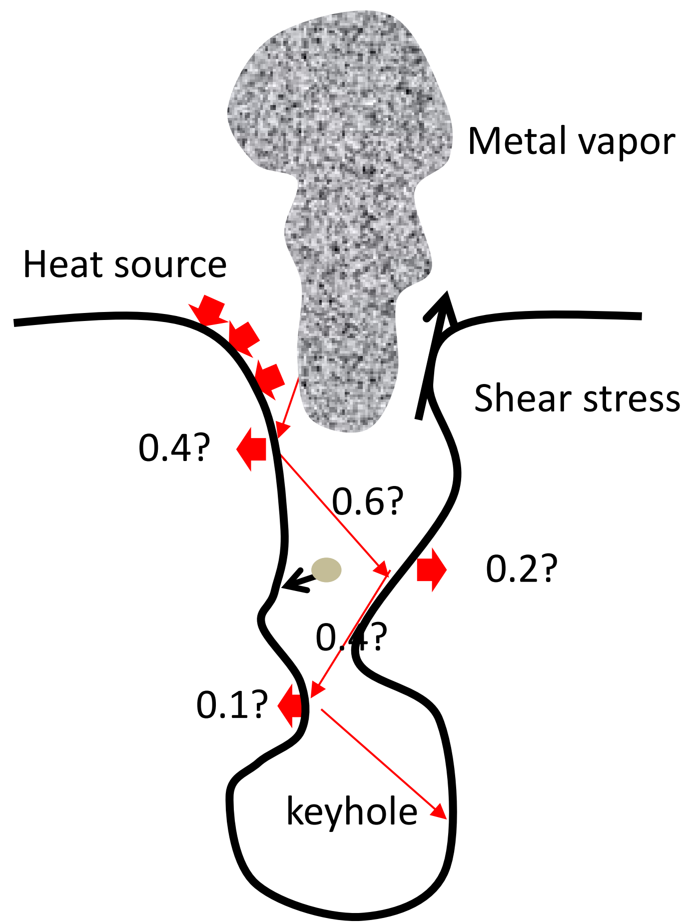

- Laser → multiple reflections by ray-tracing, scattering
- Laser-matter interaction → absorption/reflection/transmission
- Vaporization → recoil pressure
- ~~Vapor induced heat source~~
- ~~Vapor-induced shear stress~~
- Bubble formation → internal pressure

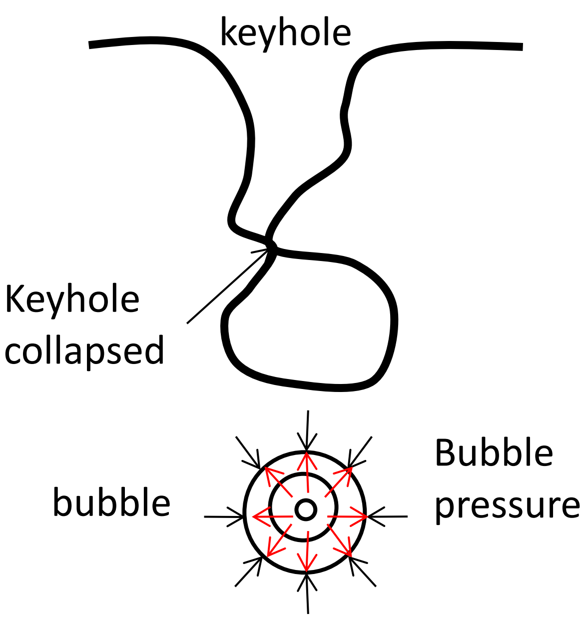

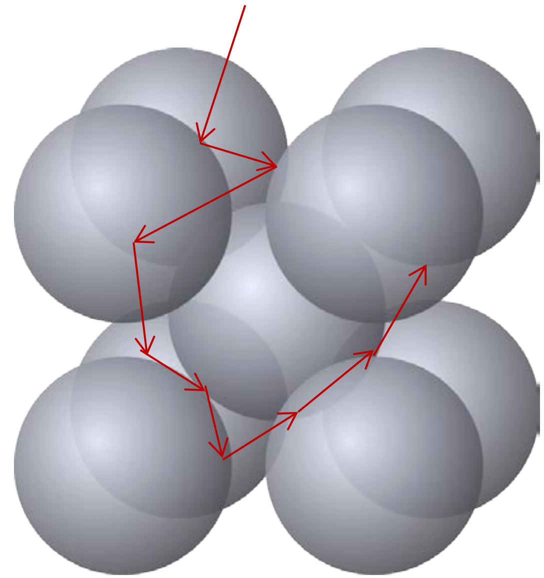

Powder Structures w/ and w/o Gap: Different Density

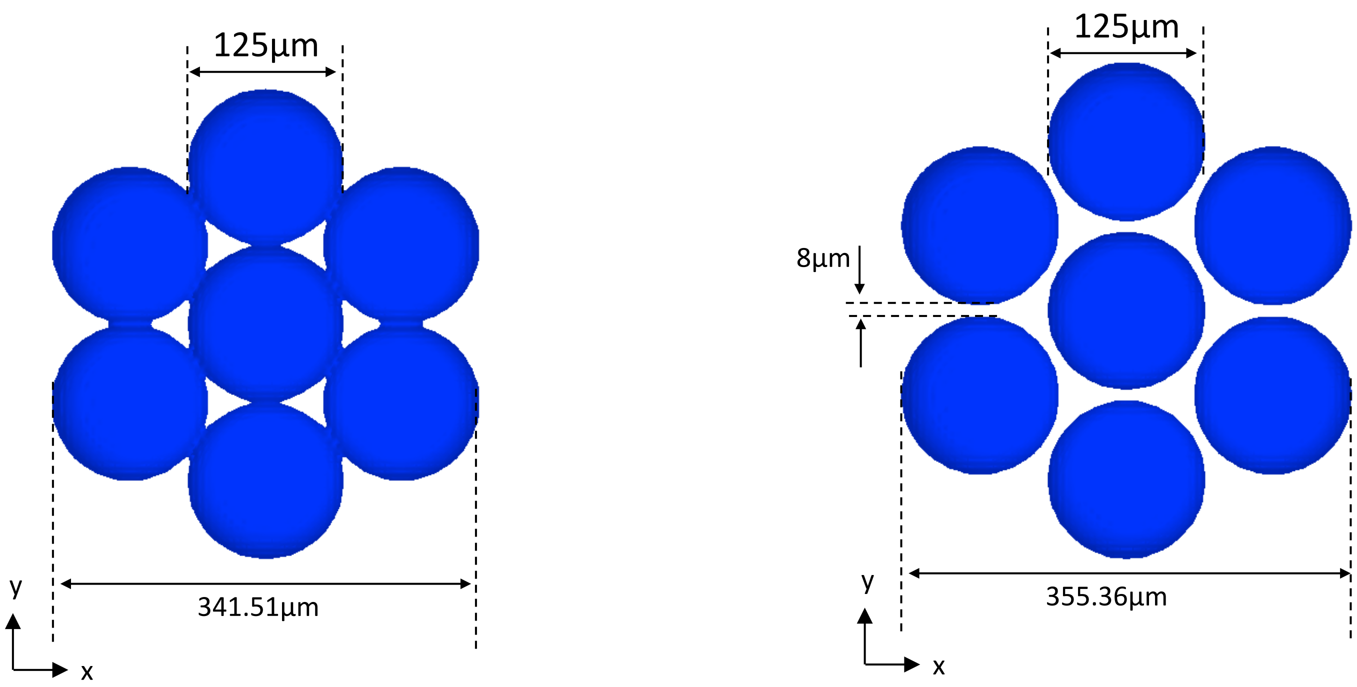

Simulation conditions

- Material : Aluminum
- Particle size : 125µm
- Beam diameter : 200µm
- Laser power : 500W

	Case 1	Case 2	Case 3
Gap	0µm	8µm	8µm
Process speed	50mm/s	50mm/s	51.28mm/s
Note		Same **process speed** with Case 1	Same **process time** with Case 1

Temperature Profile and Power Absorption

	Temperature profile		Power absorption	
	Top	Bottom	Top	Bottom
Case 1	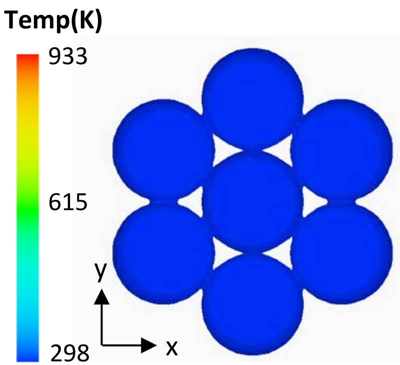	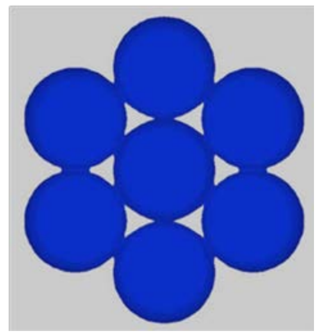	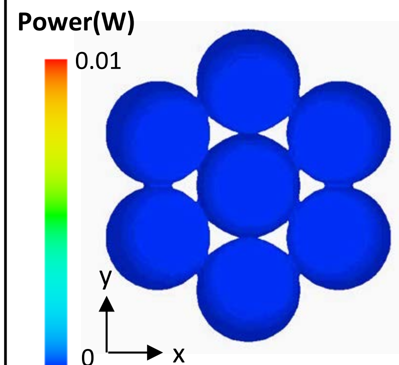	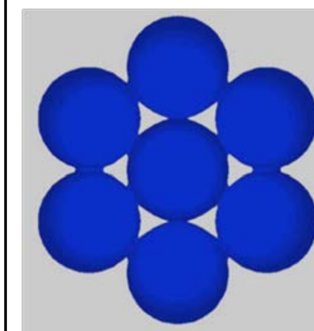
Case 2	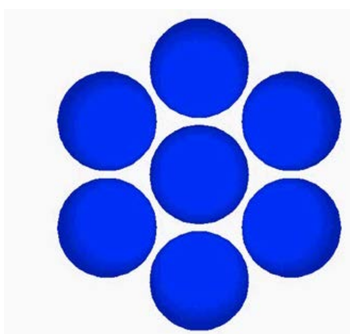	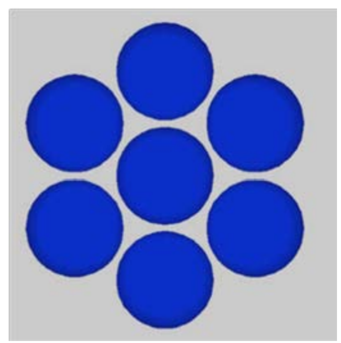	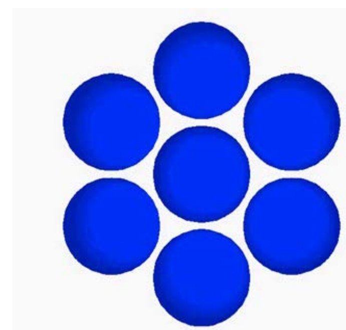	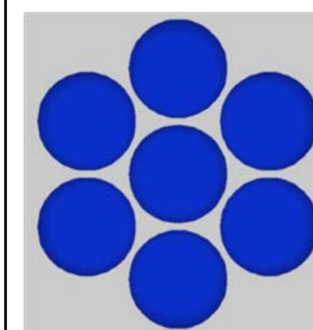
Case 3	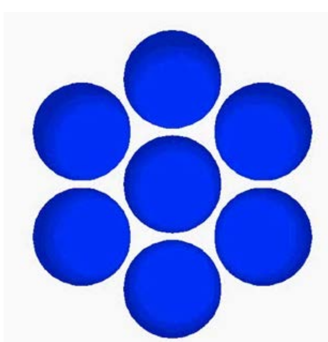	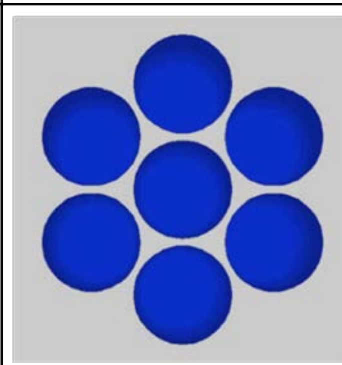	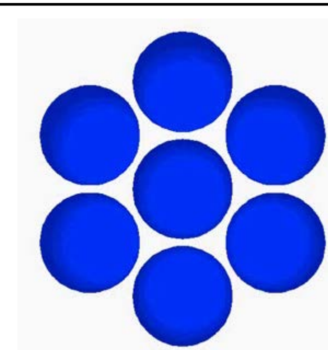	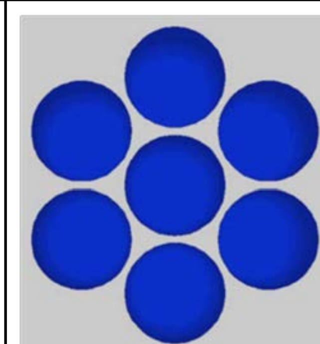

Powder Melting in Selective Laser Melting

- Irregularly distributed powder bed

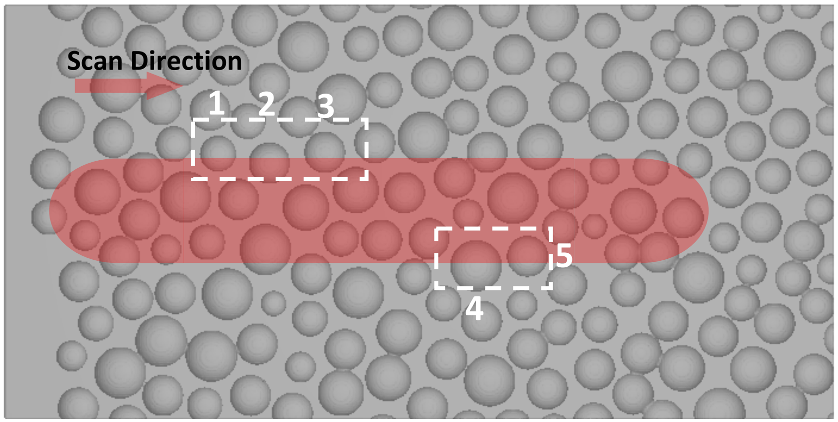

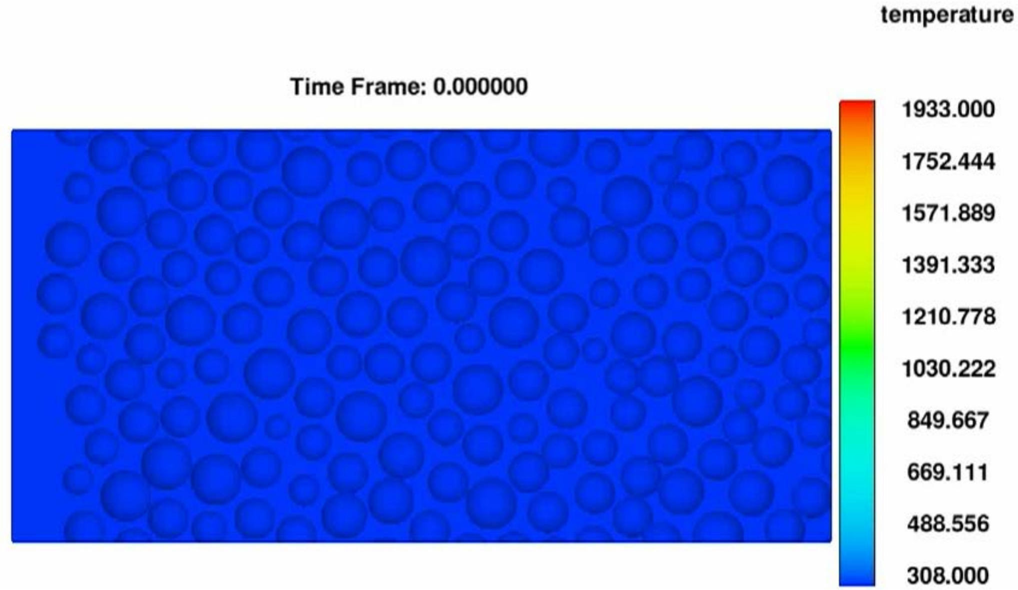

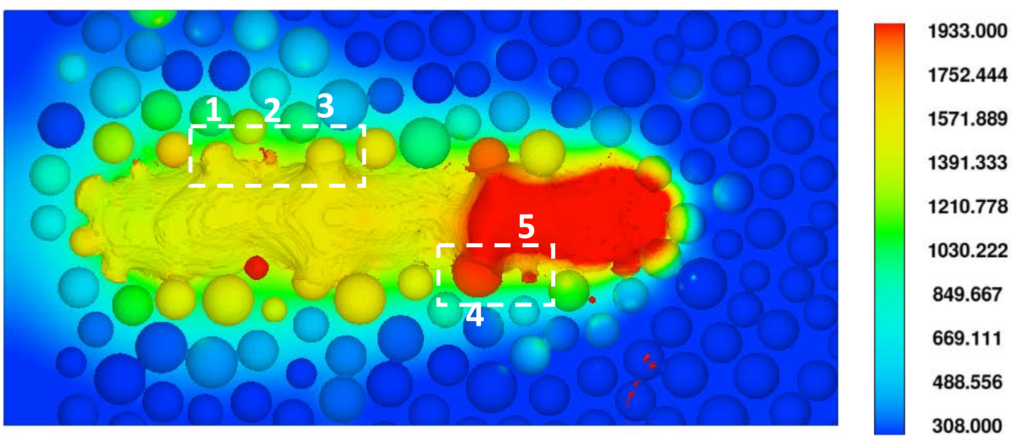

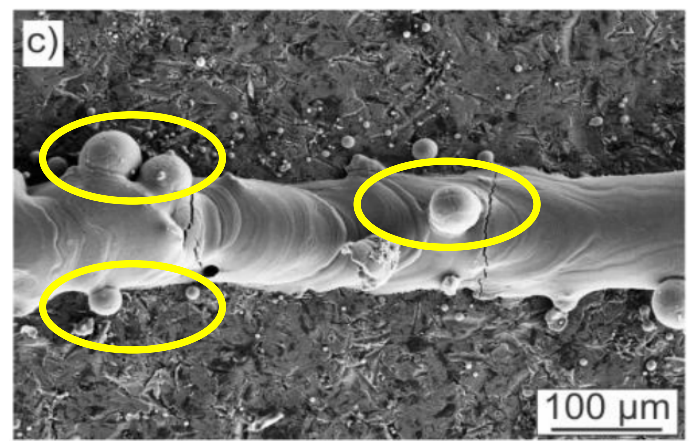

[Loeber L. et al, Selective laser melting of a beta-solidifying TNM-B1 titanium aluminide alloy, Journal of Material Processing Technology]

Powder Melting Characteristics at Different Conditions

200w-0.8m/s | 200w-1.0m/s | 200w-1.2m/s

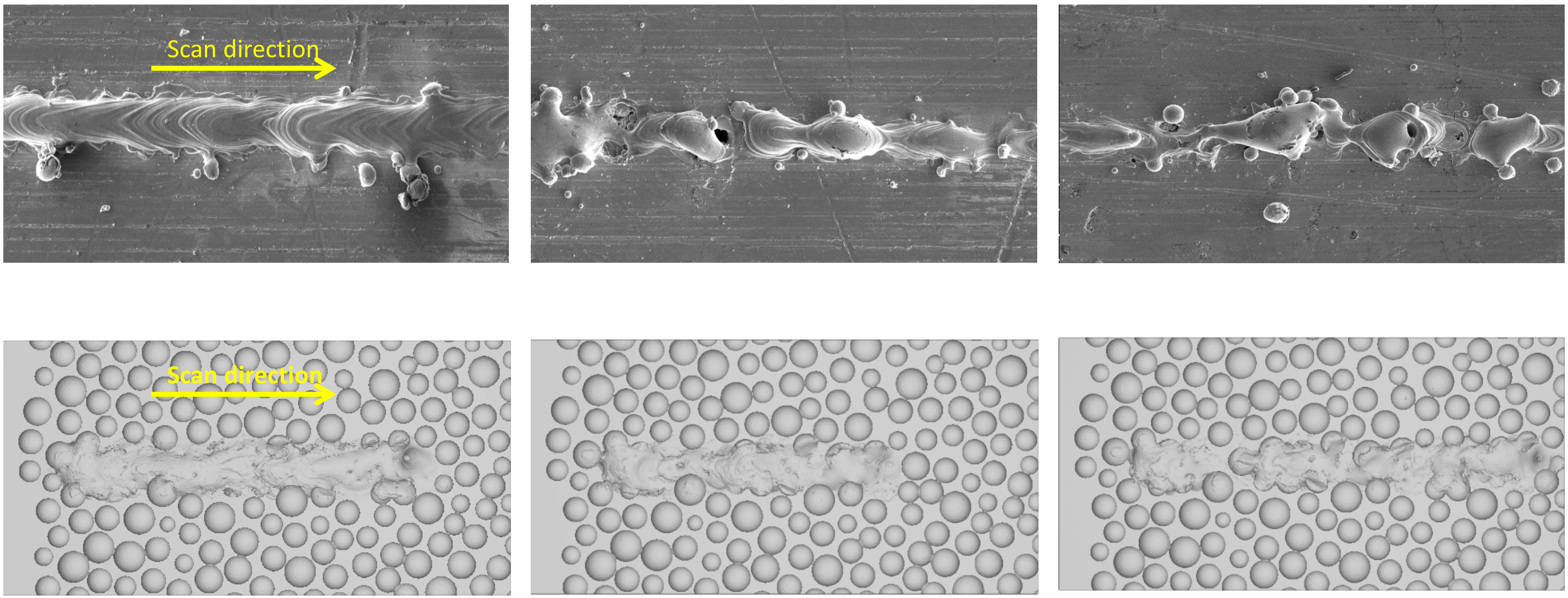

- The surface morphology: good agreement between simulations and experiments
- At lower scan speed 0.8m/s: continuous and smooth single track
- Increase of scan speed: the melt track becomes unstable and separated to small balls.

Electron Beam Welding (EBW)

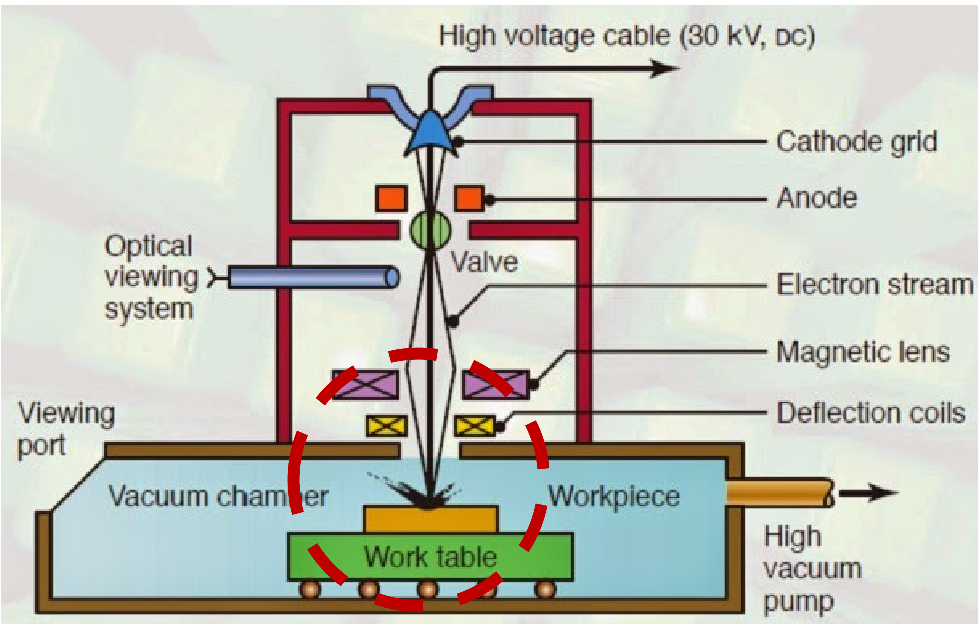

Electron Beam Melting (EBM)

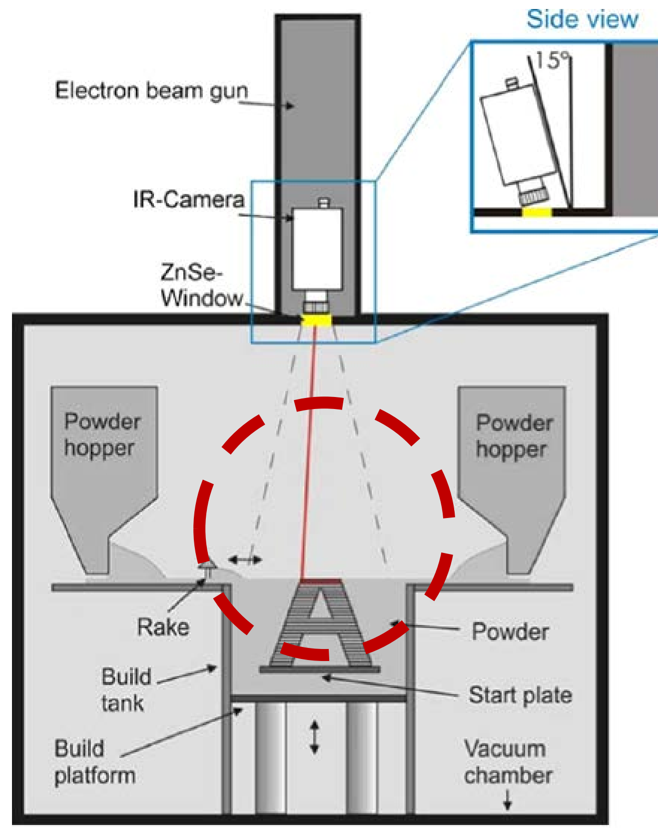

Definition of electron beam

- Cross-sectional energy flux distribution: $J = \frac{UI}{2\pi\sigma^2} exp\left(-\frac{x^2+y^2}{2\sigma^2}\right)$
- Kinetic energy of single electron: $E_0 = eU$
- Large number of electrons (*N'>100,000*) → Coordinate tracking of each electron
- The probability distribution of the coordinate (x, y) of a single electron: initial coordination

$$P(x, y) = \frac{1}{2\pi\sigma^2} exp(-\frac{x^2+y^2}{2\sigma^2})$$

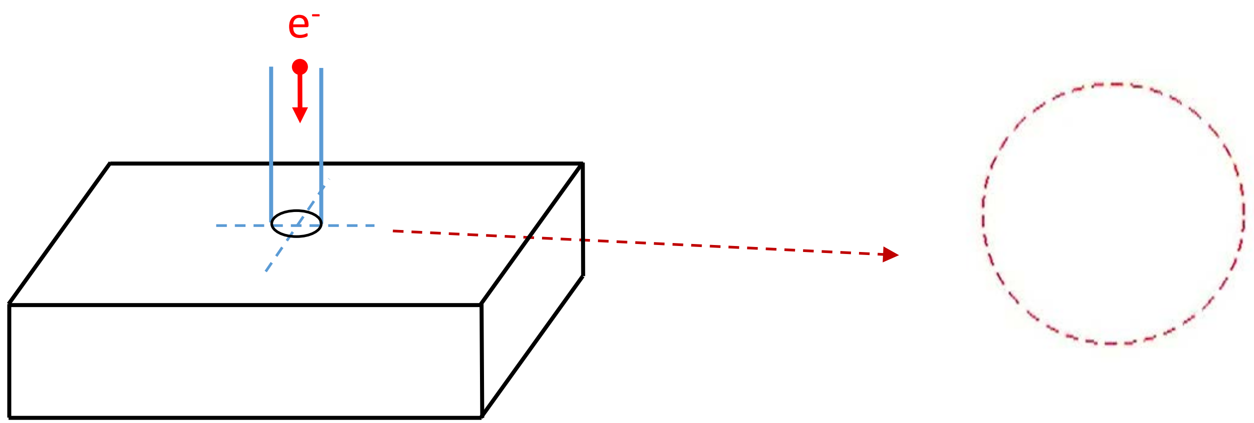

Tracking of Each Electron

- Initial coordination of each electron
- Surface cell check by surface-based ray tracing method
- Contact check → Collision point
- Absorption and backscattering at the surface cell

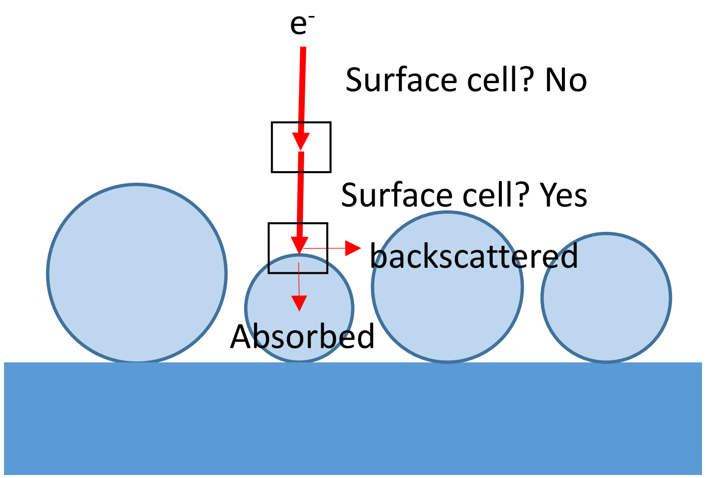

Electron beam tracking in powder bed

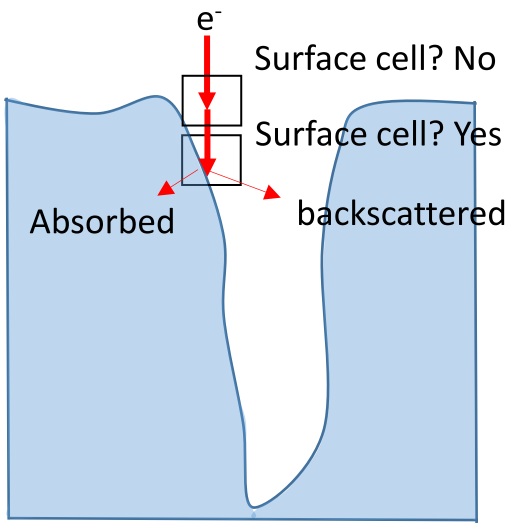

Electron beam tracking in keyhole

- Heat flux distribution $\Phi'_{(x,y,z)}$ for the sufficiently large number of electrons (*N'*) by:
  - Free-surface tracking model
  - Energy absorption model
  - Back-scattering model.

- Heat flux distribution $\Phi_{(x,y,z)}$ for the real number of electrons (*N* >> *N'*): $\Phi_{(x,y,z)} = \frac{N}{N'}\Phi'_{(x,y,z)}$

CFD Simulations of EBW and EBM

Application of the heat source in EBW simulations

Electron beam welding (EBW) in a vacuum chamber: a very deep, narrow penetration at high welding speeds.

- Material: 2219 Aluminum alloy
- Thickness: 20mm
- Beam voltage: 60kV
- Beam current： 40~60mA
- Welding speed： 10mm/s~18mm/s
- Beam radius: 0.25mm

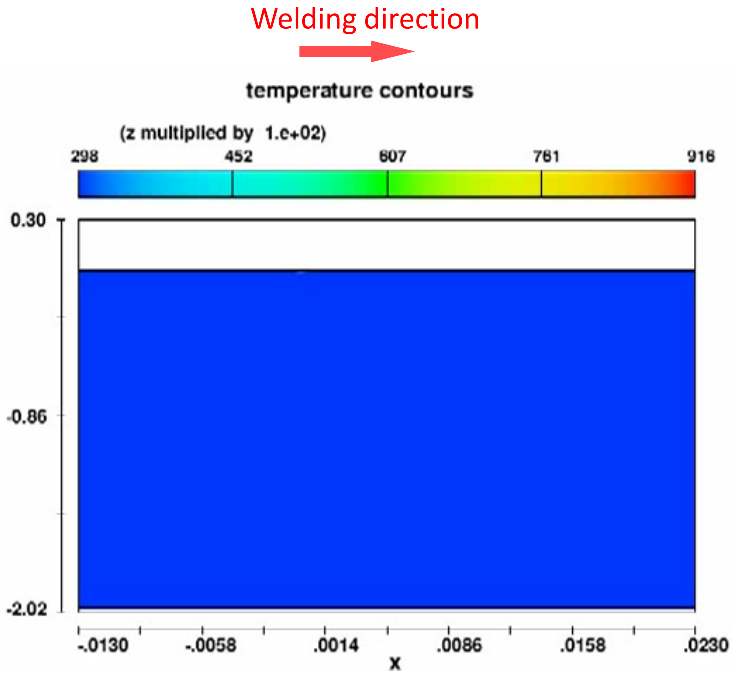

P=2400 W, V=10 mm/s

Application of the heat source in EBM simulations

Electron beam melting (EBM) for powder bed based additive manufacturing process: very promising in aerospace industry and medical implants.

- Material: Ti6Al4V
- Particle size: 45μm~110μm
- Beam voltage: 60kV
- Beam current： 0.5mA~3mA
- Scan speed： 0.05m/s~0.30m/s
- Beam radius： 0.20μm
- EBM system: Arcam AB S400

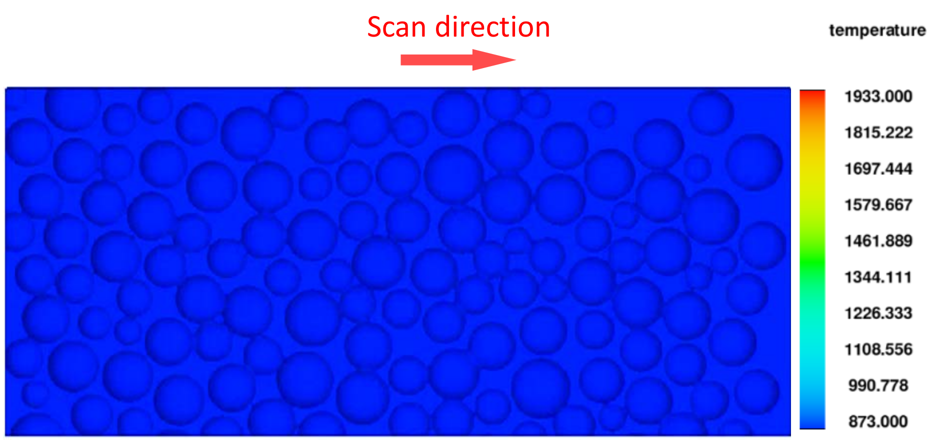

P=60 W, V=0.10 m/s

Simulations and Experiments

EBW simulation

- Molten pool:
  - Simulation results shows some trend with experiment results at the top region of the molten pool.
  - Compares to the experiments results, the bottom of the molten pool is not very sharp in the simulation.

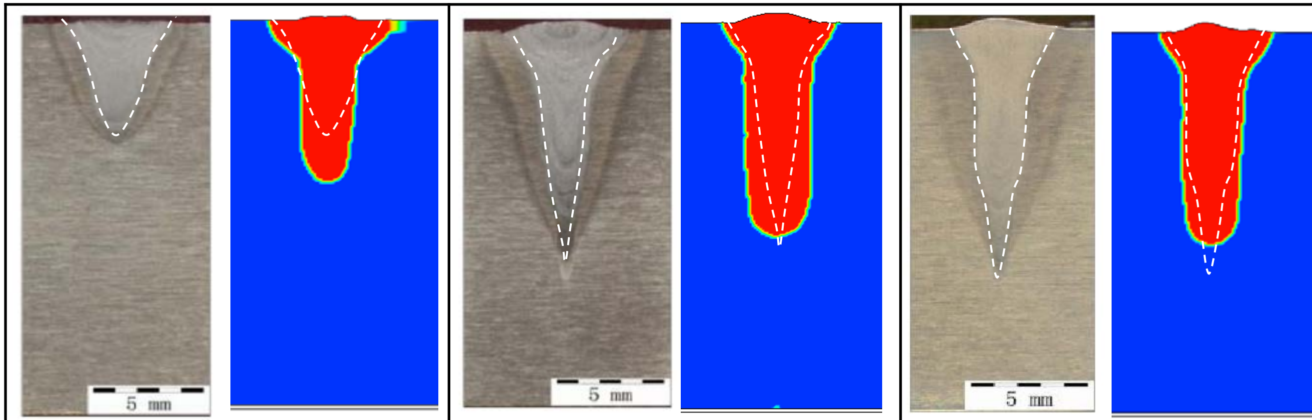

P=2400 W, V=10 mm/s | P=3600 W ,V=10 mm/s | P=3600 W, V=18 mm/s

EBM simulation

- Surface morphology:
  - The top surface morphology was divided into three patterns, balling pattern, distortion track pattern and straight track pattern.
  - Simulation results showed good agreement with experiment results.

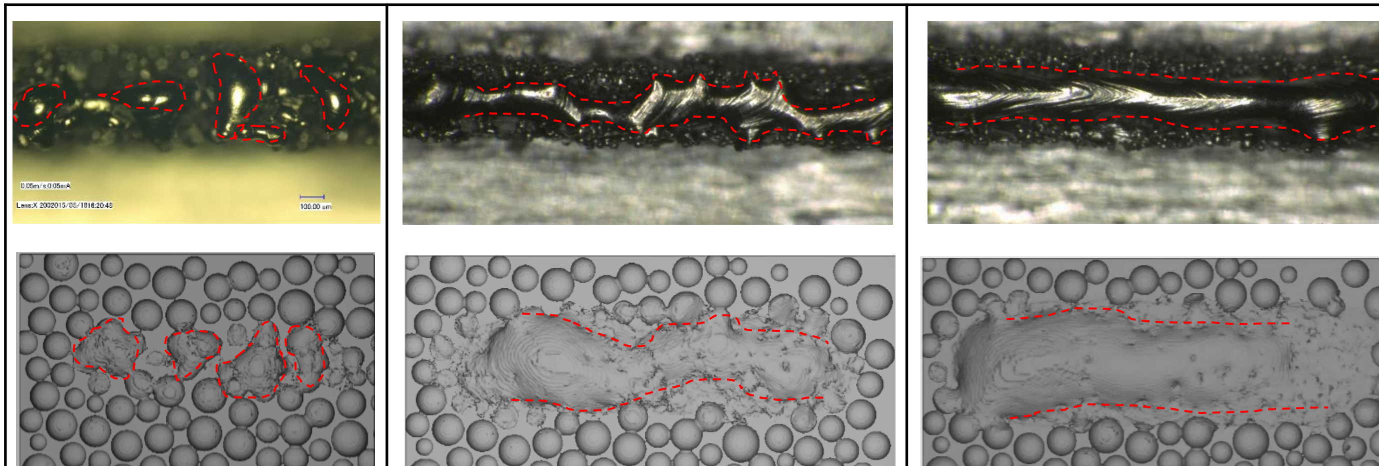

P=30w, V=0.05m/s | P=60w, V=0.10m/s | P=180w, V=0.30m/s

Friction Stir Welding (FSW)

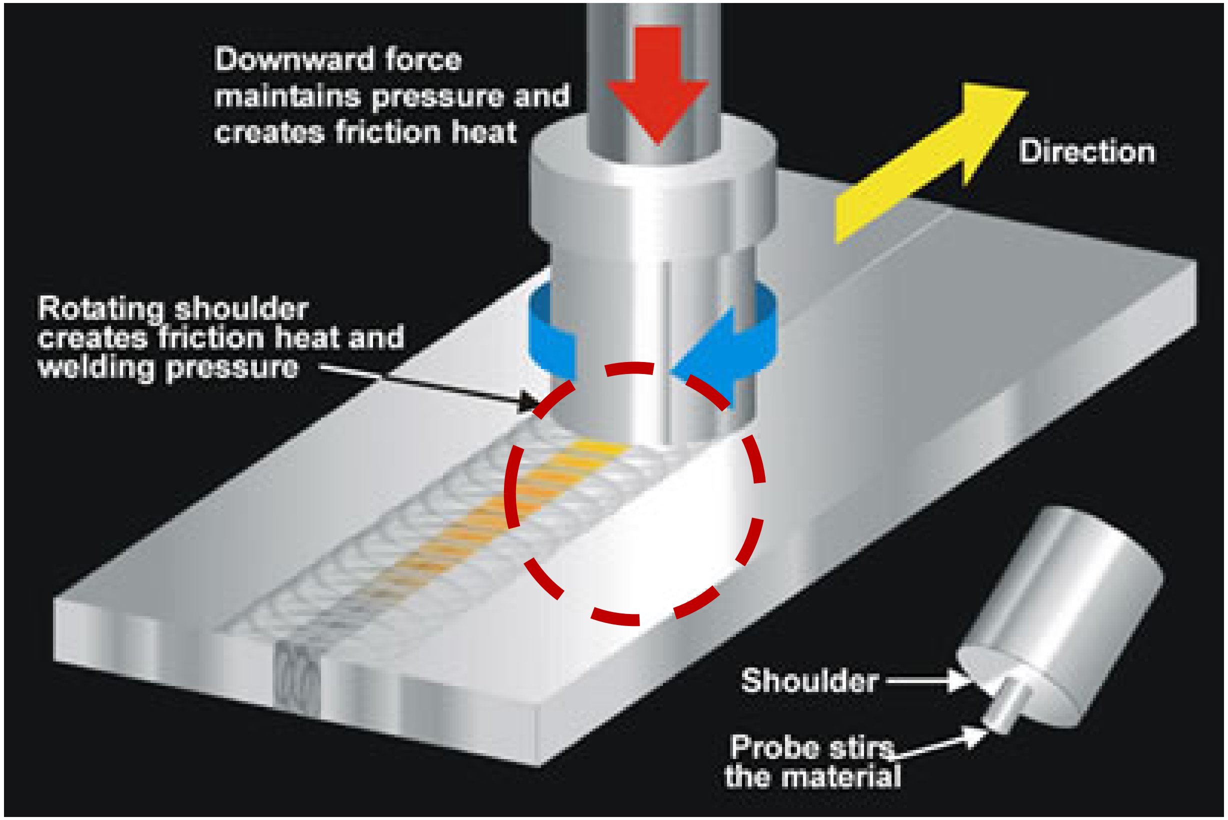

Heat Generation in Friction Stir Welding

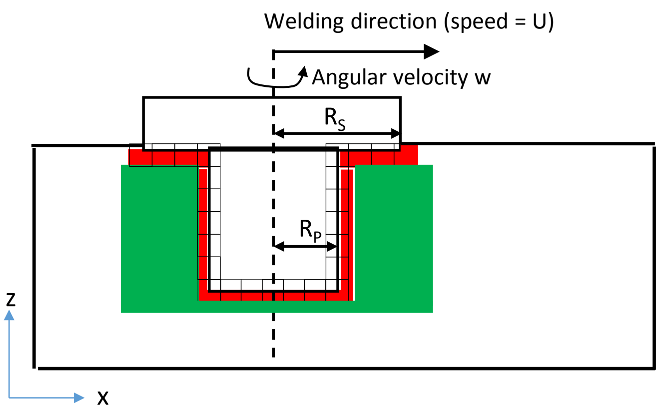

Schematic diagram for heat generation

- □ : interface cells
- ■ (red) : heat generation at tool interface cells by friction > 90%
- ■ (green) : heat generation by plastic deformation away from interface < 10%

- Energy conservation equation

$$\frac{\partial h V_F}{\partial t} + \boldsymbol{u} \cdot \nabla \mathrm{hA}_i = \frac{1}{\rho} \nabla \cdot (kAi\nabla T) + S_i + S_b$$

$h = \rho c T$

ρ and c are assumed as constant

$$S_i = \tau_{shear} v_{interface} \frac{A_r}{V} = mk(\omega r - U \sin\theta) \frac{A_r}{V}$$

where

m:friction factor

k: maximum shear stress at yielding

ω: rotational speed

r: distance from tool axis

U: welding speed

Θ: angle between x direction and rotational direction

A_r: interface area of interface cell

V: volume of a cell

$$S_b = f_m \sigma_e \dot{\varepsilon}$$

where

f_m: converted ratio from plastic deformation to heat

σ_e: flow stress, defined as $\sigma_e = \frac{1}{\alpha} \sinh^{-1}[(\frac{Z}{A})^{\frac{1}{n}}]$

Z : Zener-Hollomon parameter, defined as $Z = \dot{\varepsilon} \exp(\frac{Q}{RT})$

R : gas constant

Q, α, n, A : material dependent parameters

$\dot{\bar{\varepsilon}}$: effective strain rate, defined as $\dot{\bar{\varepsilon}} = (\frac{2}{3} \dot{\varepsilon}_{ij} \dot{\varepsilon}_{ij})$

$\dot{\varepsilon}_{ij}$: strain rate tensor, defined as $\dot{\varepsilon}_{ij} = \frac{1}{2}(\frac{\partial u_i}{\partial x_j} + \frac{\partial u_j}{\partial u_i})$

Interface Tracking

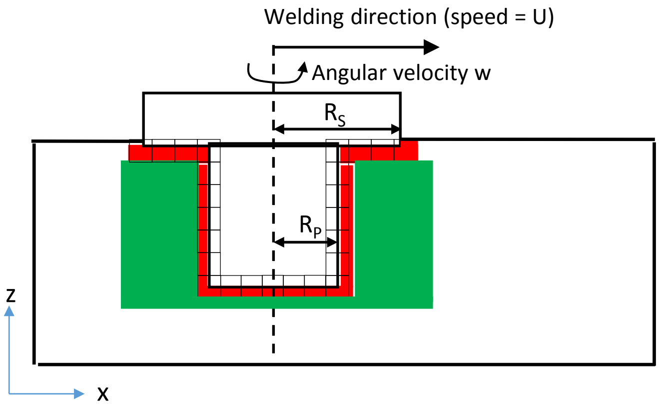

Schematic diagram for heat generation

□ : interface cells

■ (red) : heat generation at tool interface cells by friction > 90%

■ (green) : heat generation by plastic deformation away from interface < 10%

Two heat sources in FSW

Heat generation by friction: interface between tool and workpiece → Interface tracking

Tool is rotating and moving

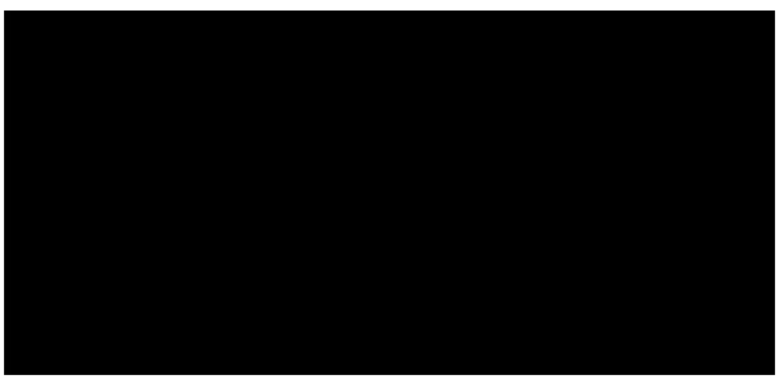

→Difficult to track the interface area between tool with complex shape and workpiece in real time

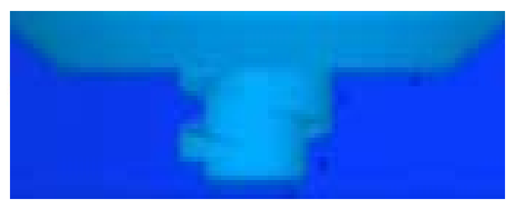

Screw type

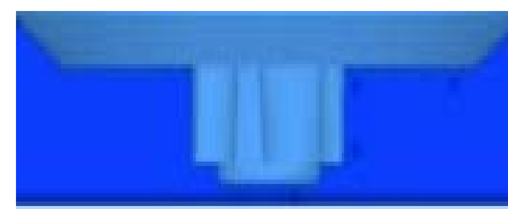

Tap type

For the design of complex tool shape

- Energy conservation equation for CFD simulation

$$\frac{\partial h V_F}{\partial t} + \boldsymbol{u} \cdot \nabla \mathrm{h} \mathrm{A}_i = \frac{1}{\rho} \nabla \cdot (kAi\nabla T) + S_i + S_b$$

$h = \rho c T$

ρ and c are assumed as constant

- V_F and A_i?

Open condition

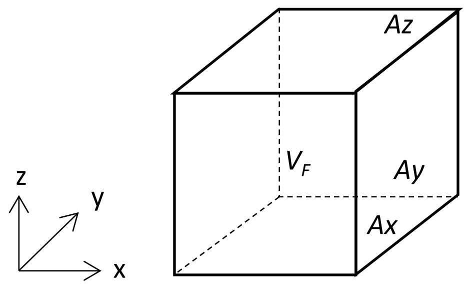

A_i = open area fraction
= 1 – closed area/area

V_F = open volume fraction
= 1 – solid volume/volume

Ax = Ay = Az = 1, V_F = 1

Partially open condition
(partially occupied by the tool)

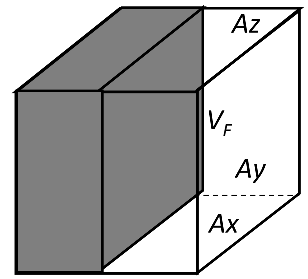

Ax ≠ Ay ≠ Az, V_F ≠ 1

- *Ax, Ay, Az and V_F* values are provided by S/W, where *Ax = 1, Ay < 1, Az < 1 and V_F < 1* in the above example → This information can be used for interface racking.

- Example

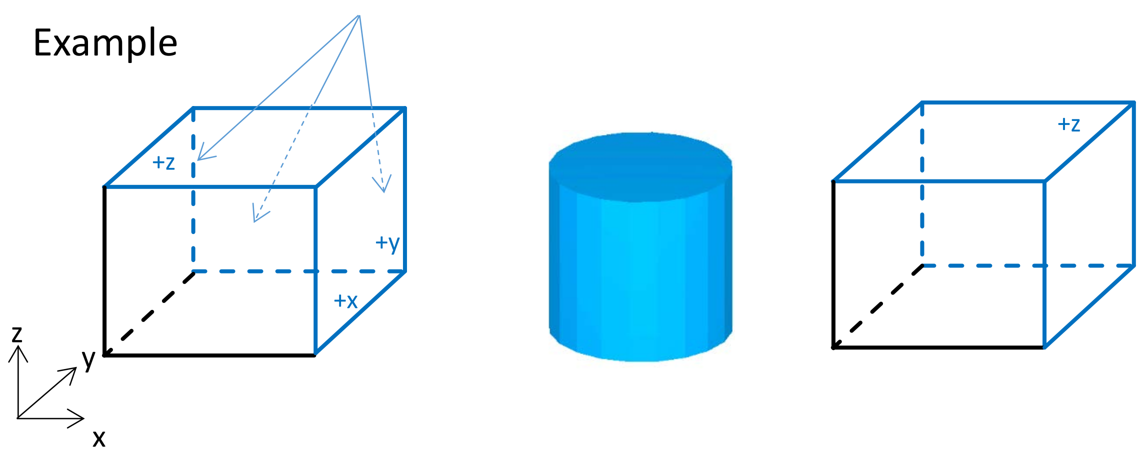

Tool surface meets +z surface
↓
Contact ratio of +z surface < 1
↓
This cell as the interface cell

Vertical Motion of Particles by Screw Type Tool

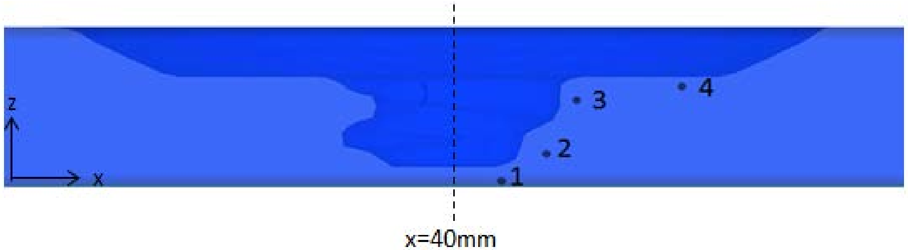

particle number	x coordinate [mm]	y coordinate [mm]	z coordinate [mm]
1	41.4	0	0.2
2	42.6	0	1
3	43.4	0	2.6
4	46.2	0	3

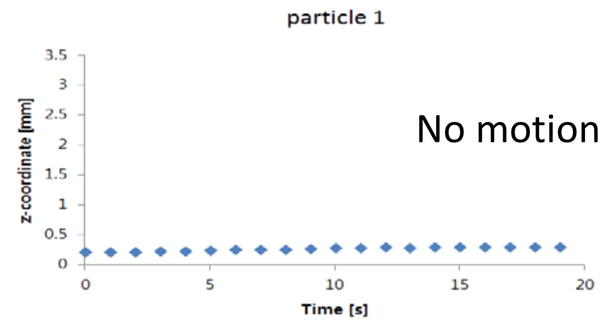

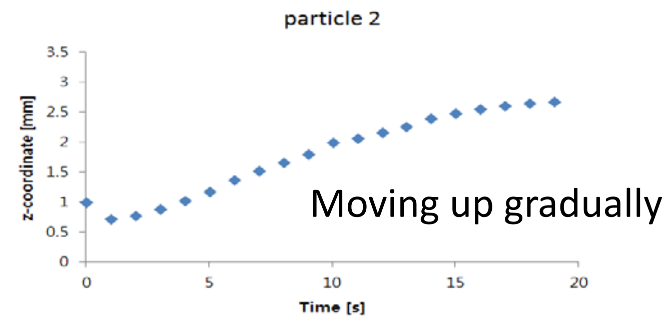

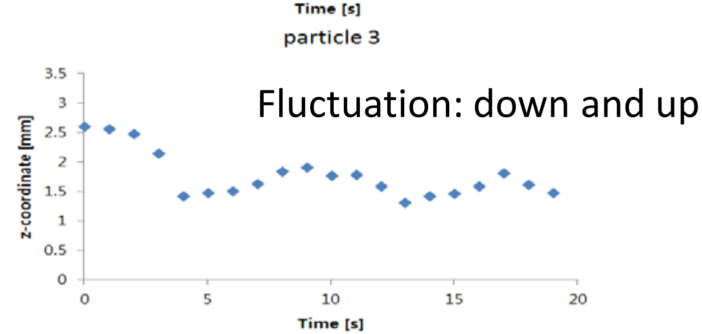

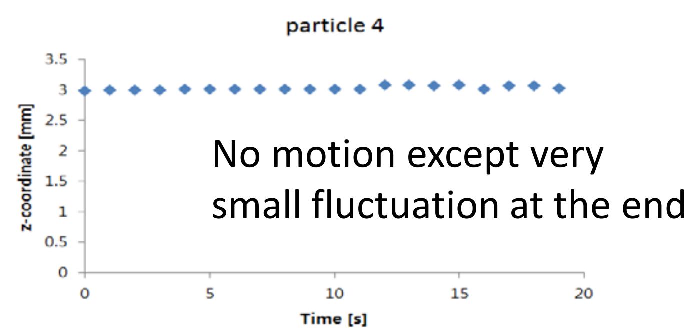

Motion in z direction

- Particle 1: below pin tip → No motion in z direction
- Particle 2: pin side → Moving up gradually
- Particle 3: below shoulder, close to screw → Fluctuating motion in z direction by screw influence
- Particle 4: below shoulder → No motion in z direction

Distribution of Velocity, ESR and Viscosity near by Tool

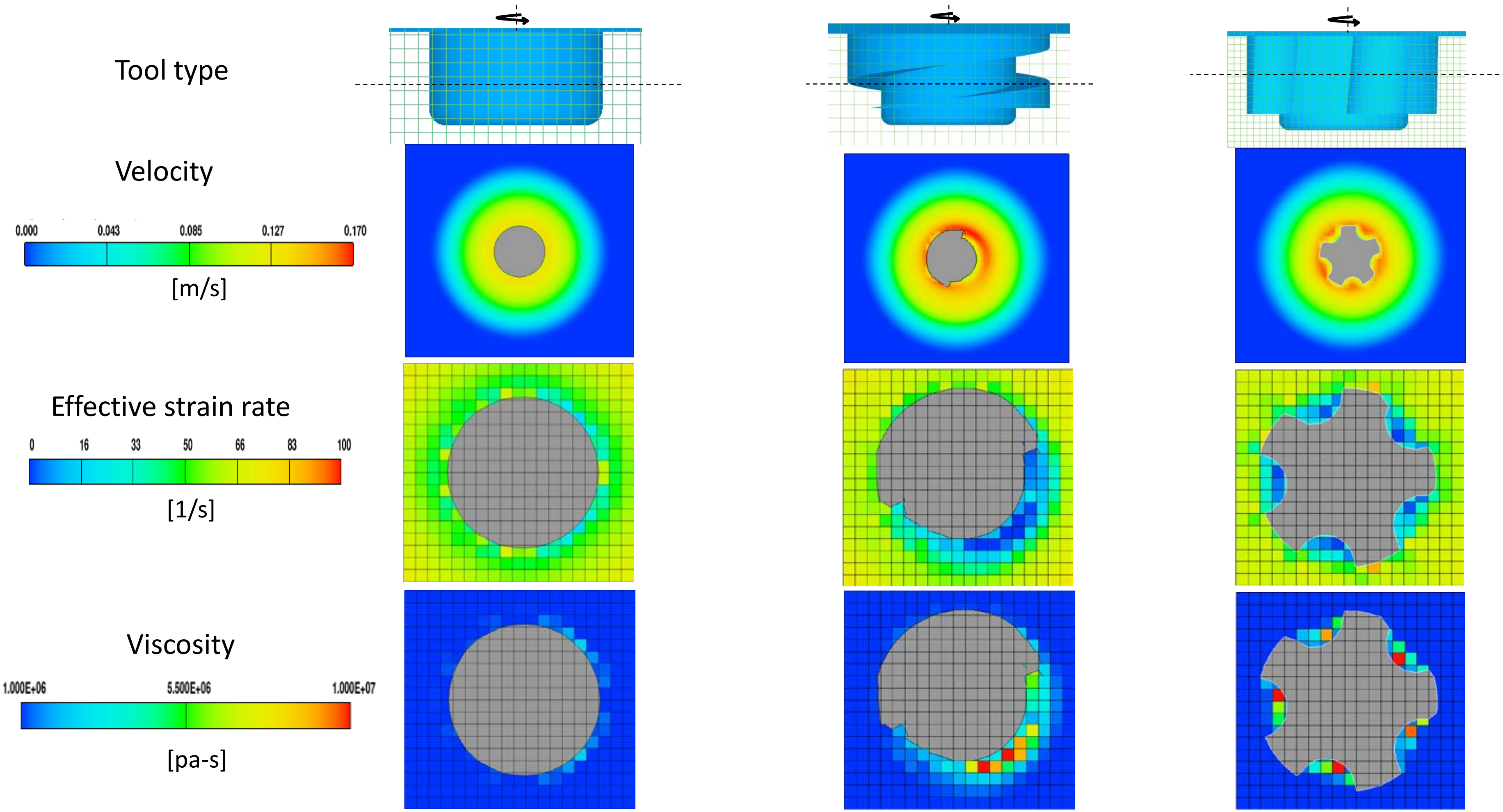

- Gradual change of velocity from tool to workpiece
- Higher effective strain rate in back side
- Higher viscosity in front side
- Relatively uniform distribution

- High velocity at heel edge area
- Lower effective strain rate in flute center area
- High viscosity in flute center area
- Relatively uniform distribution in heel area

- High velocity around the heel rotation path
- Lower effective strain rate in flute area
- Higher viscosity in flute area
- Highly non-uniform distribution

Summary: Thermal-Metallurgical-Mechanical Analysis of Weldments

Heat and Mass Transfer by CFD

Heat Source Model
- Surface heat flux by Abel inversion
- Droplet transfer from wire melting

- Accurate simulation of welding process by CFD

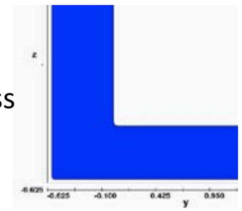

- Fundamental understanding
- Optimization of welding processes

- Temperature History
- Bead Shape
- Mixing of alloy element

- CFD-FEM coupling

- GTAW, GMAW, SAW
- LBW, LAHW, EBW, FSW
- SLM, EBM

Thermal-Metallurgical Analysis

- CCT diagram ↔ Temp., Material
- Heating and cooling rate
- Phase transformation
- Hardness prediction
- Element activation method for the weld bead formation
- Accuracy improvement by temperature history from CFD analysis
- Microstructure
- Hardness

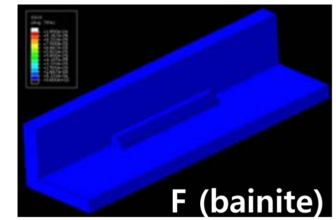

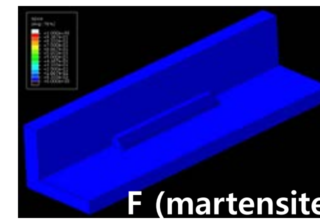

Thermal-Metallurgical-Mechanical Analysis

- Thermal-elasto-plastic behavior
- Material properties for various phases
- Stress-strain relations

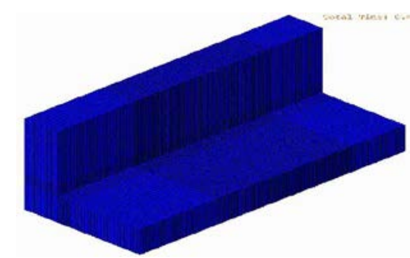

- Weld plastic strain
- Residual stress

Elastic Analysis of Welding Distortion

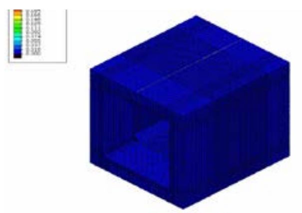

- Design of welded structures

- Weld plastic strain

Strength Prediction of Welded Joint

- Fracture strength
- Fatigue strength

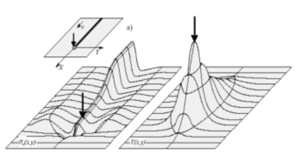

- Weld residual stress

Conclusions

1. CFD simulation results of laser materials processing can be used further for metallurgical and mechanical optimization of weldments.
2. CFD-FEM scheme is effective for thermal-metallurgical-mechanical analysis of welded structures.
3. Phase transformation plays an important role in metallurgical and mechanical behavior of weldments.
4. GMA and SA welding at various welding positions can be effectively analyzed by using arc-matter interaction models and CFD simulation of weld pool.
5. CFD simulations of laser and laser arc hybrid welding process can be realized precisely by effectively applying the laser-matter interaction in keyhole.
6. Particle tracing technique in CFD simulations is effective for understanding of element mixing behavior in laser arc hybrid welding.
7. Algorithms of ray tracing and laser-matter interaction in deep keyhole can be applied for laser welding of thin sheet metals and selective laser melting, as well as in electron beam welding and melting.
8. Friction stir welding process can be also analyzed by applying the algorithms developed for arc welding.

Thermal-Metallurgical-Mechanical Behavior of Welded Structures